Diffusion in Melts and Magmas

Youxue Zhang, Ting Gan

Department of Earth and Environmental Sciences

the University of Michigan

Ann Arbor, MI 48109-1005, USA

youxue@umich.edu; ganting@umich.edu

INTRODUCTION

Diffusion results from random motion of particles and entities. Diffusion in melts and magmas is due to thermally excited random motion of atoms, ions, and clusters, and plays a critical role in magmatic and volcanic processes. In melts and magmas, diffusion is one of the two mechanisms of mass transfer; the other being bulk flow (referred to as convection or advection). When both are present, diffusion refers to the dispersive motion relative to the mean bulk flow in a given reference frame (Richter et al. 1998). Diffusion plays critical roles in controlling magma mixing (Watson 1982; Koyaguchi 1985, 1989; Lesher 1994; Huber et al. 2009; Guo and Zhang 2020), mineral growth and dissolution rates in magmas (e.g., Watson 1982; Harrison and Watson 1983; Zhang et al. 1989; Newcombe et al. 2014; Macris et al. 2018), bubble growth and dissolution rate in magmas (Sparks 1978; Proussevitch and Sahagian 1998; Liu and Zhang 2000; Zhang 2013), and elemental and isotope fractionation during mineral

growth and dissolution (Jambon 1980; Richter et al. 1999, 2003; Watson and Muller 2009; Chopra et al. 2012; Watkins et al. 2014, 2017; Holycross et al. 2016, 2018). As a result, diffusion also plays an essential role in explosive volcanic eruptions and magma crystallization. Furthermore, diffusion has important applications in geospeedometry (Lasaga 1983, 1998; Zhang 1994, 2008; Trail et al. 2016; Zhang and Xu 2016).

Experimental investigation of diffusion in geologically relevant silicate melts began to flourish in the 1970's when micro-analytical measurements of diffusion profiles became available. In addition to the vast number of papers published since then, numerous books and reviews are available for diffusion in silicate melts. Hofmann et al. (1974) edited a book titled "Geochemical Transport and Kinetics" published by Carnegie Institution of Washington. This was the first landmark book summarizing the field. Lasaga and Kirkpatrick (1981) edited a book "Kinetics of Geochemical Processes" as volume 8 of the *Reviews in Mineralogy* (later becoming *Reviews in Mineralogy and Geochemistry*) series. Zhang and Cherniak (2010) edited "*Diffusion in Minerals and Melts*" as volume 72 of *Reviews of Mineralogy and Geochemistry* series, in which one chapter focused on diffusion theory, five chapters on diffusion in silicate melts (Behrens 2010; Lesher 2010; Liang 2010; Zhang and Ni 2010; Zhang et al. 2010), and other chapters were on experimental, analytical, and computational methods, and diffusion in minerals. Several textbooks covered the principles and applications of diffusion theories (Kirkaldy and Young 1987; Shewmon 1989; Cussler 1997; Lasaga 1998; Zhang 2008; Vrentas and Vrentas 2016), and two classic books covered the mathematics of diffusion (Carslaw and Jaeger 1959; Crank 1975). In preparing for this review chapter, we thought carefully about what to cover for this vast field, and decided to briefly go through the fundamentals of diffusion (more complete review can be found in Chakraborty 1995; Zhang 2008, 2010) and solutions to often-encountered

diffusion problems, and then focus on post-2010 diffusion studies on silicate melts and magmas. Here, melts refer to (mostly natural) silicate liquid, and magmas refer to crystal-bearing and/or bubble-bearing melts in which the continuous phase is the melt. There is a large body of work on diffusion in glasses, especially in the materials science literature, which is not covered in this review.

FUNDAMENTALS OF DIFFUSION

Fick's laws

In a compositionally homogeneous phase, diffusion (thermally activated random motion of atoms) would not result in measurable changes in the phase unless the phase is thermodynamically unstable. When there are concentration differences in the phase, diffusion tends to erase these differences and homogenize the composition. The rate at which diffusion proceeds to homogenize a phase is characterized by two Fick's laws. By analogy to Fourier's law that describes the heat flux to be proportional to the temperature gradient, the first Fick's law describes diffusive flux to be proportional to the concentration gradient. In one-dimensional space, it takes the following form:

$$\mathbf{J} = -D\frac{\partial C}{\partial x}, \tag{1}$$

where **J** is diffusive flux along x direction, D is the diffusion coefficient (or diffusivity) in m^2/s, C is concentration in kg/m^3 or mol/m^3, and $\partial C/\partial x$ is the concentration gradient along x. Symbols are summarized in Table 1. In three dimensions, Fick's first law takes the following form:

$$\mathbf{J} = -D\nabla C, \tag{2}$$

where ∇C is the concentration gradient. Melts and magmas considered in this chapter are isotropic media, and hence D does not depend on directions. Therefore, D is a scalar in this chapter (in minerals, D is in general a second-order tensor; Zhang 2010). Values of D in silicate melts are typically of the order 10^{-12} m^2/s, and hence $\mu m^2/s$ ($=10^{-12}$ m^2/s) is used as the unit of D in this chapter, where it is convenient.

Fick's first law describes the mass flux due to diffusion, and cannot be directly used to calculate how concentrations in a phase would change with time. By incorporating mass conservation into Fick's first law, it is possible to derive Fick's second law. In one-dimensional diffusion, Fick's second law takes the following form:

$$\frac{\partial C}{\partial t} = \frac{\partial}{\partial x}(D\frac{\partial C}{\partial x}). \tag{3a}$$

If D is independent of concentration and distance, the above equation becomes:

$$\frac{\partial C}{\partial t} = D\frac{\partial^2 C}{\partial x^2}. \tag{3b}$$

In three dimensions, Fick's second law takes the following form:

$$\frac{\partial C}{\partial t} = \nabla(D\nabla C) \approx D\nabla^2 C. \tag{4}$$

Equations (3) and (4) are often referred to as the diffusion equation. Given initial and boundary conditions, Equation (3) or (4) can be solved to determine changes of the concentration in space and time (Carslaw and Jaeger 1959; Crank 1975). Note that even though C in Equations (1) and (2) are in the unit of kg/m^3 or mol/m^3, C in Equations (3) and (4) can also be in other units such as mass fraction, or mass ppm as long as the mass density is roughly constant, or mole fraction if the molar density is roughly constant. To avoid confusion, w rather than C will be used when mass fraction of mass ppm is used as concentration (Table 1).

Table 1. Symbols

A: diagonal matrix in multicomponent diffusion solutions
a: radius, also a parameter for SiO_2 or H_2O_m diffusivity
$C_{i,j}$: concentration (in kg/m^3 or mol/m^3) of component i in phase j
C_{ave}: weighted average concentration in a multi-phase system; $C_{i,ave} = \phi_1 C_{i,1} + \phi_2 C_{i,2} + ...$
D: diffusivity, a scalar in melts, glasses, and magmas containing random crystals
D_0: pre-exponential factor for diffusion in the Arrhenius relation
$D_{w=0}$: diffusivity of a component when its own concentration approaches zero
D_H: diffusivity of the heavy isotope
D_L: diffusivity of the light isotope
$D_{i,j}$: diffusivity of component i in phase j
D_{bulk}: bulk diffusivity in a multiphase media, defined by $\mathbf{J}_{i,bulk} = -D_{i,bulk} \nabla C_{i,ave}$
D_{eff}: effective diffusivity in crystal-bearing and/or bubble-bearing magmas
D: diffusivity matrix
E: activation energy for diffusion in the Arrhenius relation
J: diffusion flux (a vector)
K: partition coefficient, $K=C_1/C_2 = w_1\rho_1/(w_2\rho_2)$; also equilibrium constant
L: thickness; also dissolution distance
m_H: atomic mass of a heavy isotope
m_L: atomic mass of a light isotope
M_H: molecular mass of a molecule containing the heavy isotope
M_L: molecular mass of a molecule containing the light isotope
$M_{i,j}$: diffusion mobility coefficient of component i in phase j (in ideal systems, $M_{i,j} = D_{i,j}C_{i,j}$)
N: number of components in a system
n: used in multicomponent diffusion in which $n = N–1$
P: pressure
P: eigenvector matrix
Q: diagonal matrix in multicomponent diffusion solutions
R: universal gas constant (8.31447 J mol^{-1} K^{-1})
r: radial coordinate
T: temperature (in K)
t: time
W_i: atomic mass of component i (in kg/mol)
$w_{i,j}$: mass fraction (concentration) of component i in phase j
X_i: mole fraction of component i in the gas phase, also cation mole fraction of i in a melt
x, y, z: spatial coordinate along x-direction, y-direction and z-direction
x_c: characteristic diffusion distance
α: a dimensionless parameter for calculating dissolution distance L
β: an empirical fit parameter to relate diffusivity of heavy and light isotopes to their masses
ΔM: mass gain or loss
ϕ_j: volume fraction of phase j
$\mathbf{\Lambda}$: diagonal matrix made of eigenvalues
λ_i: the ith eigenvalue
$\mu_{i,j}$: chemical potential (in J/mol) of component i in phase j
ρ_j: density of phase j
σ_j: electric conductivity of phase j.

Various kinds of diffusion and diffusivities

Numerous kinds of diffusion have been defined and discussed in the literature, and the definitions are not always consistent. Below is a summary of the many types of diffusion, often encountered in the geological literature.

Based on geometry, diffusion may be classified as one-dimensional, two-dimensional and three-dimensional diffusion. Based on the types of the diffusing material, there can be isotropic (melts, liquids, glasses and magmas and cubic symmetry minerals) or anisotropic diffusion (diffusion in lower-symmetry minerals). Based on the diffusing component or species, diffusion may be classified as follows:

Self diffusion. Strictly speaking, self diffusion means the diffusion of the exact same species in a homogeneous system, not even with isotopic differences. Such self diffusion can only be computationally studied (e.g., De Koker and Stixrude 2010), but cannot be measured analytically. In practice, measured self diffusivity means diffusion of different isotopes in an otherwise chemically homogeneous system (e.g., Liang et al. 1996a; Richter et al. 1999, 2003; Watkins et al. 2014). Self diffusion of a given isotope at constant temperature and pressure can always be well characterized by a constant diffusivity. Note that different isotopes of the same element diffuse at slightly different rate, leading to isotope fractionation (e.g., Richter et al. 1999, 2003; Watkins et al. 2017) to be discussed in a later section.

Tracer diffusion. In mostly early (1970s and 1980s) experimental studies, a tracer (often a radioactive isotope such as ^{86}Rb, Jambon and Carron 1976) is deposited on the surface of a glass of initially uniform composition. The sample is then heated to high temperature to allow the

tracer to diffuse into the sample. Such diffusion is termed tracer diffusion. Tracer diffusion can often be characterized by a constant diffusivity.

Trace element diffusion without major element concentration gradients. More recently (1990s and forward), trace element diffusion is often investigated using diffusion couple experiments (e.g., Mungall et al. 1999; Behrens and Hahn 2009; Holycross et al. 2016, 2018), with the two sides of the diffusion couple having roughly the same chemical composition except for a trace element or multiple trace elements (at < 1000 ppm level) whose diffusivities are probed. These trace element diffusivities are expected to be similar to radioactive tracer diffusivities. To distinguish from trace element diffusion in the presence of major element concentration gradients, this type of trace element diffusion will be referred to as TED1 (trace element diffusion 1).

Chemical diffusion. This category includes all other kinds of diffusion. Chemical diffusion occurs when there are major concentration gradients (or more precisely chemical potential gradients). If there are only two components in the system, the chemical diffusion is *binary diffusion* (also referred to as *mutual diffusion*). Binary diffusivity usually depends on composition. Diffusion in a system of three or more components is referred to as *multicomponent diffusion*. (If there is only one component, then it is self diffusion and cannot be measured.) To quantify multicomponent diffusion, one single diffusion coefficient is not sufficient. Instead, a *multicomponent diffusion matrix* is necessary, in which the on-diagonal terms characterize the effect of a component on its own diffusion, and the off-diagonal terms characterize the effect of other components on its diffusion. In a multicomponent system, if concentration gradients of only two components exist initially, the diffusion of these two components is referred to as *interdiffusion*. The other components can also show diffusion profiles, which are effects of

multicomponent diffusion. Diffusion of isotopes in a compositionally heterogeneous system is referred to as *isotope diffusion* (it would be self diffusion if chemically homogeneous). For the diffusion of trace elements (at <1000 ppm concentration level) in a multicomponent system with or without major chemical concentration gradients, it is *trace element diffusion*, which is further distinguished as TED1 (in the absence of major chemical concentration gradients) and TED2 (in the presence of major chemical concentration gradients) in this work. TED1 is expected to be similar to tracer diffusion, whereas TED2 displays all the complexity of multicomponent diffusion including nonmonotonic profiles (Zhang et al. 1989). In a binary or multicomponent system, if one component can be present in multiple species and we consider the diffusion of different species, the diffusion of the component is termed *multi-species diffusion*. During multicomponent diffusion, if we consider the diffusion of only one component and treat all other components as one combined "component", then the diffusion is called *effective binary diffusion* (EBD, which may mean either effective binary diffusion, or effective binary diffusivity). EBD has been further classified into first kind and second kind (Zhang et al. 2010). The first kind of effective binary diffusion (*FEBD*) is when all concentration gradients are due to one component, all other components being diluted by the component. FEBD is similar to tracer diffusion or TED1 except the concentration of the diffusing component can be higher in FEBD. The second kind of effective binary diffusion (*SEBD*) includes all other situations. In this work, we reclassify EBD into principally one-concentration-gradient diffusion (POCGD, same as FEBD), interdiffusion (ID), and other types of EBD (OEBD). EBD treatment can only handle concentration profiles that are monotonic. If a component displays mass motion from low concentration to high concentration leading to a nonmonotonic profile, it is called *uphill diffusion*, which cannot be treated by EBD.

Dependence of *D* on temperature, pressure, and melt composition

The value of D characterizes the diffusion rate. Hence, it is critical to know D under various conditions, and how it varies with other parameters. Based on experimental studies, it is known that D of a component in silicate melts depends strongly on temperature, weakly on pressure, in a complex manner on the melt composition, and sometimes on its own concentration.

The dependence of D on temperature is well characterized by the Arrhenius relation:

$$D = D_0 e^{-E/(RT)}, \tag{5}$$

where R is the universal gas constant (8.31447 J mol^{-1} K^{-1}), T is temperature in K, E is the activation energy (the energy difference between the activated state and normal state), and D_0 is, for lack of a better term, the pre-exponential factor. D_0 is also the hypothetical diffusivity when $T = \infty$. Even though viscosity of melt-glass has often been found to be and successfully modeled as non-Arrhenian (e.g., Hess and Dingwell 1996; Zhang et al. 2003; Hui and Zhang 2007; Giordano et al. 2008), it is difficult to think of a case where D is unambiguously non-Arrhenian.

The dependence of D on pressure is weaker but also more complicated. A relation including both the temperature and pressure dependence is:

$$D = D_0 e^{-(E+P\Delta V)/(RT)}, \tag{6}$$

where P is pressure and ΔV is the activation volume (the volume difference between the activated state and normal state). In this equation, $P\Delta V$ is an energy term and plays a similar role as the activation every E. However, unlike the activation energy, which is always positive for diffusion, ΔV may be either positive (D decreasing with P) or negative (D increasing with P); it may also change signs as pressure varies. For example, Shimizu and Kushiro (1984) showed that oxygen self diffusivity decreases with pressure in diopside melt (positive ΔV) but increases with

pressure in jadeite melt (negative ΔV) at $P \leq 2$ GPa, and Tinker and Lesher (2001) showed that Si and O self diffusivity in dacite melt increases with pressure from 1 to 4 GPa (negative ΔV), and then decreases with further increase of pressure to 5.7 GPa (positive ΔV). Experimental data by Chen and Zhang (2008) show that the effective binary diffusivity of MgO in basalt melt is roughly independent of pressure from 0.5 to 1.4 GPa.

Diffusivity in silicate melts depends on the major oxide composition of the melts. For example, diffusivity of an element in dry basalt melt is higher than in dry rhyolite melt at the same temperature and pressure, except for He, Li and Na (Behrens 2010; Henderson 1985, Zhang et al., 2010). The dependence of D on melt composition is complicated and there is no theoretical formulation. Many authors tried to develop empirical relations. Mungall (2002) made great effort to model tracer diffusivity of many elements in silicate melts as a function of viscosity and compositional parameters such as ionic radius r, Z^2/r (where Z is valence), Al/(Na+K+H), and M/O ratio where M is the total number of divalent and univalent cations, and O is total number of oxygen. Later studies (e.g., Behrens and Hahn 2009; Zhang et al. 2010; Yu et al. 2019) evaluated the empirical model of Mungall (2002) and concluded the model may be used as an order of magnitude estimate for tracer diffusivities but not accurate enough for practical applications. Fanara et al. (2017) provided fits of diffusivities and obtained $D\eta^{0.7} = 10^{-9.98}$ for trivalent cations, $D\eta^{0.59} = 10^{-9.42}$ for divalent cations, and $D\eta^{0.13}/r^3 = 10^{-1.76}$ for univalent cations, where η is viscosity in Pa·s, D is in m^2/s, and r is ionic radius in angstrom. The equation for the univalent cations does not seem to be correct. These equations do not distinguishing diffusivities of different divalent cations (i.e., treating diffusivities of Mg, Ca, Sr and Ba to be the same) or different trivalent cations (treating diffusivities of REE, Al, Cr^{3+} and Ga^{3+} to be the same), and hence, they at the best would provide an order of magnitude estimate

of diffusivities. In addition to these general models, other authors have examined how diffusivity of a given component in a specific system depends on composition using simple and empirical composition parameters, often in the form of ln*D* being linear to some concentration (mass fraction or mole fraction), such as H_2O (Behrens and Zhang 2001), or SiO_2 (Watson 1982; Lesher and Walker 1986; Koyaguchi 1989; Macris et al. 2018), or Si+Al (Zhang et al. 2010; Zhang and Xu 2016; Yu et al. 2019), or ASI = Al/(Na+K+2Ca+2Mg) (Behrens 2010). Occasionally, a linear dependence of ln*D* on the square root of H_2O concentration seems to fit data best (e.g., Zhang et al. 2010, REE diffusion). Nonetheless, the compositional dependence of diffusivity is still not well quantified due to the large number of components that may affect a given diffusivity in natural silicate melts.

The diffusivity of some components in silicate melts may depend on its own concentration, such as SiO_2 (e.g., Watson 1982; Koyaguchi 1989; Macris et al. 2018), and H_2O (Shaw 1974; Zhang et al. 1991a; Zhang and Behrens 2000; Ni and Zhang 2008, 2018). In the former case, SiO_2 is a major component and controls the melt structure (e.g., degree of polymerization). Hence, the dependence of SiO_2 diffusivity on its own concentration is not surprising, and in fact, Yu et al. (2019) showed that it is Si+Al rather than Si that controls Si diffusion. Hence, the dependence on its own concentration in this case is related to the compositional or structural effect. In the latter case, H_2O diffusivity depends on H_2O concentration due to two factors. One is that H_2O dissolves in silicate melts as two species: molecular H_2O (H_2O_m) and hydroxyl (OH) (Stolper 1982a,b). H_2O_m diffuses more rapidly than OH (Doremus 1969; Zhang et al. 1991a; Ni and Zhang, 2018), and the proportion of H_2O_m in total H_2O (H_2O_t) increases as H_2O_t concentration increases (Stolper 1982a,b). This leads to a rough linearity between H_2O_t diffusivity and H_2O_t concentration at low H_2O_t concentrations (< 2 wt%). The second factor is

that $\ln D_{H_2O_m}$ (as well as $\ln D$ of many other elements) increases linearly with H_2O_t leading to faster than linear increase between $D_{H_2O_t}$ and H_2O_t (Zhang and Behrens 2000; Ni and Zhang 2008, 2018). Hence, part of the dependence of H_2O diffusivity on its own concentration is due to the speciation of H_2O, and part of it is due to compositional dependence. The diffusion of SiO_2 and H_2O will be discussed further in this chapter.

The relation between self or tracer diffusivity and viscosity has been examined extensively and many famous equations (such as the Stokes-Einstein equation, Einstein 1905, and the Eyring equation, Eyring 1936) of inverse proportionality between diffusivity and viscosity have been developed. Some authors have taken these equations for granted. However, these equations cannot be applied to the diffusion of most components. For example, self and tracer diffusivities may either increase with melt viscosity (for He, Li, and Na; Behrens 2010; Henderson et al. 1985; Zhang et al. 2010), or decrease with melt viscosity (for most other elements). Even when self or tracer diffusivity decreases with viscosity, the Stokes-Einstein equation and the Eyring equation often do not work well (Zhang and Ni 2010; Zhang et al. 2010; Ni et al. 2015). For example, for O diffusion in hydrous silicate melts, the error by either of these equations may be many orders of magnitude (Zhang and Ni 2010). The best applications seem to be the Eyring equation for Si or O self diffusivity in anhydrous silicate melts to within a factor of 3 (e.g., Shimizu and Kushiro 1984; Reid et al. 2001; Tinker et al. 2004). Dingwell (1990) and Fanara et al. (2017) discussed the relations between diffusivity of different ions and viscosity. As discussed earlier, Mungall (2002) and Fanara et al. (2017) made effort to quantify relations between diffusivity of different groups of elements and viscosity. We will not examine diffusivity-viscosity relations further.

SOME USEFUL SOLUTIONS TO THE DIFFUSION EQUATION AND EXPERIMENTAL DESIGNS FOR OBTAINING DIFFUSIVITY

Analytical solutions for some often encountered and relatively simple diffusion problems (Fig. 1) are provided in this section without derivations. Readers interested in the associated derivations are referred to textbooks such as Carslaw and Jaeger (1959), Crank (1975), and Zhang (2008). These solutions are often used in experimental studies of diffusion and can sometimes be applied to treat natural diffusion problems by using approximations and simplifications.

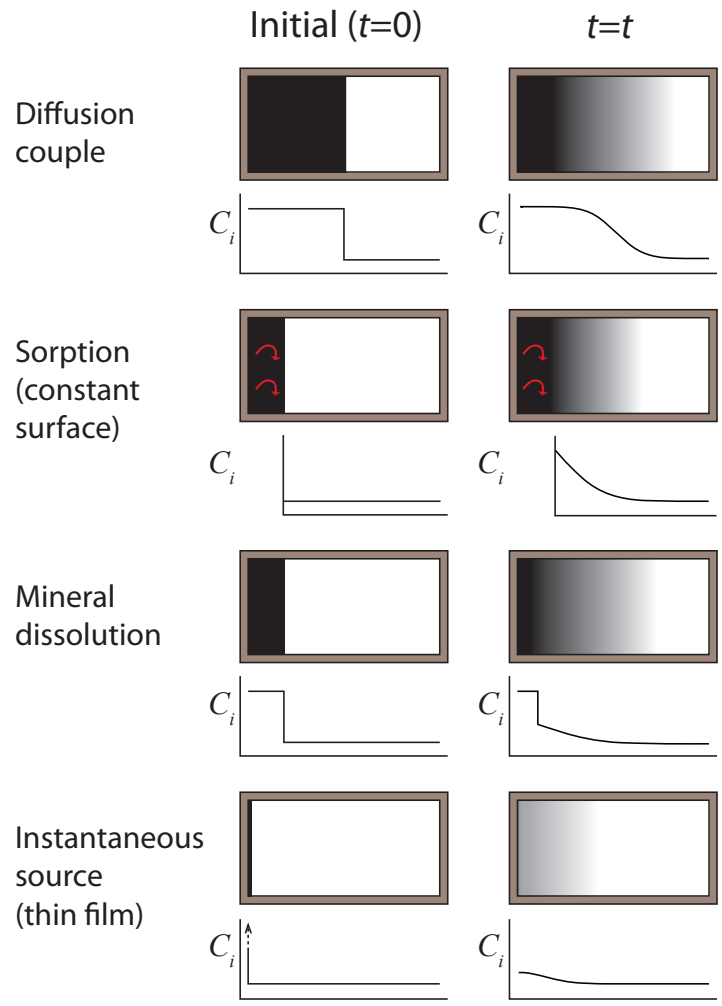

Figure 1. Four diffusion problems that are often encountered in experimental determination of diffusion coefficients and in geological applications. The left-hand side shows the initial configuration and the initial concentration profile, and the right-hand side shows the effect of diffusion on the distribution of the diffusant and the concentration profile. For the case of diffusion couple setup, the black part means the initial high concentration at $x < 0$ (where x=0 is the interface). For the case of sorption, the black part means the ambient convecting and uniform gas phase. For the case of mineral dissolution, the black part means the dissolving mineral. For the case of instantaneous source, the initial concentration at the surface (an infinitesimally thin film) is very high as indicated by the arrow. Modified after Watson and Dohmen (2010).

Diffusion couples

When two melts of different compositions (each melt is uniform in composition) are brought into contact in the laboratory or in nature, the diffusion problem is referred to as a diffusion couple (Fig. 1). Define the contact plane to be $x = 0$. Then, one side is at $x < 0$, and the other side is at $x > 0$. Consider the situation when the diffusion distance is small compared to the thickness of the two melts (i.e., diffusion from the interface has not reached the far ends). For self diffusion, binary diffusion with a constant diffusivity, trace or minor element diffusion in a roughly uniform major oxide composition, or for a component in a multicomponent system that can be characterized by a constant effective binary diffusivity, the analytical solution is (Carslaw and Jaeger 1959; Crank 1975):

$$w = \frac{w_A + w_B}{2} + \frac{w_B - w_A}{2} \operatorname{erf} \frac{x}{\sqrt{4Dt}}, \tag{7}$$

where w_A and w_B are the initial mass fraction of the component in melt at $x < 0$ and at $x > 0$, w is the mass fraction of the component at any x and any $t > 0$, and erf is the error function (Carslaw and Jaeger 1959; Crank 1975; Zhang 2008). Equation (7) shows that at a given time t, the diffusion profile (meaning w versus x) is an error function. The diffusion profiles for diffusion couples at $t = 0$ and $t = t$ are shown in Fig. 1. As t increases, the length of the diffusion profile increases. An example of actual experimental data and fit of the data by Equation (7) is shown in Fig. 2.

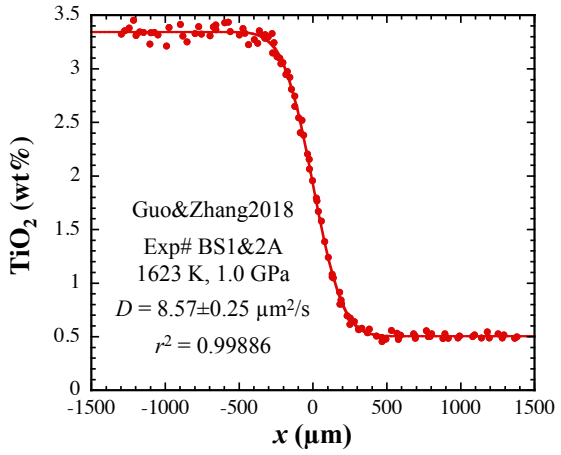

Figure 2. TiO_2 diffusion profile from a multicomponent diffusion couple experiment. It is treated as effective binary diffusion with a constant diffusivity. Points are measured data. The flat regions on each side show that diffusion has not reached the far ends. The solid curve is a nonlinear least-squares fit using Equation (7). The fit is excellent, and provides the effective binary diffusivity. From Guo and Zhang (2018).

Sorption or desorption

A gas component may dissolve into or exsolve from a melt or glass that may contain some uniform initial concentration of the component w_{initial}. Often the surface concentration of the gas component is fixed by the external gas pressure to be w_{surface} (Sorption in Fig. 1). Define the position of the surface to be $x = 0$. If the diffusivity is constant and diffusion has not reached the far end (if sorption from two parallel surfaces, then diffusion has not reached the center) of the melt or glass, the analytical solution is:

$$w = w_{\text{surface}} + (w_{\text{initial}} - w_{\text{surface}})\text{erf}\frac{x}{\sqrt{4Dt}}. \tag{8}$$

If the surface concentration is zero (desorption into vacuum), the above equation becomes:

$$w = w_{\text{initial}}\text{erf}\frac{x}{\sqrt{4Dt}}. \tag{8a}$$

If the initial concentration is zero (sorption), then Equation (8) becomes:

$$w = w_{\text{surface}}\left(1 - \text{erf}\frac{x}{\sqrt{4Dt}}\right) = w_{\text{surface}}\text{erfc}\frac{x}{\sqrt{4Dt}}. \tag{8b}$$

These equations are often used to fit diffusion profiles resulting from sorption or desorption. An example of experimentally generated concentration data with a fit using Equation (8) is shown in Fig. 3. In addition to gas diffusion, isotope diffusion is sometimes accomplished by using an

isotopically enriched gas to maintain a constant isotope ratio at the mineral or glass surface and allowing the isotope to diffuse into the solid (e.g., Williams 1965; Ryerson et al. 1989).

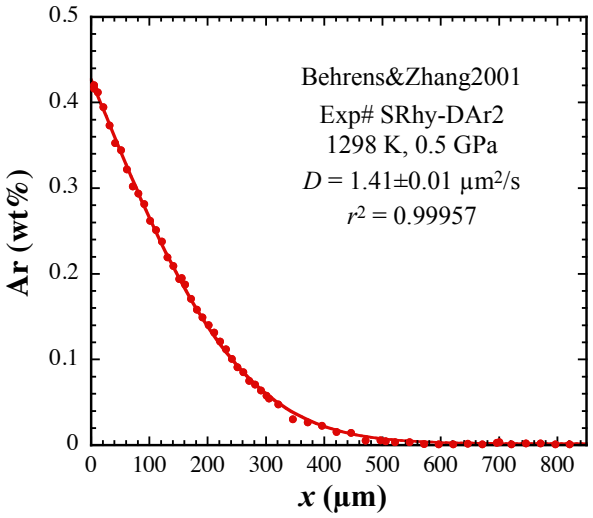

Figure 3. Experimental Ar diffusion profile from an Ar sorption experiment. Points are measured data. The solid curve is a nonlinear least-squares fit using Equation (8). The fit is excellent, and provides the effective binary diffusivity (POCGD). From Behrens and Zhang (2001).

In sorption or desorption experiments, sometimes the concentration profile at a given time is not measured due to, e.g., analytical difficulty, but the mass gain or loss of the sample is measured as a function of time. Consider a sample that is a thin plate with uniform thickness L with sorption or desorption from both surfaces. Define ΔM_t and ΔM_∞ to be the amount of the gas component entering (or exiting) the plate at time t and time ∞. When $\Delta M_t/\Delta M_\infty \leq 0.6$, the mass gain or loss can be described by the following equation:

$$\frac{\Delta M_t}{\Delta M_\infty} = \frac{4\sqrt{D}}{L\sqrt{\pi}}\sqrt{t}\,. \tag{9}$$

By plotting $\Delta M_t/\Delta M_\infty$ versus $\sqrt{t}$, one would get a straight line passing through the origin (0,0). Fitting the straight line by a proportionality equation, D can be calculated from the slope.

Diffusion in melts during diffusive mineral dissolution

One method to experimentally investigate diffusion in melts is to use crystal dissolution to provide a source for some component (e.g., Harrison and Watson 1983). Often, interface equilibrium between the dissolving crystal and the melt is rapidly reached (Zhang et al. 1989; Zhang 2008; Chen and Zhang 2008; Yu et al. 2016), meaning that the interface melt composition is fixed, and the dissolving mineral recedes (Mineral dissolution in Fig. 1). Consider the case when convection in the melt can be ignored (e.g., the mineral does not sink in the melt). Assume that the diffusion of a component can be described as by a constant effective binary diffusivity. If the dissolution thickness of the crystal is negligible compared to the diffusion distance, and diffusion has not reached the far end, then the analytical solution for one-dimensional diffusion would be similar to that of the sorption problem Equation (8). If the dissolution thickness is not negligible, the analytical solution for one-dimensional diffusive dissolution is as follows:

$$w = w_{\text{initial}} + (w_{\text{interface}} - w_{\text{initial}}) \frac{\operatorname{erfc} \frac{(x-L)}{\sqrt{4Dt}}}{\operatorname{erfc} \frac{(-L)}{\sqrt{4Dt}}}, \tag{10}$$

where w_{initial} and $w_{\text{interface}}$ are the initial and interface concentrations in the melt, and L is the growth thickness of the melt, which is related to the dissolution thickness of the crystal (L_c) by $L = L_c(\rho_{\text{crystal}}/\rho_{\text{melt}})$, and can be calculated as follows:

$$L = \alpha\sqrt{4Dt}\,, \tag{10a}$$

with α solved from:

$$\frac{(w_{\text{interface}} - w_{\text{initial}})}{(w_{\text{crystal}} - w_{\text{interface}})} = \sqrt{\pi}\alpha e^{\alpha^2} \operatorname{erfc}(-\alpha), \tag{10b}$$

where w_{crystal} is the concentration in the crystal. An example of experimental data and a fit to the data is shown in Fig. 4.

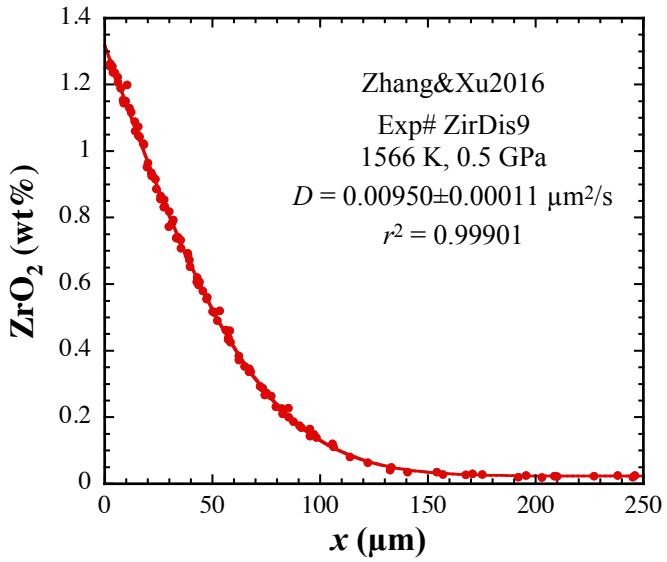

Figure 4. Experimental ZrO_2 diffusion profile from a zircon dissolution experiment. Points are measured data. The solid curve is a nonlinear least-squares fit using Equation (10) in which the melt growth thickness L = 0.9 μm as obtained from experimental data. The fit is excellent, and provides the effective binary diffusivity (POCGD) of Zr. From Zhang and Xu (2016).

Thin-source diffusion

In this method, a fixed (and often undefined) amount of substance (often a radioactive tracer) is deposited on the surface as a thin layer with uniform thickness. Tracer diffusivity is typically constant. If the thin layer (the location is defined as $x = 0$) is sandwiched between two cylinders, then diffusion goes to both directions. Before diffusion reaches the far end, the analytical solution is:

$$C = \frac{M_0}{\sqrt{4\pi Dt}} \mathrm{e}^{-x^2/(4Dt)}, \tag{11}$$

where C is concentration in kg/m^3 or mol/m^3, and M_0 is deposited mass per unit area (kg/m^2 or mol/m^2). Often M_0 is not known, and the concentration profile is measured at a given time. Hence, the concentration profile would be fit in the following form:

$$C = C_0 \mathrm{e}^{-x^2/(4Dt)}, \tag{11a}$$

where C_0 is concentration at $x = 0$.

If the thin layer is on the surface of a cylinder and diffusion goes to one direction only (Instantaneous source in Fig. 1), then, at a given x, the concentration is two times the concentration given by Equation (11):

$$C = \frac{M_0}{\sqrt{\pi Dt}} \mathrm{e}^{-x^2/(4Dt)} = C_0 \mathrm{e}^{-x^2/(4Dt)}. \tag{12}$$

Measured concentration profiles at a given time t also follows Equation (11a) but C_0 in the case of one-sided diffusion is two times C_0 in the case of two-sided diffusion for a given M_0.

Isotropic diffusion in spheres

Degassing or regassing of a spherical melt or glass belongs to this class of diffusion problems. Melt and glass are isotropic so that D does not vary with diffusion directions. Assume a constant initial concentration (w_{initial}) in the sphere, a constant surface concentration (w_{surface}), and a constant diffusivity D. Then the analytical solution is:

$$\frac{C - C_{\text{surface}}}{C_{\text{surface}} - C_{\text{initial}}} = \frac{2a}{\pi r} \sum_{n=1}^{\infty} \frac{(-1)^n}{n} \sin \frac{n\pi r}{a} \mathrm{e}^{-n^2\pi^2 Dt/a^2}, \tag{13a}$$

where a is the radius of the sphere, and r is the radial coordinate. The concentration at the center (r=0) can be found by

$$\frac{C_{\text{center}} - C_{\text{surface}}}{C_{\text{surface}} - C_{\text{initial}}} = 2\sum_{n=1}^{\infty} (-1)^n \mathrm{e}^{-n^2\pi^2 Dt/a^2}. \tag{13b}$$

The total amount of mass entering or leaving the sphere is:

$$\frac{\Delta M_t}{\Delta M_\infty} = 1 - \frac{6}{\pi^2} \sum_{n=1}^{\infty} \frac{1}{n^2} \mathrm{e}^{-n^2\pi^2 Dt/a^2}, \tag{13c}$$

where ΔM_∞ is the final mass gain or loss as t approaches ∞. In other words, ΔM_∞ is the mass gain or loss at equilibrium, and equals $4\pi a^3(C_{\text{surface}} - C_{\text{initial}})/3$. $\Delta M_t/\Delta M_\infty$ is a measure of how

close the system is to equilibrium. If $\Delta M_t/\Delta M_\infty = 0$, then diffusion is just beginning. If $\Delta M_t/\Delta M_\infty = 1$, it means that equilibrium is reached.

Equations (13a)-(13c) converge rapidly for $Dt/a^2 > 0.1$. For smaller Dt/a^2 values, the following three equations may be used for rapid convergence:

$$\frac{C - C_{\text{initial}}}{C_{\text{initial}} - C_{\text{surface}}} = \frac{a}{r}\sum_{n=0}^{\infty}\left[\text{erfc}\frac{(2n+1)a - r}{\sqrt{4Dt}} - \text{erfc}\frac{(2n+1)a + r}{\sqrt{4Dt}}\right], \tag{14a}$$

$$\frac{C_{\text{center}} - C_{\text{initial}}}{C_{\text{initial}} - C_{\text{surface}}} = \frac{2a}{\sqrt{\pi Dt}}\sum_{n=0}^{\infty} e^{-(2n+1)^2 a^2/(4Dt)}, \tag{14b}$$

$$\frac{\Delta M_t}{\Delta M_\infty} = \frac{6}{\sqrt{\pi}}\frac{\sqrt{Dt}}{a}\left[1 + 2\sqrt{\pi}\sum_{n=1}^{\infty}\text{ierfc}\frac{na}{\sqrt{Dt}}\right] - 3\frac{Dt}{a^2}, \tag{14c}$$

where ierfc is integrated complementary error function. An example of fitting can be found in Zhang (2008, Fig. 3-30a).

Variable diffusivity along a profile

Solutions presented above are all for constant diffusivity along a diffusion profile, which typically happens when the variation in every major oxide concentration is small (e.g., $\Delta w < 4$ wt%). Sometimes, one-dimensional diffusion profiles deviate clearly from error functions and cannot be fit by constant-D solutions. In such cases, there is often no analytical solution. To fit the data, one may guess a relation between D and the composition (e.g., ln$D$ is linear to concentration, meaning D is an exponential function of the concentration), numerically solve the diffusion problem, and use the numerical solution to fit the experimental diffusion profile (Zhang et al. 1991a; Zhang and Behrens 2000; Yang et al. 2016; Macris et al. 2018; Yu et al. 2019). For example, Fig. 5 shows an SiO_2 diffusion profile during quartz dissolution. Total SiO_2 concentration variation is very large, 50 wt% to about 90 wt%. The effective binary diffusivity

D_{SiO_2} across the profile is not constant due to such major composition variations. Fitting the concentration profile by a constant D using Equation (10) (blue dashed curve in Fig. 5) does not match the data points well. By assuming that D_{SiO_2} depends exponentially on SiO_2 wt% ($D = D_{w=0}e^{-aw}$, where $D_{w=0}$ and a are two fit parameters and w is wt% of SiO_2), the fit curve (red solid curve) matches the data very well.

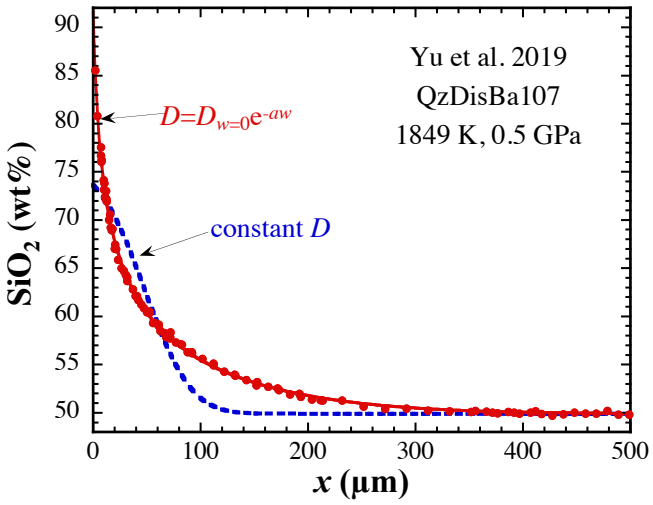

Figure 5. Experimental SiO_2 diffusion profile from a quartz dissolution experiment. Points are measured data. The data indicate very steep slope near the interface ($x = 0$), which descends into a much shallower slope at larger x (e.g., $x = 50$ μm), implying much smaller diffusivity near the interface than in the far-field. The dashed blue curve is a nonlinear least-squares fit using constant D (Eqn. 10) in which $L = 34.9$ μm as obtained from experimental data. The fit does not match the data. The solid red curve is a nonlinear least squares fit by assuming D_{SiO_2} decreases exponentially as SiO_2 concentration increases. The fit is excellent, and verifies the chosen functional dependence of D_{SiO_2}. From Yu et al. (2019).

If one wishes to examine the relation between D and composition without any bias of a presumed functional form, then Boltzmann analysis may be applied to the diffusion couple problem (Matano 1933: Sauer and Freise 1962), sorption problem, or mineral dissolution problem (Watson 1982; Yu et al. 2019). For a diffusion couple experiment, from the concentration profile $w(x)$ at a given time t, one method to obtain D at a given position x_0 or a given concentration w_{x_0} (w_{x_0} is w at $x = x_0$) is the Boltzmann-Matano method (Matano 1933):

$$D_{x=x_0} = \frac{\int_{w_{x_0}}^{w_\infty} x\,\mathrm{d}w}{2t(\mathrm{d}w/\mathrm{d}x)|_{x=x_0}}, \qquad (15)$$

where x is distance from the Matano interface, x_0 is the position at which D is calculated, and t is the experimental duration. In using the above equation, it is necessary to first smooth the concentration profile $w(x)$, and also obtain the Matano interface position so that

$$\int_{w_{-\infty}}^{w_{\infty}} x\,\mathrm{d}w = \int_{0}^{\infty}(w_{\infty}-w)\mathrm{d}x - \int_{-\infty}^{0}(w-w_{-\infty})\mathrm{d}x = 0\,. \tag{16}$$

An alternative Boltzmann method to calculate D at a given position or concentration based on a diffusion couple profile without finding the Matano interface is given by Sauer and Freise (1962):

$$D = \frac{1}{2t(\mathrm{d}y/\mathrm{d}x)|_{x=x_0}}\left[y_{x_0}\int_{x_0}^{\infty}(1-y)\mathrm{d}x + (1-y_{x_0})\int_{-\infty}^{x_0} y\,\mathrm{d}x\right], \tag{17a}$$

where $y = (w–w_{\mathrm{min}})/(w_{\mathrm{max}}–w_{\mathrm{min}})$ so that $y = 0$ at $x = -\infty$ and $y = 1$ at $x = \infty$ (that is, minimum concentration w_{min} is at $x = -\infty$, and maximum concentration w_{max} is at $x = \infty$). If the side of $x > 0$ has lower concentration so that $y = 1$ at $x = -\infty$ and $y = 0$ at $x = \infty$, then the equation becomes:

$$D = \frac{-1}{2t(\mathrm{d}y/\mathrm{d}x)|_{x=x_0}}\left[(1-y_{x_0})\int_{x_0}^{\infty} y\,\mathrm{d}x + y_{x_0}\int_{-\infty}^{x_0}(1-y)\mathrm{d}x\right]. \tag{17b}$$

The advantage of the Sauer and Freise (1962) method is that there is no need to find the Matano interface.

For diffusive mineral dissolution experiments, D at a given position x_0 can be calculated using the following equation (Yu et al. 2019):

$$D = \frac{1}{2t(\mathrm{d}w/\mathrm{d}x)|_{x=x_0}}\left[\int_{w_{x_0}}^{w_{\infty}} x\,\mathrm{d}w + \frac{(w_{\infty}-w_{x_0})}{(w_{\mathrm{c}}-w_{\infty})}\int_{w_0}^{w_{\infty}} x\,\mathrm{d}w\right], \tag{18}$$

where $w_0 = w|_{x=0}$ is the concentration at the interface melt (note that $x = 0$ is the mineral-melt interface, which is directly measured, rather than calculated as the Matano interface), and w_{c} is the concentration of the component in the dissolving crystal.

Diffusion distance and square root of time relation

The analytical solutions (Eqns. 7, 8, 10, and 11) for one-dimensional diffusion typically indicate that concentration depends on $x/(4Dt)^{1/2}$. That is, at a given $x/(4Dt)^{1/2}$, or at $x = 2a(Dt)^{1/2}$ where a is a constant, the concentration is constant regardless any variations in x and t. Hence, diffusion distance is proportional to $\sqrt{Dt}$. At a given D, the diffusion distance is proportional to square root of time. This is referred to as the square root of time relation, or sometimes the parabolic relation. Often a characteristic distance x_c is roughly defined as

$$x_c \approx \sqrt{Dt} \,. \tag{19}$$

To be more precise, Zhang (2008) defined the mid-concentration distance to be the distance from the interface at which the concentration is $0.5(w_{\text{interface}}+w_{\text{farfield}})$. For constant D, the mid-concentration distance x_{mid} for diffusion couple and sorption/desorption can be expressed as (Zhang, 2008):

$$x_{\text{mid}} = 0.953872\sqrt{Dt} \,. \tag{20}$$

Because diffusion distance is proportional to square root of time, diffusion-controlled processes (such as diffusion-controlled crystal growth, crystal dissolution, oxidation, dehydration, etc.) are often said to follow the parabolic law (t is linear to x^2, e.g., Yu et al. 2016). Conversely, if a process follows the parabolic law, the process is often identified to be diffusion controlled.

MULTICOMPONENT DIFFUSION

Natural silicate melts typically contain 5 to 10 major oxides (≥ 1 wt%) plus minor (0.1 to 1.0 wt%) and trace components (<0.1 wt%). Therefore, diffusion in geological melts is always

multicomponent in nature even though usually treated by EBD. The general theory of multicomponent diffusion is well developed. Because the concentration gradient of any one component would affect the diffusive flux of not only itself, but also other components, multicomponent diffusion must be described by a diffusion matrix (De Groot and Mazur 1962; Zhang 2008, 2010; Liang 2010). There are at least two manifestations of multicomponent diffusion compared to binary diffusion. One is uphill diffusion in a stable phase, in which a component diffuses from low concentration to high concentration, resulting in a non-monotonic concentration profile, such as one maximum or minimum during mineral dissolution (Na_2O profile in Fig. 6), or a pair of minimum and maximum in diffusion couples (e.g., see Al_2O_3, FeO, CaO and Na_2O profiles in Fig. 7 later). Applying the effective binary diffusion treatment would fail because the extracted D values would vary from positive to negative, and negative D values are incorrect for stable phases. Another manifestation of multicomponent diffusion is the coordinated motion among many components, resulting in concentration profiles of similar lengths (Fig. 6) for components with widely different self or tracer diffusivities. Coordinated diffusion, with many components showing similar diffusion distances, is often observed when the major concentration gradient is in SiO_2 (Fig. 6). One explanation for coordinated motion of many different components is that a few slowly diffusing major components (such as SiO_2 and Al_2O_3 for aluminosilicate melts) control the chemical potential of other components. The components that diffuse more rapidly redistribute following the chemical potential gradients of the slowly diffusing components, which means more rapidly diffusing components follow the concentration gradients of SiO_2 and Al_2O_3 (Watson 1976, 1982; Zhang 1993), with similar apparent diffusivity. The effect of SiO_2 and Al_2O_3 on the chemical potential and diffusion of other components may be roughly modeled (Zhang 1993). The coordinated motion can still be

treated by the effective binary diffusion method even though the extracted EBD can only be applied to diffusion problems with similar concentration gradients and composition.

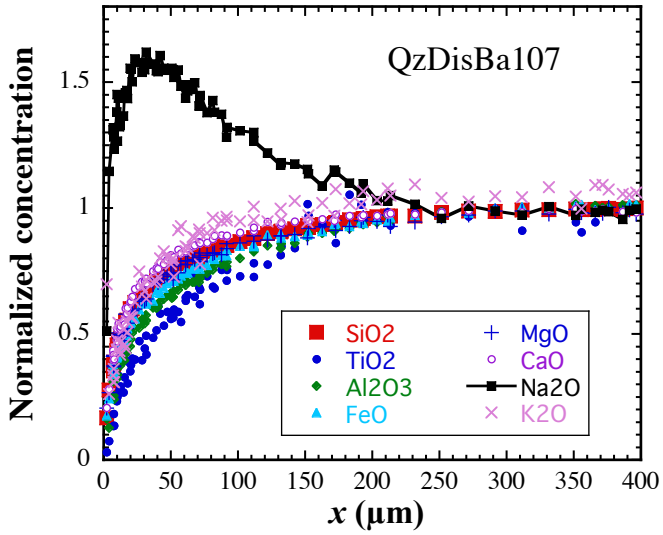

Figure 6. Concentration profiles in the melt during quartz dissolution in basalt (Yu et al. 2019). For easier comparison, the concentration profiles are normalized so that the far-field concentration is 1, and the interface concentration is zero. Na_2O (black solid squares) displays obvious uphill diffusion. All other oxides show similar diffusion distance, even though their tracer diffusivity may differ by orders of magnitude. In terms of profile lengths, Ti > Al > Fe ≥ Si ≈ Mg ≥ Ca > K. This sequence is different from the sequence for tracer diffusivities (see Eqn. 28 later).

Liang (2010) provided a thorough review of multicomponent diffusion work. Because the EBD approach is not disappearing anytime soon, especially for minor and trace elements, here we first briefly review and reclassify the effective binary diffusion approach. We then outline the theory of multicomponent diffusion following De Groot and Mazur (1962) and Zhang (2008). Finally, we discuss recent multicomponent diffusion work since the review by Liang (2010).

Effective binary diffusion

Up to a few years ago, the only practical approach in treating diffusion in natural basalt to rhyolite melts, which are multicomponent in nature, is the effective binary diffusion treatment. Cooper (1968) discussed limitations and applications of the effective binary treatment. Although significant progress has been made and we are beginning to use multicomponent diffusion matrix to treat diffusion in basalt (e.g., Guo and Zhang 2018, 2020), our opinion is that we still have a

long way to go to treat multicomponent diffusion in numerous natural silicate melts using the diffusion matrix approach. Hence, effective binary diffusion treatment is here to stay in the near future (e.g., next 20 years) in dealing with major element diffusion in natural silicate melts. Furthermore, we are very far from using multicomponent diffusion matrix to treat minor and trace element diffusion. For all these reasons, effective binary diffusion still deserves attention. Rigorously speaking, even tracer diffusion is still in the presence of concentration gradients of other components and hence may be regarded as a kind of effective binary diffusion although the main concentration gradient is in one component (the tracer) only.

When using the effective binary approach, the diffusivity is termed effective binary diffusivity (EBD) or effective binary diffusion coefficient (EBDC). In this approach, the diffusant of interest is treated as one component, and all other components are treated as one combined "component". All solutions to the binary diffusion problems (Eqns. 5-20) are applicable to effective binary diffusion. This treatment can only treat monotonic profiles. For example, Figs. 2-5 are all effective binary diffusion profiles. Nonmonotonic profiles, such as Na_2O profile in Fig. 6, and Al_2O_3, FeO, CaO, and Na_2O profiles in Fig. 8 in a later section, cannot be treated using the effective binary approach. There is a modified effective binary diffusion model (Zhang 1993), which can treat nonmonotonic diffusion profiles, but it has not been much applied.

Because effective binary diffusion covers many different scenarios of diffusion, we suggest that when effective binary diffusivities are mentioned, the type of experiments is included, such as EBD of Zr during zircon dissolution, or EBD of SiO_2 during cassiterite dissolution into a rhyolite melt, etc. Zhang (2010) divided effective binary diffusion into two categories: the first type of effective binary diffusion (abbreviated as FEBD) and the second type of effective binary

diffusion (SEBD). In this work, we aim to improve the classification rational, and classify the types of EBD based on how an EBD can be uniquely specified: (i) principally one-concentration-gradient diffusion (POCGD) in multicomponent system, (ii) interdiffusion (ID) in multicomponent system, and (iii) other types of effective binary diffusion (OEBD) in multicomponent system. These are further elucidated below.

POCGD (same as FEBD in Zhang 2010) is the diffusion of a component A into or out of an initially uniform composition (such as sorption, desorption, and thin source diffusion). Other components diffuse mainly in response to the concentration gradient of this component A and their diffusion is typically not considered. POCGD also includes diffusion couples in which the initial concentration gradient is only in a single component A and all other components are the same except for the dilution by component A. When the concentration of the component in POCGD is below 1000 ppm, then it becomes TED1. For example, sorption of Ar into a glass or melt (Carroll 1991; Carroll and Stolper 1991; Behrens and Zhang 2001), hydration or dehydration of a glass or melt or H_2O diffusion couples (Shaw 1974; Zhang et al. 1991a; Zhang and Stolper 1991; Zhang and Behrens 2000; Ni et al. 2013; Ni and Zhang 2018), Zr diffusion in a melt during zircon dissolution into the melt (Harrison and Watson 1983; Zhang and Xu 2016), SiO_2 diffusion in a melt during quartz dissolution into the melt (Watson 1982; Yu et al. 2019), Sn diffusion in a melt during cassiterite dissolution into the melt (Yang et al. 2016), are all examples of POCGD. Diffusivities of POCGD depend only on the bulk composition including the concentration of the diffusing component, but not on other factors (other concentration gradients are all related to the diffusion of the component in consideration). Therefore, when specifying POCGD, one only needs to specify the bulk composition in addition to temperature and pressure. If one is interested in the diffusion of other components (such as Si diffusion in the

melt during cassiterite dissolution in a rhyolite), EBD of these other components would be other types of EBD and depend on the major concentration gradients.

Another type of diffusion in the category of effective binary diffusion that is worth special mention is **interdiffusion (ID)**, in which the initial concentration gradients exist only for two compensating components A and B. Because of the motion of other components, effective binary diffusivity of component A may differ from that of B. Components other than A and B typically cannot be treated by effective binary diffusion due to uphill diffusion. To specify an interdiffusivity, it is necessary to include both the bulk composition and the counter-diffusion component, such as interdiffusivity of SiO_2 during SiO_2-K_2O interdiffusion in a basalt, or that of SiO_2 during SiO_2-Al_2O_3 interdiffusion in a basalt. The interdiffusivity of SiO_2 during SiO_2-K_2O interdiffusion in basalt does not necessarily equal to the interdiffusivity of K_2O during SiO_2-K_2O interdiffusion in basalt, or the interdiffusivity of SiO_2 during SiO_2-Al_2O_3 interdiffusion in basalt. For example, interdiffusivity (effective binary diffusivity) of SiO_2 in a haplobasalt2 at 1773 K and 1.0 GPa is 15.7±1.5 $\mu m^2/s$ for SiO_2-Al_2O_3 interdiffusion, and 103±20 $\mu m^2/s$ for SiO_2-K_2O interdiffusion (Guo and Zhang 2016), a variation by a factor of 6. The interdiffusivity of SiO_2 in basalt11a at 1773 K and 1.0 GPa is 6.6±1.6 $\mu m^2/s$ for SiO_2-TiO_2 interdiffusion, and 88±11 $\mu m^2/s$ for SiO_2-K_2O interdiffusion, a variation by a factor of 13 (Guo and Zhang, 2020). The interdiffusivity of CaO in haplobasalt2 is 60±2 $\mu m^2/s$ for SiO_2-CaO interdiffusion, and 116±7 $\mu m^2/s$ for MgO-CaO interdiffusion (Guo and Zhang 2016).

All other types of effective binary diffusivities are more complicated, and are termed, lacking a better term, other types of effective binary diffusion (**OEBD**). Some examples include: SiO_2 diffusion during cassiterite dissolution into a rhyolite melt, Na_2O diffusion during hydration of a melt, Al_2O_3 diffusion during quartz dissolution, diffusion of all components in a basalt-rhyolite

diffusion couple or during diopside dissolution into a basalt. Because EBD values depend on directions and relative magnitudes of concentration gradients, specification of the experiments may guide users in choosing the most appropriate EBDs. For example, to model olivine growth in a basalt (Newcombe et al. 2014, 2020), the most appropriate MgO EBD (an OEBD) is that during olivine dissolution in a similar basalt, rather than MgO EBD during diopside dissolution, or MgO EBD in a basalt-rhyolite diffusion couple, or Mg tracer diffusivity or self diffusivity. To model diffusion during mixing of two melts, the most appropriate EBDs are those extracted from diffusion couples made of these two melts.

In terms of applicability, POCGD has the widest applicability. It depends only on the bulk composition (in addition to temperature and pressure). Interdiffusivity depends on both the bulk composition and the counter-diffusion component. Once these are specified, then interdiffusivity is also specified. The other EBDs, or OEBDs, have limited applicability: one must specify the bulk composition as well as concentration gradients to apply. The concentration gradients can be specified in a number of ways, such as MORB-rhyolite diffusion couple, diopside dissolution/growth in a basalt, etc.

Multicomponent diffusion theory

Fick's first law (Eqn. 1) describes diffusive flux in a binary system. In an N-component system ($N \geq 3$), because the summation of concentrations of all components must be 100%, there are N-1 independent components. Define the Nth component to be the dependent component, and let $n = N$-1. Because the concentration gradient of any component would contribute to the diffusion of other components, the expanded Fick's law for one-dimensional diffusion takes the

following form (the intricacy of the reference frame is not discussed here; interested readers are referred to Brady 1975; Chakraborty 1995; Zhang 2008):

$$\mathbf{J}_1 = -D_{11}^{[N]}\frac{\partial C_1}{\partial x} - D_{12}^{[N]}\frac{\partial C_2}{\partial x} - \cdots - D_{1n}^{[N]}\frac{\partial C_n}{\partial x},$$

$$\mathbf{J}_2 = -D_{21}^{[N]}\frac{\partial C_1}{\partial x} - D_{22}^{[N]}\frac{\partial C_2}{\partial x} - \cdots - D_{2n}^{[N]}\frac{\partial C_n}{\partial x},$$

.....

$$\mathbf{J}_n = -D_{n1}^{[N]}\frac{\partial C_1}{\partial x} - D_{n2}^{[N]}\frac{\partial C_2}{\partial x} - \cdots - D_{nn}^{[N]}\frac{\partial C_n}{\partial x},$$

where $D_{ii}^{[N]}$ characterizes the diffusive flux of component *i* due to its own concentration gradient $\partial C_i/\partial x$ when the *N*th component is used as the dependent component, and $D_{ij}^{[N]}$ $(i\neq j)$ characterizes the diffusive flux of component *i* due to concentration gradient of another component *j*, $\partial C_j/\partial x$. In other words, $D_{ij}^{[N]}$ $(i\neq j)$ describes the cross effect of concentration gradient of component *j* on the diffusion of component *i*. In matrix notation, the above set of equations can be written as:

$$\begin{pmatrix} \mathbf{J}_1 \\ \mathbf{J}_2 \\ \vdots \\ \mathbf{J}_n \end{pmatrix} = \begin{pmatrix} D_{11}^{[N]} & D_{12}^{[N]} & \cdots & D_{1n}^{[N]} \\ D_{21}^{[N]} & D_{22}^{[N]} & \cdots & D_{2n}^{[N]} \\ \vdots & \vdots & \vdots & \vdots \\ D_{n1}^{[N]} & D_{n2}^{[N]} & \cdots & D_{nn}^{[N]} \end{pmatrix} \begin{pmatrix} \partial C_1/\partial x \\ \partial C_2/\partial x \\ \vdots \\ \partial C_n/\partial x \end{pmatrix} = \mathbf{D}^{[N]}\frac{\partial}{\partial x}\begin{pmatrix} C_1 \\ C_2 \\ \vdots \\ C_n \end{pmatrix}, \qquad (21)$$

where $\mathbf{D}^{[N]}$ is referred to as the diffusion matrix, and the superscript [*N*] means that the *N*th component is taken as the dependent component.

Fick's second law in a multicomponent system takes the following form:

$$\frac{\partial}{\partial t}\begin{pmatrix} C_1 \\ C_2 \\ \vdots \\ C_n \end{pmatrix} = \frac{\partial}{\partial x}\left[\mathbf{D}^{[N]}\frac{\partial}{\partial x}\begin{pmatrix} C_1 \\ C_2 \\ \vdots \\ C_n \end{pmatrix}\right]. \tag{22}$$

If the **D**-matrix is independent of composition and x, then

$$\frac{\partial}{\partial t}\begin{pmatrix} C_1 \\ C_2 \\ \vdots \\ C_n \end{pmatrix} = \mathbf{D}^{[N]}\frac{\partial^2}{\partial x^2}\begin{pmatrix} C_1 \\ C_2 \\ \vdots \\ C_n \end{pmatrix}. \tag{22a}$$

Because melt density is roughly constant, the concentration above may be in either kg/m^3, or mass fraction or wt% (w). If a different component k is used as the dependent component, then the concentration vector would be different, (C_1,..., C_{k-1}, C_{k+1},..., C_N), and the **D** matrix would be different. Methods for obtaining $\mathbf{D}^{[k]}$ from $\mathbf{D}^{[N]}$ can be found in Guo and Zhang (2016).

The above diffusion equation can be solved by the diagonalization of **D** using eigenvalues and eigenvectors:

$$\mathbf{D} = \mathbf{P}\mathbf{\Lambda}\mathbf{P}^{-1}, \tag{23}$$

where $\mathbf{\Lambda}$ is a diagonal matrix with each diagonal element λ_i being the eigenvalues, and **P** is the eigenvector matrix, with column j corresponding to eigenvalue λ_j.

A number of analytical solutions have been obtained for the case of constant multicomponent diffusion matrix. For a diffusion couple, before diffusion reaches the far ends, the solution is (Liang, 2010):

$$\mathbf{w} = \frac{\mathbf{w}_\mathrm{A} + \mathbf{w}_\mathrm{B}}{2} + \mathbf{P}\mathbf{Q}\mathbf{P}^{-1}\frac{\mathbf{w}_\mathrm{B} - \mathbf{w}_\mathrm{A}}{2}, \tag{24}$$

where **w** is a column vector of concentrations, $\mathbf{w}_A$ and $\mathbf{w}_B$ are the initial concentration vectors at $x < 0$ and $x > 0$, **P** is the eigenvector matrix, and **Q** is a diagonal matrix with each diagonal term $Q_{ii} = \mathrm{erf}(x/\sqrt{4\lambda_i t})$ and off-diagonal terms $Q_{ij} = 0$ for $i \neq j$.

For one-dimensional diffusive mineral dissolution, the analytical solution is (Guo and Zhang 2016):

$$\mathbf{w} = \mathbf{w}_{\text{initial}} + \mathbf{PAP}^{-1}(\mathbf{w}_{\text{interface}} - \mathbf{w}_{\text{initial}}), \tag{25}$$

where **P** is the eigenvector matrix, and **A** is a diagonal matrix with $A_{ij} = 0$ if $i \neq j$, and

$$A_{ii} = \frac{\mathrm{erfc}\dfrac{(x-L)}{\sqrt{4\lambda_i t}}}{\mathrm{erfc}\dfrac{(-L)}{\sqrt{4\lambda_i t}}}, \tag{26}$$

where L is the melt growth distance (see Eqn. 10). For a discussion of determining $\mathbf{w}_{\text{interface}}$ and L, please refer to Guo and Zhang (2016).

Varshneya and Cooper (1972) used eigenvectors of diffusion matrices to infer exchange mechanisms and also hinted that the eigenvectors might be independent of temperature in ternary SiO_2-SrO-K_2O melts. Chakraborty et al. (1995b) found that diffusion eigenvectors are insensitive to composition in ternary SiO_2-Al_2O_3-K_2O melts and to temperature, and each eigenvalue depends on temperature following the Arrhenius relation and on melt composition. The constancy of eigenvectors and the Arrhenian behavior of eigenvalues significantly simplify the quantification of multicomponent diffusion. Claireaux et al. (2016, 2019) and Guo and Zhang (2016, 2018, 2020) applied and extended the concepts and approaches to multicomponent diffusion in a quaternary SiO_2-Al_2O_3-CaO-Na_2O melt (NCAS in Table 2), a seven-component haplobasalt (haplobasalt2 in Table 2) and an eight-component basalt (basalt11a in Table 2).

The above summary highlights that the general multicomponent diffusion theory is well developed. The difficulty in applying the theory is in the unavailability of the diffusion matrix. Below we summarize recent efforts to determine the diffusion matrix in aluminosilicate melts.

Recent studies of multicomponent diffusion

There has been major progress in multicomponent diffusion in silicate melts since the review of Liang (2010). Watkins et al. (2014) expanded multicomponent diffusion theory to treat simultaneous isotope diffusion and multicomponent diffusion. Claireaux et al. (2016, 2019) carried out diffusion couple experiments at 1473 to 1633 K to quantify multicomponent diffusion in a quaternary system SiO_2-Al_2O_3-CaO-Na_2O (NCAS). Guo and Zhang (2016) studied multicomponent diffusion in a seven component Fe-free haplobasalt SiO_2-TiO_2- Al_2O_3-MgO-CaO-Na_2O-K_2O (haplobasalt2 in Table 2) at 1773 K. Pablo et al. (2017) examined multicomponent diffusion in a ternary sodium borosilicate melt (average composition 68SiO_2-18B_2O_3-14Na_2O by mol%) at 973-1373 K. Guo and Zhang (2018, 2020) investigated multicomponent diffusion in an eight component basalt (basalt11a in Table 2) at 1533 to 1773 K, which has a similar composition to a MORB from Juan de Fuca Ridge except with increased K_2O to resolve the effect of K_2O. The compositions of these silicate melts except for the borosilicate melts are listed in Table 2, and the results from these studies are summarized below.

Table 2. Nominal composition of melts (wt%) investigated for multicomponent diffusion

Melt	SiO_2	TiO_2	Al_2O_3	FeO	MgO	CaO	Na_2O	K_2O	References
NCAS	64.5		11.4			10.8	13.3		1,2
haplobasalt2	50.0	1.50	15.0		10.0	19.0	3.00	1.50	3
basalt11a	51.0	2.00	14.0	11.5	6.5	10.5	3.00	1.50	4,5

References: 1. Claireaux et al. (2016); 2. Claireaux et al. (2019); 3. Guo and Zhang (2016); 4. Guo and Zhang (2018); 5. Guo and Zhang (2020). Effort is made so that the name of each melt is the same or similar to those in Table 1 of Zhang et al. (2010) for easy cross reference. For example, the composition of basalt11a in this Table is similar to that of basalt11 in Table 1 of Zhang et al. (2010).

Multicomponent diffusion in NCAS quaternary system. Claireaux et al. (2016, 2019) investigated multicomponent diffusion in the quaternary system SiO_2-Al_2O_3-CaO-Na_2O (composition NCAS in Table 2) at 1473, 1553 and 1633 K. They obtained the diffusion matrix at each of the three temperatures, and found that the eigenvectors of the three diffusion matrices are similar, and the eigenvalues depend on temperature following the Arrhenius relation, which are consistent with previous studies of multicomponent diffusion in silicate melts of the following compositions: 68SiO_2-17SrO-21K_2O (Varshneya and Cooper 1972), 40SiO_2-20Al_2O_3-40CaO (Sugawara et al. 1977; Oishi et al. 1982), SiO_2- Al_2O_3-K_2O with ~75 wt% SiO_2 (Chakraborty et al. 1995a,b), SiO_2-$NaAlSi_3O_8$-$KAlSi_3O_8$-H_2O (Mungall et al. 1998), 60SiO_2-15Al_2O_3-25CaO and 45SiO_2-20Al_2O_3-35CaO (Liang and Davis 2002). Table 3 lists the three common eigenvectors using SiO_2 as the dependent component, and the Arrhenius equation for calculating the eigenvalues. The eigenvector corresponding to the smallest eigenvalue (λ_1 in Table 3) is mostly the exchange of Al_2O_3 with CaO plus some SiO_2 (the eigenvector component for the Al_2O_3 component is positive, those for CaO and SiO_2 are negative; and 0.06 for Na_2O is considered to be small and negligible here), that to the middle eigenvalue (λ_2 in Table 3) is mostly the exchange of CaO with SiO_2 plus some Al_2O_3, and that to the greatest eigenvalue (λ_3 in Table 3) is mostly the exchange of Na_2O with CaO plus a little SiO_2. These eigenvectors and associated eigenvalues are consistent with expectation that exchange of higher-valence (or network forming) components is slow and that involving lower-valence components is rapid. To calculate the diffusion matrix at a given temperature, one uses Equation (23), in which $\mathbf{P}$ is the three-component eigenvector matrix in Table 3 (by removing the SiO_2 row) and $\mathbf{\Lambda}$ is a diagonal matrix with diagonal elements being λ_1, λ_2 and λ_3.

Table 3. Eigenvectors and eigenvalues for NCAS melt in Table 2 at 1473-1633 K

Eigenvalues in m^2/s	λ_1 $e^{-9.967-29267/T}$	λ_2 $e^{-6.195-32624/T}$	λ_3 $e^{-13.697-15541/T}$
Eigenvectors	$\mathbf{v}_1$	$\mathbf{v}_2$	$\mathbf{v}_3$
SiO_2	-0.33	-0.67	-0.10
Al_2O_3	0.83	-0.32	-0.01
CaO	-0.56	0.95	-0.65
Na_2O	0.06	0.04	0.76

Data are from Claireaux et al. (2019). Eigenvalues are arranged by increasing size. SiO_2 is the dependent component. All-component eigenvectors are listed for convenience of examining diffusion exchange mechanisms. The SiO_2 component of each eigenvector is calculated to be the negative sum of all the independent components. The all-component eigenvectors are not unitized. The unitized independent three-component eigenvectors (matrix **P** used in Eqns. 23-25) can be obtained by removing the SiO_2 row.

Multicomponent diffusion in haplobasalt2. Guo and Zhang (2016) carried out this study to develop the best strategy for tackling multicomponent diffusion in natural basalt, one of the most common crustal rock types. An Fe-free haplobasalt (haplobasalt2 in Table 2) was chosen. Trial and Spera (1994) suggested that in an *N*-component system, at least *N*–1 "orthogonal" diffusion couples are required to extract the diffusion coefficient matrix. Hence, for this 7-component system, 6 orthogonal diffusion couples are a minimum. Guo and Zhang (2016) designed the experiments as follows. The haplobasalt2 composition in Table 2 is used as the base composition. Each diffusion couple is made of two halves, in which one half deviates from the base composition by +1.5 wt% in component *i* (often SiO_2) and –1.5 wt% in another component *j* ($i \neq j$), so that the total is 100 wt%, and the other half is opposite, containing 1.5 wt% less in component *i*, and 1.5 wt% more in component *j* compared to the base composition. Hence, the number of different glasses with specific compositions that must be prepared is two times the number of diffusion couple experiments. Guo and Zhang (2016) carried out 9 diffusion couple experiments. The first six of them have concentration gradients in SiO_2 and another component, TiO_2, Al_2O_3, MgO, CaO, Na_2O, and K_2O respectively. These six diffusion couples may be

regarded as the necessary 6 "orthogonal" couples. Three additional diffusion couple experiments were carried out, with opposing (or interdiffusing) components of TiO_2-MgO, MgO-CaO, CaO-Na_2O. Furthermore, an anorthite dissolution experiment in the base melt composition was carried out. The diffusion matrix is a 6×6 matrix and has been obtained from the first six diffusion couple experiments (which are deemed a minimum) denoted as $\mathbf{D_1}$ matrix (Guo and Zhang 2016), all nine diffusion couple experiments ($\mathbf{D_2}$ matrix; Guo and Zhang 2016), and combined fitting of nine diffusion couple experiments plus one anorthite dissolution experiments ($\mathbf{D_3}$ matrix; Guo and Zhang 2018). With more experiments, the error on the **D** matrix is reduced slightly. The mean relative error (here the mean relative error on a matrix is defined to be $\sum\sigma_{ij}/\sum|D_{ij}|$, summed over all matrix elements) is 7.3% for $\mathbf{D_1}$, 6.3% for $\mathbf{D_2}$, and 5.7% for $\mathbf{D_3}$ (Guo and Zhang 2016, 2018, note that there are corrections; Guo and Zhang 2019a,b). The relative error decreases fairly slowly as the number of experiments increases. A linear extrapolation suggests that 23 experiments at a given temperature would be needed for this 7-component system to reach a mean relative error of ≤ 1%. Table 4 shows matrix $\mathbf{D_3}$ (based on 9 diffusion couple experiments and one dissolution experiment) as well as associated eigenvalues and eigenvectors. Fig. 7 shows fits to experimental concentration profiles in an experiment (Guo and Zhang 2018).

The diffusion eigenvectors listed in Table 4 are explained as follows. The eigenvector corresponding to the smallest eigenvalue is largely due to Si-Al exchange. That to the second smallest eigenvalue is largely due to Si-Ti exchange (more specifically, exchange of Ti and minor Ca+Mg with Si and minor amount of other components). That to the third smallest eigenvalue is due to divalent cations exchanging with all other components. That to the fourth smallest (also the third largest) eigenvalue is due to Ca exchanging with other components. That

to the second largest eigenvalue is due to Ca+K exchanging with all other components. And the eigenvector corresponding to the largest eigenvalue is due to the exchange of Na with all other components. Note that there is no simple Na-K exchange eigenvector. The exchange mechanisms and associated eigenvalues are also consistent with expectation.

Table 4. Diffusion matrix $D^{[Si]}$ for haplobasalt2 melt at 1773 K

D ($\mu m^2/s$)	TiO_2	Al_2O_3	MgO	CaO	Na_2O	K_2O
TiO_2	18.78±0.32	-0.81±0.23	-4.20±0.47	-11.10±1.16	-27.13±2.85	-15.54±3.27
Al_2O_3	-4.72±0.96	8.96±0.43	-17.40±0.96	-36.01±1.95	-60.32±4.74	-80.65±5.33
MgO	-6.77±1.13	0.22±0.58	39.02±1.23	-39.62±2.38	-82.61±5.54	-45.38±7.01
CaO	-11.20±1.30	-4.56±0.62	-27.62±1.29	64.89±2.58	-31.03±5.49	30.37±7.40
Na_2O	27.40±1.25	11.66±0.64	48.66±1.28	59.90±1.83	341.56±3.92	98.05±6.13
K_2O	5.39±0.50	5.98±0.22	11.67±0.46	15.20±0.93	-0.37±1.88	114.29±2.43
Eigenvalues	λ_1	λ_2	λ_3	λ_4	λ_5	λ_6
in $\mu m^2/s$	13.73±0.26	19.88±0.34	35.59±0.99	80.95±2.26	122.02±3.29	315.33±4.55
Eigenvectors	$\mathbf{v}_1$	$\mathbf{v}_2$	$\mathbf{v}_3$	$\mathbf{v}_4$	$\mathbf{v}_5$	$\mathbf{v}_6$
SiO_2	-0.88	-0.95	-0.45	0.07	-0.15	-0.34
TiO_2	-0.03±0.02	0.90±0.18	-0.15±0.03	-0.06±0.02	-0.05±0.02	-0.08±0.03
Al_2O_3	0.99±0.13	-0.20±0.15	-0.35±0.05	-0.09±0.03	-0.37±0.04	-0.15±0.05
MgO	-0.07±0.02	0.18±0.05	0.69±0.06	-0.57±0.14	-0.27±0.10	-0.26±0.08
CaO	0.07±0.01	0.30±0.03	0.58±0.04	0.80±0.20	0.63±0.15	-0.09±0.03
Na_2O	-0.02±0.003	-0.12±0.01	-0.14±0.01	-0.01±0.01	-0.33±0.03	0.95±0.51
K_2O	-0.06	-0.11	-0.18	-0.14	0.54	-0.03

The composition of the haplobasalt2 melt (Guo and Zhang 2016) is listed in Table 2. Data in the table are mostly from Guo and Zhang (2018) but error estimation of eigenvalues and eigenvectors is from Guo and Zhang (2020). See footnote in Table 3 for all-component eigenvectors (i.e., the calculation of the SiO_2 component in an eigenvector).

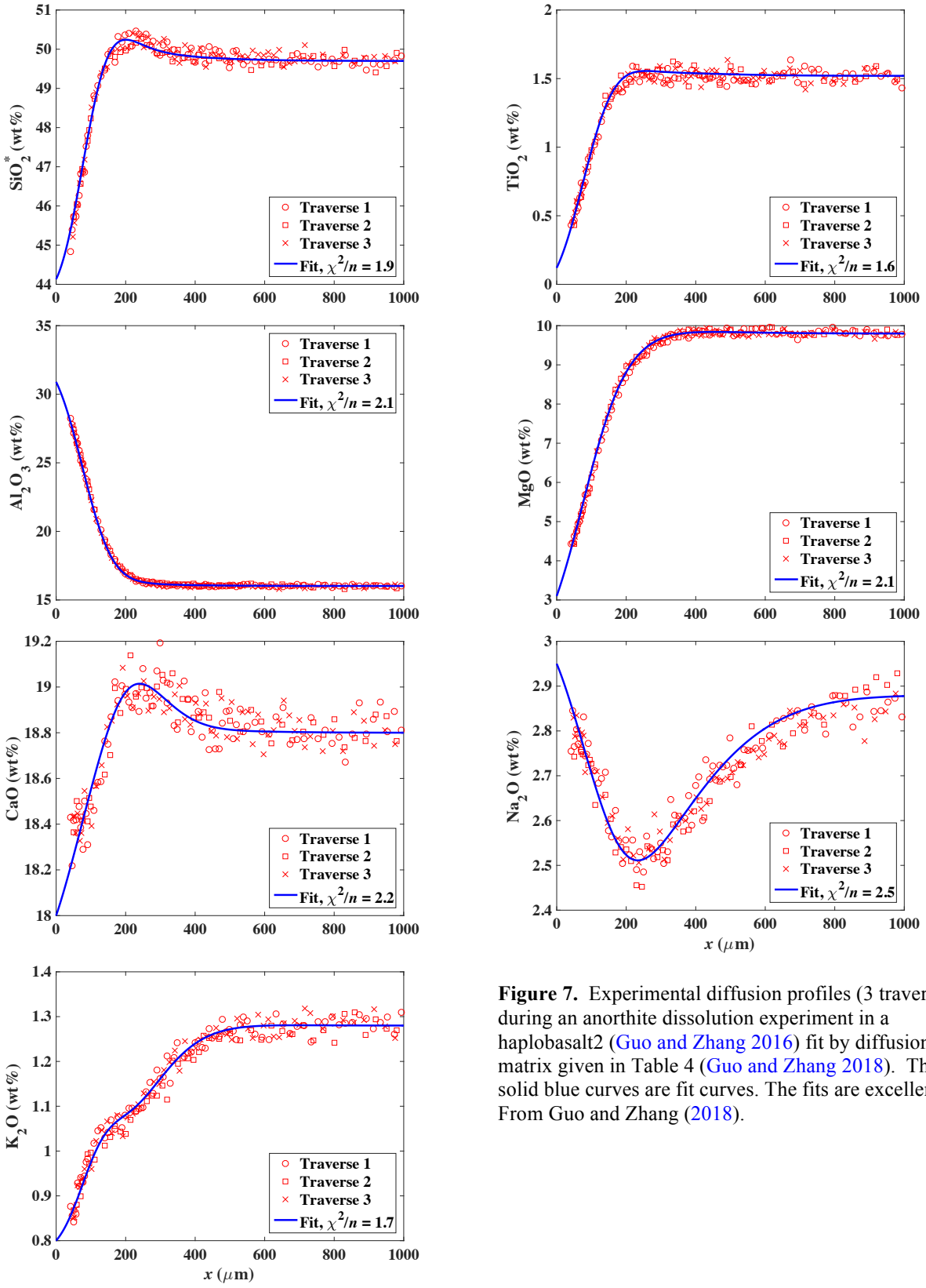

Figure 7. Experimental diffusion profiles (3 traverses) during an anorthite dissolution experiment in a haplobasalt2 (Guo and Zhang 2016) fit by diffusion matrix given in Table 4 (Guo and Zhang 2018). The solid blue curves are fit curves. The fits are excellent. From Guo and Zhang (2018).

Multicomponent diffusion in a basalt. Following the study on haplobasalt2 discussed above, Guo and Zhang (2018) investigated an eight-component FeO-bearing basalt (basalt11a in Table 2) at 1623 K. The experimental strategy is similar to that in Guo and Zhang (2016). All diffusion couples have initial concentration gradients in only two components. That is, they were interdiffusion experiments. Seven diffusion couple experiments were carried out, with initial concentration gradients in SiO_2 and one of the other seven components in turn. Two other experiments are Al_2O_3-CaO and MgO-K_2O interdiffusion couples. Diffusion matrix was obtained from nine diffusion couple experiments ($\mathbf{D_1}$), as well as nine diffusion couple experiments plus results of mineral dissolution experiments from literature ($\mathbf{D_2}$). The latter diffusion matrix, which is best constrained, is shown in Table 5, together with eigenvalues and eigenvectors. The diffusion profiles of all oxides in one of the experiments and the fits of the profiles are shown in Fig. 8. It can be seen that all major features are well fit, including the uphill diffusion profiles. Nonetheless, there are still small misfits, and future improvements are necessary.

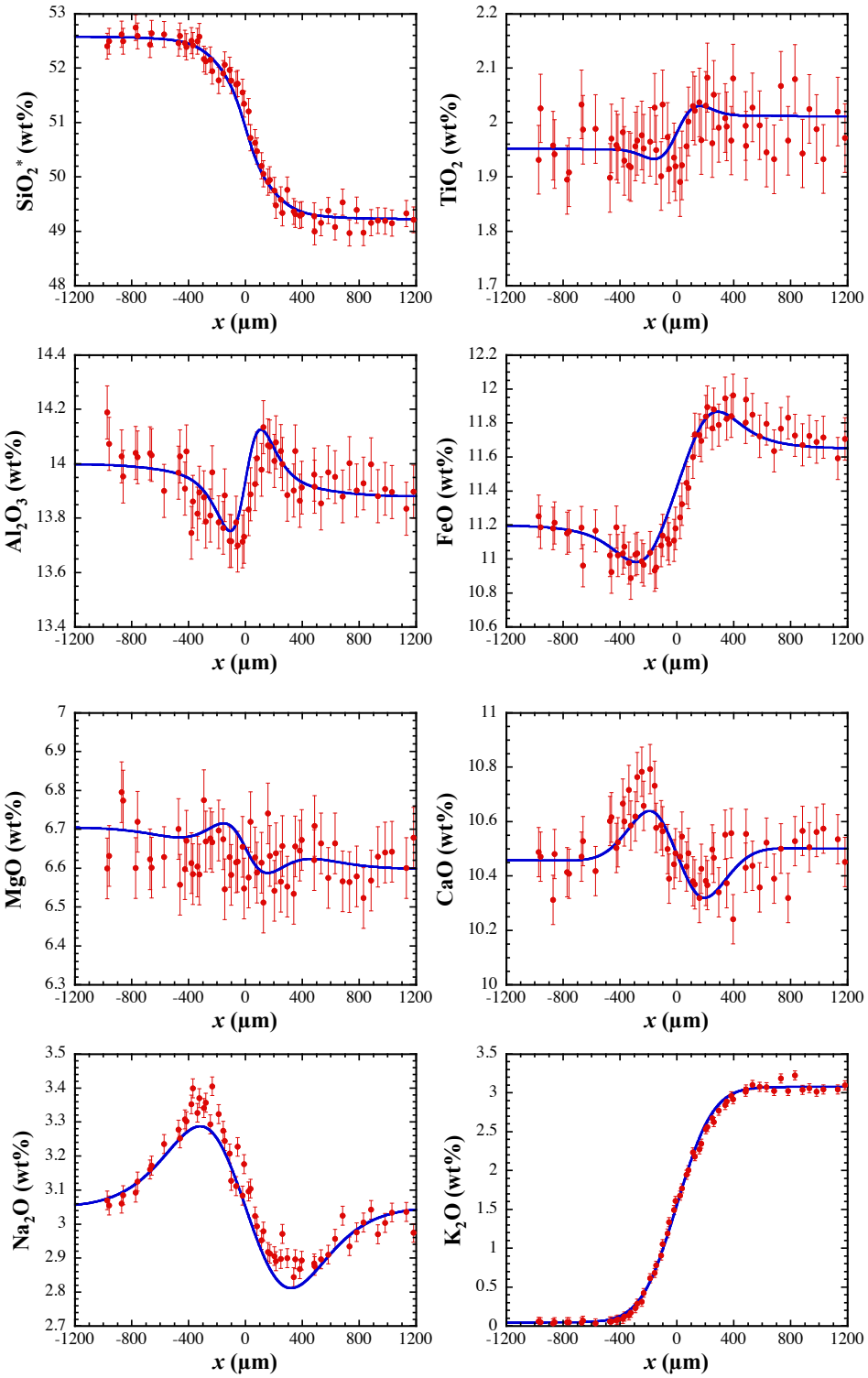

Figure 8. Concentration profiles in a diffusion couple experiment on multicomponent diffusion in a basalt. Solid blue curves are fit curves using [*D*] matrix in Table 5. From Guo and Zhang (2018).

The diffusion eigenvectors listed in Table 5 are explained as follows. The eigenvector corresponding to the smallest eigenvalue is largely due to Si-Al exchange. That to the second smallest eigenvalue is largely due to Si exchange with Al+Ti+Fe. That to the third smallest eigenvalue is due to divalent cations exchanging with all other components. That to the fourth smallest (also the fourth largest) eigenvalue is due to Fe+K exchanging with other components. That to the third largest eigenvalue is due to Fe+Ca exchanging with mostly Mg. That to the second largest eigenvalue is largely due to Ca exchanging with other components. And the eigenvector corresponding to the largest eigenvalue is due to exchange of Na with all other components. These eigenvectors are mostly similar to those in the seven-component haplobasalt2 although the presence of three divalent cations introduces some complexity. Hence, studies of the haplobasalt2 and basalt systems are revealing similar diffusion mechanisms.

Table 5. Diffusion matrix $D^{[Si]}$ for basalt melt at 1623 K

D ($\mu m^2/s$)	TiO_2	Al_2O_3	FeO	MgO	CaO	Na_2O	K_2O
TiO_2	7.81±0.32	-0.25±0.07	-1.53±0.23	-2.02±0.31	-2.76±0.46	-6.43±1.67	-3.17±0.72
Al_2O_3	-0.81±0.70	5.69±0.14	-7.85±0.43	-6.77±0.55	-14.96±0.82	-29.73±2.90	-20.57±1.43
FeO	-21.66±1.30	-3.70±0.27	23.21±0.91	-31.24±1.08	-38.91±1.57	-72.85±5.73	-46.15±2.48
MgO	-5.52±0.73	1.11±0.16	-7.93±0.55	27.21±0.64	-21.46±0.90	-39.21±3.11	-7.33±1.54
CaO	13.58±1.48	-4.62±0.21	-17.94±0.69	-8.93±0.80	37.88±1.16	-38.15±4.14	15.44±1.66
Na_2O	19.68±1.90	10.28±0.29	28.83±0.90	39.57±0.87	57.21±1.31	243.78±4.65	77.02±1.74
K_2O	5.54±0.33	1.42±0.07	3.24±0.19	4.47±0.28	8.47±0.44	21.37±1.51	39.83±0.73
Eigenvalues	λ_1	λ_2	λ_3	λ_4	λ_5	λ_6	λ_7
in $\mu m^2/s$	6.43±0.12	8.18±0.28	14.95±0.27	31.43±0.61	41.68±1.00	58.24±0.77	224.52±4.70
Eigenvectors	$\mathbf{v}_1$	$\mathbf{v}_2$	$\mathbf{v}_3$	$\mathbf{v}_4$	$\mathbf{v}_5$	$\mathbf{v}_6$	$\mathbf{v}_7$
SiO_2	-1.06	-1.44	-0.23	-0.45	0.04	0.05	-0.28
TiO_2	0.04±0.02	0.57±0.06	-0.16±0.03	-0.03±0.01	0.01±0.01	-0.01±.003	-0.02±0.01
Al_2O_3	0.99±0.22	0.75±0.27	-0.64±0.14	-0.25±0.03	0.13±0.02	-0.08±0.01	-0.11±0.01
FeO	0.07±0.01	0.30±0.04	0.55±0.10	0.83±0.09	-0.51±0.09	-0.42±0.05	-0.30±0.03
MgO	-0.04±0.01	0.02±0.03	0.37±0.06	-0.24±0.08	0.75±0.19	-0.30±0.04	-0.16±0.02
CaO	0.10±0.02	-0.01±0.03	0.31±0.05	-0.09±0.04	-0.39±0.10	0.84±0.10	-0.14±0.03
Na_2O	-0.06±0.01	-0.08±0.01	-0.15±0.03	-0.17±0.01	0.06±0.01	-0.15±0.01	0.92±0.12
K_2O	-0.04	-0.11	-0.04	0.39	-0.08	0.06	0.09

The composition of the basalt melt is listed in Table 2. Data are mostly from Guo and Zhang (2018) but error estimation of eigenvalues and eigenvectors is from Guo and Zhang (2020). See footnote in Table 3 for all-component eigenvectors.

Guo and Zhang (2020) continued the study of Guo and Zhang (2018) and examined the temperature dependence of diffusion in basalt11a (Table 2). They reported 18 new diffusion couple experiments, nine each at 1533 K and 1773 K. Diffusion matrices and at the two temperatures were determined from the experimental diffusion profiles. These results were combined with those at 1623 K in Guo and Zhang (2018) to examine the temperature dependence of the diffusion matrix, diffusion eigenvectors and eigenvalues. The hypothesis of constant eigenvectors (Varshneya and Cooper 1972; Chakraborty et al. 1995) is roughly but not rigorously verified: the eigenvectors at three different temperatures show similarity but are not identical within error. In addition, they found that some eigenvalues are nearly identical, and defined the phenomenon as near degeneracy of eigenvalues. In mathematical (strict) degeneracy of eigenvalues, eigenvectors are not uniquely defined because any linear combination of two eigenvectors is another eigenvector. In the case of near degeneracy of eigenvalues, eigenvectors are still uniquely defined but more constraints (e.g., more experimental data or higher quality data) are needed to resolve the eigenvectors. This difficulty to resolve the eigenvectors might explain that the extracted eigenvectors at three different temperatures are not identical within error. The occurrence of near degeneracy means that an increase of only one additional component from haplobasalt2 and basalt11a significantly increases the level of difficulty of obtaining accurate eigenvectors. Guo and Zhang (2020) nonetheless made effort to estimate average eigenvectors based on the data at the three temperatures, and redetermined eigenvalues at each temperature using the average eigenvectors. The eigenvalues are shown in Fig. 9 in an Arrhenius plot. The average eigenvectors and temperature-dependent eigenvalues are listed Table 6. Diffusion matrix in basalt at a given temperature between 1533 and 1773 K can be

estimated using Equation (23), where **P** is the temperature-invariant eigenvector matrix (Table 6) and each λ_i is calculated at the given temperature using expressions in Table 6. Using the formulation, a diffusion matrix was calculated at 1673 K and was used to predict diffusion profiles during mineral dissolution with preliminary success except for the K_2O diffusion profiles (Guo and Zhang 2020). Magma mixing in the Bushveld Complex at 1473 K is also calculated, revealing possible mixing-generated sulfide ore formation (Guo and Zhang 2020).

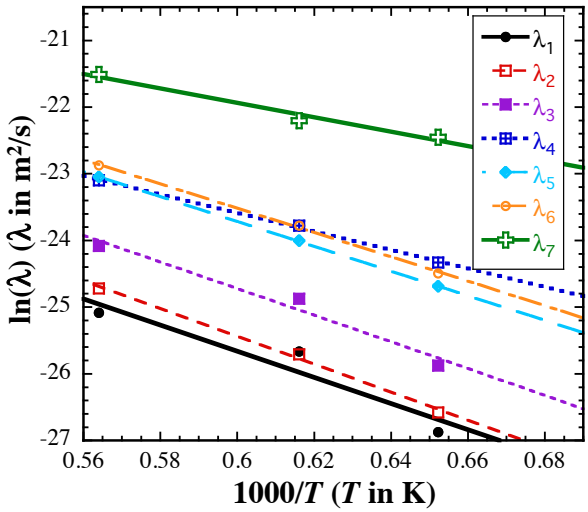

Figure 9. Arrhenius plot of eigenvalues for diffusion in basalt11a. Data are from Guo and Zhang (2020). The lines are least-squares linear fits. The fit equations are provided in Table 6. Eigenvalues λ_1 and λ_2 are nearly degenerate (difference is ≤ 0.4 natural logarithm units). λ_4, λ_5 and λ_6 are triply nearly degenerate. From Guo and Zhang (2020).

Table 6. Temperature dependence of eigenvalues [$\lambda(T)$] and the invariant eigenvector matrix **P** for basalt11a in the temperature range from 1533 to 1773 K

	Eigenvalues (m^2/s)						
	λ_1	λ_2	λ_3	λ_4	λ_5	λ_6	λ_7
	$e^{-13.88-19636/T}$	$e^{-12.89-20912/T}$	$e^{-12.73-19987/T}$	$e^{-15.26-13880T}$	$e^{-12.57-18569/T}$	$e^{-12.55-18279/T}$	$e^{-15.45-10808/T}$
	Invariant eigenvectors						
	v_1	v_2	v_3	v_4	v_5	v_6	v_7
TiO_2	–0.76	–0.20	–0.18	–0.02	–0.02	–0.02	–0.02
Al_2O_3	–0.18	0.97	–0.47	–0.15	–0.01	–0.07	–0.10
FeO	–0.51	0.00	0.66	0.86	0.06	–0.41	–0.36
MgO	–0.17	–0.03	0.41	–0.14	–0.71	–0.32	–0.15
CaO	–0.22	0.12	0.33	–0.33	0.70	0.79	–0.08
Na_2O	0.17	–0.04	–0.18	–0.12	–0.04	–0.19	0.91
K_2O	0.13	–0.02	–0.09	0.32	–0.10	0.25	0.06

Note: T is in K, and λ_i values are in m^2/s. Eigenvectors are for independent components with SiO_2 as the dependent component.

In summary, major progresses have been made in recent years on multicomponent diffusion in silicate melts, including natural basalt. Even in an extensively studied basalt, there is still uncertainty in the eigenvectors and eigenvalues, likely due to additional complexity introduced by near degeneracy of eigenvalues. There are still misfits in reproducing experimental diffusion profiles, especially in mineral dissolution experiments. Future work will need to rigorously test whether eigenvectors in natural silicate melts depend on temperature as well as melt composition. If eigenvectors do not depend on temperature or composition, then we would be well on our way to use multicomponent diffusion matrix to treat major oxide diffusion in natural silicate melts in various magmatic processes.

TRACER AND EFFECTIVE BINARY DIFFUSION DATA

In volume 72 (titled "*Diffusion in Minerals and Melts*") of *Reviews in Mineralogy and Geochemistry* published in 2010, five chapters (Behrens 2010; Lesher 2010; Liang 2010; Zhang and Ni 2010; Zhang et al. 2010) thoroughly reviewed diffusion coefficients in silicate melts, covering noble gases (He, Ne, Ar, Kr, Xe, and Rn, Behrens 2010), H, C, and O (Zhang et al. 2010), plus diffusion data on 59 other elements. For most elements, some diffusion data were available. However, no diffusion data were available for N, As, Bi, Se, I, V, Cu, Mo, In, Tm, Ru, Rh, Pd, Ag, Os, Ir, Pt, Au, and Hg (plus most synthetic elements) in natural or nearly natural silicate melts as of 2010. The order of elements/oxides ranked by tracer diffusivity and POCGD from high to low is roughly as follows in rhyolite melt (Zhang et al. 2010; Behrens et al. 2010; Ni et al. 2017):

$$H_2 > He > Li \approx Na > Cu > K > Ne > Ar \approx CO_2 \approx Cl \approx Rb \approx Sb \approx F > Ba \approx Cs \approx Sr > Ca$$
$$> Mg > Be \approx B \approx Ta \approx Nb \approx Y \approx REE > Zr \approx U \approx Hf \approx Ti \approx Ge \approx Th \approx Si \approx P. \quad (27)$$

Rare earth elements have similar diffusivity, but there is consistently slight decrease of diffusivity from D_{La} to D_{Lu}. H_2O diffusivity is not included in the sequence because it depends strongly on total H_2O concentration (see discussion below). In other melts, the sequence is similar, although there may be small variations. For example, in basalt melt, the updated sequence is roughly (Behrens 2010; Zhang et al. 2010, and new data):

$$\mathrm{He}>\mathrm{Ne}>\mathrm{Li}>\mathrm{Na}\approx Cu>\mathrm{F}\approx\mathrm{Cd}>\mathrm{Cl}\approx\mathrm{Mn}\approx\mathrm{Co}\approx\mathrm{Ca}\approx\mathrm{Sr}>Rb\approx\mathrm{Br}\approx\mathrm{CO_2}\approx\mathrm{Ba}>V\approx$$
$$\mathrm{Tl}\approx\mathrm{Cs}\approx\mathrm{Pb}\approx\mathrm{Y}\approx\mathrm{REE}>Sc>\mathrm{Te}\approx\mathrm{Ti}\approx\mathrm{O}\approx U\approx Nb>Th\approx Zr\approx Ta>Hf>P\geq Si, \quad (28)$$

where the position of Cu, Rb, V, Sc, U, Nb, Th, Zr, Ta, Hf, P and Si are based on new data (Watson et al. 2015; Holycross and Watson 2016, 2018) to be reviewed below. Many empirical fit equations were given in Behrens (2010), Zhang and Ni (2010), and Zhang et al. (2010) for the purpose of estimating elemental diffusivities.

Since the reviews in 2010, new diffusion data and models have been reported for H_2O (Persikov et al. 2010, 2014; Fanara et al. 2013; Ni et al. 2013; Zhang et al. 2017; Ni and Zhang 2018; Kuroda and Tachibana 2019; Newcombe et al. 2019), Li (Holycross et al. 2018), F and Cl (Bohm and Schmidt 2013), Al (Yu et al. 2016), Si (Gonzalez-Garcia et al. 2017; Yu et al. 2019), P (Watson et al. 2015), S (Frischat and Szurman 2011; Lierenfeld et al. 2018), Cl (Yoshimura 2018), Cu (Ni and Zhang 2016; Ni et al. 2017; Ni et al. 2018), Zr (Zhang and Xu 2016), Sn (Yang et al. 2016), Sr and Ba (Fanara et al. 2017), and Mo and W (Zhang et al. 2018). Hence, Cu and Mo no longer belong to the list of elements with no diffusion data. Still, diffusion of 16 nonradioactive elements (N, As, Bi, Se, I, V, In, Tm, Ru, Rh, Pd, Ag, Os, Ir, Pt, Au, and Hg) has not been investigated yet, most of which are chalcophile and siderophile elements. Absence of Tm diffusion data is not expected to be much missed because REE diffusivities are highly

consistent and Tm diffusivity can be predicted from diffusivities of other REE's (see Eqns. 45a-45c later).

In addition, some papers reported diffusion data on a large number of elements. Holycross and Watson (2016) determined trace element diffusivity (close to TED1) of 25 elements (Sc, V, Rb, Sr, Y, Zr, Nb, Ba, La, Ce, Pr, Nd, Sm, Eu, Gd, Tb, Dy, Ho, Er, Yb, Lu, Hf, Ta, Th and U) in nominally dry basalt melt. Holycross and Watson (2018) measured trace element diffusivity (close to TED1) of 21 elements (Sc, V, Y, Zr, Nb, La, Ce, Pr, Nd, Sm, Eu, Gd, Tb, Dy, Ho, Er, Yb, Lu, Hf, Th and U) in hydrous rhyolite melt. Gonzalez-Garcia et al. (2017, 2018) obtained effective binary diffusivities (OEBD) of 19 major and trace elements (Si, Ti, Fe, Mg, Ca, K, Rb, Cs, Sr, Ba, Co, Sn, Eu, Ta, V, Cr, Hf, Th, U; other elements show uphill diffusion) in shoshonite-rhyolite diffusion couples. Posner et al. (2018) evaluated self diffusivity of O, Si, Mg, and Ca, and interdiffusivity of Ni and Co in a peridotite melt at very high pressures of 4- 24 GPa and very high temperatures (≥2150 K). These heroic efforts greatly expanded the diffusion database.

We review below experimental diffusion data since 2010. The following review will not be nearly as systematic as the several chapters in 2010 (Behrens 2010; Lesher 2010; Liang 2010; Zhang and Ni 2010; Zhang et al. 2010), but will focus on new advances on diffusion in natural or nearly natural melts in recent years. In addition, more emphasis will be on TED1 and POCGD because they only depend on the bulk composition and not on concentration gradients. As it will be seen, the Holy Grail of determining the composition dependence of diffusivity is still elusive, and empirical equations accounting for compositional dependence developed in earlier papers often cannot predict later published data in melts with different compositions.

H_2O diffusion

H_2O diffusion is the best example of multi-species diffusion. Due to the importance of H_2O diffusion in volcanic eruption dynamics, exsolution of hydrothermal fluids, bubble growth as well as the importance of H_2O in controlling magma evolution, and due to the complexity of the H_2O diffusion process, H_2O diffusion has been investigated extensively and is probably the best studied diffusion problem in geology literature (e.g., Shaw 1974; Delaney and Karsten 1981; Karsten et al. 1982; Stanton et al. 1985; Wasserburg 1988; Zhang and Stolper 1991; Zhang et al. 1991a, 1991b; Jambon et al. 1992; Nowak and Behrens 1997; Zhang and Behrens 2000; Freda et al. 2003; Behrens et al. 2004, 2007; Liu et al. 2004; Okumura and Nakashima 2004, 2006; Ni and Zhang 2008; Ni et al. 2009a,b; Wang et al. 2009; Persikov et al. 2010, 2014; Zhang and Ni 2010; Fanara et al. 2013; Ni et al. 2013; Zhang et al. 2017, 2019; Ni and Zhang 2018; Kuroda and Tachibana 2019; Newcombe et al. 2019). Because there is major advancement since 2010, below we briefly summarize the earlier developments and then focus on recent progress since the review of Zhang and Ni (2010). The compositions of silicate melts that have been investigated for H_2O diffusion are listed in Table 7.

Dissolved H_2O component in silicate melts is present as at least two species, neutral and free H_2O molecules (referred to as H_2O_m), and charged and bonded hydroxyl groups (referred to as OH) (Stolper 1982a,b). The two species interconvert in the melt structure:

$$H_2O_m \text{ (melt)} + O \text{ (melt)} \rightleftharpoons 2OH \text{ (melt)}, \tag{29}$$

with an equilibrium constant

$$K = [OH]^2/([H_2O_m][O]), \tag{30}$$

where brackets mean mole fractions, increasing with temperature (Zhang et al. 1995, 1997). Due to the above speciation reaction, OH is the dominant species at low total H_2O content (referred to as H_2O_t hereafter; H_2O refers to the component) such as ≤ 1 wt%, and H_2O_m is the dominant

species at high H_2O_t such as ≥ 5 wt%. According to the above reaction, the mole fraction of H_2O_t is expressed as:

$$[H_2O_t] = [H_2O_m] + 0.5[OH]. \quad (31)$$

Table 7. Chemical composition in H_2O diffusion studies in geology literature

Melt	SiO_2 wt%	TiO_2 wt%	Al_2O_3 wt%	FeO wt%	MgO wt%	CaO wt%	Na_2O wt%	K_2O wt%	X_{Si}	W g/mol	Ref.
rhyolite14a	76.6	0.07	13.2	0.64	0.05	0.57	4.15	4.83	0.711	32.52	1-12
CBS-NSL	75.9	0.20	10.2	4.33	0.0	0.09	5.19	4.61	0.704	33.23	13,14
GMR-MAC	72.7	0.16	15.2	1.02	0.16	0.76	4.21	4.01	0.686	32.60	11,13
dacite5	67.5	0.77	15.7	4.28	1.43	4.40	3.58	2.15	0.632	33.49	15
HA2	66.3	0	17.6	0	1.38	2.50	10.45	0	0.592	33.05	12
Ab75Di25	65.8	0	15.1	0	3.17	7.0	8.93	0	0.582	33.53	16
dacite3a	65.4	0.73	15.9	4.44	2.02	4.96	3.88	2.59	0.608	33.84	17-19
andesite7	62.5	0.7	16.7	5.55	2.97	6.48	3.2	1.69	0.583	34.13	12
HA1a	62.3	0	19.8	0.02	2.30	10.2	4.12	1.00	0.570	33.55	20,21
Ab50Di50	62.2	0	10.5	0	6.79	14.2	6.34	0	0.555	34.45	16
trachyte0b	60.5	0.48	17.8	7.14	0.21	1.72	5.22	7.28	0.553	35.25	22
trachyte0a	59.9	0.39	18.0	3.86	0.89	2.92	4.05	8.35	0.555	34.94	23
phonolite1a	58.9	0.76	19.9	3.61	0.69	3.90	5.96	6.87	0.529	35.04	24
andesite1a	57.2	0.84	17.5	7.58	4.27	7.59	3.31	1.60	0.530	34.98	17
haplobasalt3	52.0	1.06	16.3	0.03	11.2	15.3	2.79	0.89	0.465	35.04	24
basalt11	50.6	1.88	13.9	12.5	6.56	11.4	2.64	0.17	0.475	36.59	25
An36Di64	49.6	0.02	17.5	0.03	9.89	23.8	0.07	0.01	0.448	35.55	26
green glass	48.3	0.39	8.17	15.9	17.4	8.98	0	0	0.450	37.16	27
basalt0	46.1	1.50	16.1	10.8	7.60	13.3	3.56	0.76	0.423	37.15	15
LB2a	43.6	3.46	8.96	21.8	13.1	8.74	0.01	0.00	0.419	38.59	26
yellow glass	43.5	3.11	7.86	21.9	13.2	8.24	0.44	0	0.422	38.69	27

Compositions are listed in decreasing SiO_2 order. Similar melt compositions (defined to be ≤ 1.5 wt% difference in every oxide concentrations) are averaged, e.g., rhyolite14a includes many high-silica rhyolites and AOQ(Ab38Or34Qz28). HA: haploandesite. LB, green glass, and yellow glass: lunar basalts. X_{Si} is cation mole fraction of Si on dry basis. W is mass of the melt per mole of oxygen on dry basis (Stolper 1982a,b; Zhang 1999). See footnotes in Table 2 for more explanation of melt names.

References: 1. Shaw 1974; 2. Delaney and Karsten 1981; 3. Karsten et al. 1982; 4. Stanton et al. 1985; 5. Zhang et al. 1991a; 6. Jambon et al. 1992; 7. Nowak and Behrens 1997; 8. Zhang and Behrens 2000; 9. Okumura and Nakashima 2004; 10. Behrens et al. 2007; 11. Ni and Zhang 2008; 12. Persikov et al. 2014; 13. Behrens and Zhang 2009; 14. Wang et al. 2009; 15. Okumura and Nakashima 2006; 16. Persikov et al. 2010; 17. Behrens et al. 2004; 18. Liu et al. 2004; 19. Ni et al. 2009a; 20. Ni et al. 2009b; 21. Ni et al. 2013; 22. Fanara et al. 2013; 23. Freda et al. 2003; 24. Zhang et al. 2017; 25. Zhang and Stolper 1991; 26. Newcombe et al. 2019; 27. Zhang et al. 2019.

On the other hand, the mass fraction of H_2O_t is expressed as:

$$w_{H_2O_t} = w_{H_2O_m} + w_{OH}, \quad (32)$$

where w_{OH} does not mean the actual OH mass fraction, but by convention it means the mass fraction of H_2O that is present in the melt or glass as OH (Stolper 1982a,b; Zhang 1999). The mole fractions are defined on a single oxygen basis as follows:

$$[H_2O_t] = (w_{H_2O_t}/18.015)/\{w_{H_2O_t}/18.015 + (1-w_{H_2O_t})/W\}, \quad (33a)$$

$$[H_2O_m] = [H_2O_t]w_{H_2O_m}/w_{H_2O_t}, \quad (33b)$$

$$[OH] = 2\{[H_2O_t] - [H_2O_m]\}, \quad (33c)$$

$$[O] = 1 - [H_2O_m] - [OH], \quad (33d)$$

where 18.015 is the molecular mass of H_2O in g/mol, and W is the mass of the dry melt per mole of oxygen in g/mol. Values of W for investigated melts are listed in Table 7.

Experimental studies of H_2O diffusion before 1990 (Shaw 1974; Delaney and Karsten 1981; Karsten et al. 1982; Stanton et al. 1985) found that H_2O diffusivity depends strongly on H_2O concentration in addition to the temperature dependence. Zhang et al. (1991a) investigated H_2O diffusion in rhyolite14a containing ≤ 1.7 wt% H_2O_t. Based on measured H_2O_m and OH concentration profiles by FTIR, they considered the contribution of both H_2O_m and OH and treated one-dimensional diffusion of H_2O_t using the following multi-species diffusion equation:

$$\frac{\partial[H_2O_t]}{\partial t} = \frac{\partial}{\partial x}\left(D_{H_2O_m}\frac{\partial[H_2O_m]}{\partial x} + D_{OH}\frac{\partial[OH]/2}{\partial x}\right), \quad (34)$$

where $D_{H_2O_m}$ and D_{OH} are the diffusivity (POCGD) of H_2O_m and OH. Hence, $D_{H_2O_t}$ is related to species diffusivities as follows:

$$D_{H_2O_t} = D_{H_2O_m}\frac{d[H_2O_m]}{d[H_2O_t]} + D_{OH}\left(1 - \frac{d[H_2O_m]}{d[H_2O_t]}\right). \quad (35)$$

The differential in the above equation can be found as (Wang et al. 2009):

$$\frac{d[H_2O_m]}{d[H_2O_t]} = 1 - \frac{(0.5 - X)}{\sqrt{X(1-X)(\frac{4}{K} - 1) + 0.25}}, \quad (36)$$

where $X = [H_2O_t]$. Zhang et al. (1991a) found that in rhyolite melt and glass, $D_{H_2O_m}$ was roughly constant in their samples (0.1 to 1.7 wt% H_2O_t), and D_{OH} is too small (compared to $D_{H_2O_m}$) to be resolved. That is, OH diffusion is negligible and the diffusion of the H_2O component is accomplished by H_2O_m diffusion and interconversion of OH and H_2O_m. Even when H_2O_t is as low as 0.18 wt%, meaning that more than 90% of H_2O_t is present as OH, contribution of OH diffusion to H_2O_t diffusion is still negligible and unresolvable. The speciation-diffusion model leads to a proportionality between $D_{H_2O_t}$ and H_2O_t content at low H_2O_t (e.g., <2 wt%).

Nowak and Behrens (1997) found that $D_{H_2O_t}$ is no longer proportional to H_2O_t when H_2O_t is > 3 wt%. Zhang and Behrens (2000) extended the multi-species H_2O diffusion model in rhyolite to high H_2O_t, and found that H_2O_m diffusivity ($D_{H_2O_m}$) is no longer a constant, but depends on H_2O_t concentration exponentially:

$$D_{H_2O_m} = D_{X=0} e^{aX}, \quad (37)$$

where $X = [H_2O_t]$, a is a constant depending on T, and $D_{X=0}$ is $D_{H_2O_m}$ at zero H_2O_t. D_{OH} was still not resolved from the experimental data. This formulation has been adopted by subsequent studies until 2013 (Okumura and Nakashima 2004, 2006; Behrens et al. 2004, 2007; Liu et al. 2004; Ni and Zhang 2008; Wang et al. 2009; Ni et al. 2009a,b; Persikov et al. 2010a,b; Fanara et al. 2013).

Behrens et al. (2004) hinted at OH contribution to H_2O diffusion in diffusion couple experiments in andesite1a melt at 1608-1848 K. Ni et al. (2013) were the first to resolve the noticeable role of OH diffusion contributing to H_2O_t diffusion in a haploandesite melt (HA1a in Table 7) when H_2O_t is low (< 1 wt%) at 1619-1842 K and 1 GPa. They assumed constant OH

diffusivity and found $D_{OH}/D_{X=0}$ (note that $D_{X=0}$ is $D_{H_2O_m}$ at zero H_2O_t) ranging from 0.09 to 0.24. Zhang et al. (2017) (note that this Zhang is L. Zhang) investigated H_2O diffusion in haplobasalt3 melt containing 0.03-2.02 wt% H_2O_t and quantified both OH and H_2O_m diffusivities, obtaining $D_{OH}/D_{X=0}$ ranging from 0.10 to 0.17. The success in resolving OH diffusivity in haploandesite (Ni et al. 2013) and haplobasalt (Zhang et al. 2017) confirmed the importance of OH diffusion in depolymerized melt at magmatic temperatures and low H_2O_t.

Ni and Zhang (2018) constructed a general model for H_2O diffusivity in calc-alkaline silicate melts and glasses using literature data. The model did not include trachyte (Freda et al. 2003; Fanara et al. 2013), phonolite (Fanara et al. 2013), or peralkaline rhyolite (Behrens et al. 2009; Wang et al. 2009). The model parameterized K, a and $D_{X=0}$, and D_{OH} as a function of the cation mole fraction of Si in dry melt (X_{Si}; values are listed in Table 7), T and P as follows:

$$\ln K = X_{Si}(2.6 - \frac{4339}{T}), \tag{38a}$$

$$a = -94.07 + 74.112X_{Si} + \frac{198508 - 166674X_{Si}}{T}, \tag{38b}$$

$$\ln D_{X=0} = 8.02 - 31X_{Si} + 2.348X_{Si}P + \frac{121824X_{Si} - 118323\sqrt{X_{Si}} - (10016X_{Si} - 3648)P}{T}, \tag{38c}$$

$$\ln \frac{D_{OH}}{D_{X=0}} = -56.09 - 115.93X_{Si} + \sqrt{X_{Si}}(160.54 - \frac{3970}{T}), \tag{38d}$$

where P is in GPa, T is in K, and $D_{X=0}$ and D_{OH} are in m^2/s. Once K, a, $D_{X=0}$ and D_{OH} are calculated from Equations (38a)-(38d), $D_{H_2O_m}$ can be calculated from Equation (37), and then $D_{H_2O_t}$ can be calculated from Equation (35) with the differential from Equation (36). A supplementary excel file is available in Ni and Zhang (2018) for the calculation. Calculations indicate that OH contribution to H_2O diffusion increases with increasing temperature and

decreasing SiO_2 concentration. Ni and Zhang (2018) concluded that in rhyolite and dacite glass and melt, contribution of OH to H_2O diffusion is rarely noticeable, whereas in andesite and basalt melt, contribution of OH to H_2O diffusion becomes important at $T \geq 1200$ K.

The synthesis model of H_2O speciation and diffusion by Ni and Zhang (2018) represents a major step forward. Nonetheless, the model is unlikely to be the last word on H_2O diffusion. In their model, data to constrain OH diffusivity are limited. In addition, the compositional coverage by the model does not include peralkaline rhyolite, or phonolite, or trachyte. Newcombe et al. (2019) investigated H_2O diffusion in An36Di64 melt and lunar mare basalt, and found their data on An36Di64 are in reasonable agreement with the model, but those on lunar mare basalt (lower SiO_2 and Al_2O_3 and much higher FeO) are off the model by a factor of 6. Zhang et al. (2019) determined H_2O_t diffusivity in lunar green glass and yellow glass, and their data are off the model of Ni and Zhang (2018) by a factor of 3 to 8. Future improvement is expected to require more data at low H_2O_t to better resolve OH diffusivity and how it depends on H_2O_t, as well as more compositional coverage (e.g., the role of Al_2O_3, FeO, and alkalis).

Diffusion of alkalis

Zhang et al. (2010) reviewed alkali diffusion data. Li tracer diffusivity does not vary much with composition in dry Ab39Or61, albite, rhyolite, dacite, andesite and basalt melts (Zhang et al. 2010), and Rb tracer diffusivity does not vary much with composition in dry jadeite, albite, rhyolite, haploandesite, trachyte and phonolite. The primary dependence is on temperature. Rb diffusivity increases with H_2O content. Na, K, and Cs tracer diffusivity depends more on melt composition.

Ni (2012) reevaluated existing data on alkali tracer diffusion and developed specific models for each alkali element. The new empirical equation for calculation of D_{Li} is (Ni 2012):

$$\ln D_{\mathrm{Li}} = -13.09 - \frac{9722.7 + 1171.4 f_1 + 4943 f_2}{T}, \tag{39}$$

where

$$f_1 = \frac{\mathrm{K\#}}{\mathrm{K\#} + 0.1(1 - \mathrm{K\#})}, \tag{39a}$$

and

$$f_2 = \frac{\mathrm{Ca\#}}{\mathrm{Ca\#} + 3(1 - \mathrm{Ca\#})}, \tag{39b}$$

where K# = K/(K+Na), Ca# = Ca/(Ca+K+Na), with Na, K and Ca being cation mole fractions. For Na, K, Rb, and Cs, Ni (2012) developed the following empirical equations:

$$\ln D_{\mathrm{Na}} = -13.77 - \frac{8815.8 + 1308.2 f_1 + 15164 f_2}{T}, \tag{40}$$

$$\ln D_{\mathrm{K}} = -14.81 - \frac{11125 + 1277.6 f_3}{T}, \tag{41}$$

$$\ln D_{\mathrm{Rb}} = -15.73 - \frac{11376 + 4022.9 f_3}{T}, \tag{42}$$

$$\ln D_{\mathrm{Cs}} = -11.87 - \frac{5352.8 f_1 + 233.52 F - 30124\,\mathrm{AI}}{T}, \tag{43}$$

where

$$f_3 = \frac{\mathrm{Na\#}}{\mathrm{Na\#} + 0.1(1 - \mathrm{Na\#})} = \frac{1 - \mathrm{K\#}}{1 - 0.9\,\mathrm{K\#}},$$

F = SiO_2+TiO_2+Al_2O_3+P_2O_5 in wt%, and AI is peralkalinity defined to be the greater of (Na+K–Al)/O (where Na, K, Al and O are atomic fractions) and zero.

Holycross et al. (2018) studied Li trace element diffusivity (TED1) in wet rhyolite (6.0 wt% H_2O). The data are not used to evaluate the model of Ni (2012) because the latter does not contain data from hydrous melts. Gonzalez-Garcia et al. (2018) obtained OEBD of Rb in

shoshonite-rhyolite diffusion couple using the Boltzmann-Matano method. These OEBD values are not expected to be similar to tracer diffusivities, and hence are not used to test the model of Ni (2012). Holycross and Watson (2016) reported new Rb trace element diffusion (close to TED1) data in nominally dry basalt melt, which can be used to test Equation (42). The predicted Rb diffusivity using Equation (42) is lower than the experimental data by 0.87 to 1.52 ln$D$ units, which is not too bad. On the other hand, due to the weak dependence of Rb diffusivity on melt composition, if the Rb Arrhenius equation for rhyolite (Eqn. 13 in Zhang et al. 2010) is used to predict Rb diffusivity, the predicted values are lower than experimental data by only 0.51 to 1.16 ln$D$ units, better than the predicted values using Equation (42). Hence, except for its ability to reconcile Rb diffusivity in orthoclase melt, the Rb diffusivity model by Ni (2012) does not improve prediction compared to simply assuming no variation from rhyolite to basalt.

Cu diffusion

The absence of Cu diffusion data in natural silicate melts has been remedied by three recent papers (33 data points). Ni and Zhang (2016) investigated Cu diffusion in basalt1a (composition listed in Table 8) melt using diffusion couples. Ni et al. (2017, 2018) reported Cu diffusion data in various rhyolite melts. The diffusion data in the three papers may all be viewed as POCGD, and they are highly consistent (note that Ni et al. 2017 and Ni et al. 2018 are different authors from different laboratories). Fig. 10 shows all available Cu diffusion data in natural melts (and comparison with Li, Na and K diffusivity shown as numbered lines). Cu diffusivity is very high in rhyolite to basalt melts, higher than H_2O_t diffusivity at the same H_2O concentration. In dry basalt, Cu diffusivity is similar to Na diffusivity (overlapping in Fig. 10). In dry rhyolite, Cu diffusivity lies between Na and K and closer to K (Ni et al. 2017). These observations can be explained by Cu diffusion as univalent cation Cu^+. For the composition (including H_2O) effect,

Ni et al. (2017) found that a single compositional parameter Si+Al–H seems to adequately capture the dependence of D_{Cu} on composition, where Si, Al and H are cation mole fractions on wet basis. The pressure effect was not well resolved by Ni et al. (2017). Their equation without including the pressure effect predicts the later published data in Ni et al. (2018) well (within 0.22 ln$D$ units) except for the data at low pressures of 0.15 GPa. Following Ni et al. (2017) but including the pressure effect, the following empirical equation is obtained for Cu diffusivity in dry basalt and dry and wet (up to 6 wt% H_2O) rhyolite at 973-1848 K and ≤1.5 GPa:

$$\ln D_{Cu} = -16.68 + 2.872(\text{Si+Al–H}) - \frac{5103 + 8259(\text{Si+Al–H}) + 411.7P}{T}, \quad (44)$$

where P is in GPa and D is in m^2/s. The above equation predicts all Cu diffusion data in Ni and Zhang (2016) and Ni et al. (2017, 2018) to within 0.23 ln$D$ units (1σ error 0.12 ln$D$ units). This accuracy is among the highest of all empirical predictive equations for diffusivity data across different compositions. We recommend its use to predict Cu^+ diffusion in other natural silicate melts if no experimental data are available.

Table 8. Chemical compositions (on dry basis) for trace element diffusion studies

	SiO_2	TiO_2	Al_2O_3	FeO	MnO	MgO	CaO	Na_2O	K_2O	Ref.
rhyolite14b	76.8	0.15	13.3	0.78	0.08	0.08	0.62	4.04	3.91	1
rhyolite8a	73.2	0.11	13.8	2.14	0.08	0.18	0.92	4.22	5.31	2
NCO	72.9	0.22	14.2	1.93	0.06	0.18	0.86	4.73	4.24	3
rhyolite3a	70.4	0.29	16.3	1.21	0.00	0.59	1.69	3.93	5.15	4
dacite3a	65.0	0.54	16.5	3.88	0.10	2.23	4.97	4.49	1.52	5
phonolite2	58.5	0.68	19.9	3.53	0.21	0.36	0.74	9.90	5.67	6
shoshonite	53.3	0.69	16.4	8.14	0.21	4.64	8.04	5.46	3.05	2
basalt8a	50.0	1.62	16.0	9.40	0.25	8.50	10.79	3.00	0.20	7,8
basalt11	49.9	1.83	13.5	12.9	0.22	6.81	10.8	2.65	0.17	3
basalt6	48.5	2.7	13.8	12.7	0.00	7.55	10.9	2.50	0.41	9
basalt1a	46.9	1.65	17.66	10.6	0.00	5.86	10.6	4.43	2.02	10
peridotite	46.1		4.0	8.8		37.5	3.6			11

References: 1. Holycross and Watson (2018); 2. Gonzalez-Garcia et al. (2017, 2018); 3. Yu et al. (2019); 4. Zhang et al. (2018); 5. Lierenfeld et al. (2018); 6. Bohm and Schmidt (2013); 7. Watson et al. (2015); 8. Holycross and Watson (2016); 9. Lesher et al. (1996); 10. Ni and Zhang (2016); 11. Posner et al. (2018). The peridotite composition includes 1 wt% NiO on one side and 1 wt% CoO on the other side. See footnotes in Table 2 for melt names.

A note about the calculation of cation mole fractions of Si, Al and H. Often the oxide wt% is given on the dry basis for easy comparison with other melts and then H_2O wt% is separately given. In such cases, calculation of cation mole fractions on dry basis is straightforward. However, for the calculation of cation mole fractions on wet basis (i.e., cation mole fraction of H is also calculated), the non-H_2O oxide wt% must first be calculated by multiplying $(1\text{-}w_{H_2O})$, where w_{H_2O} is the mass fraction of H_2O. Then the reported H_2O wt% and the recalculated wt% of other oxides are used to calculate cation mole fraction. If the oxide wt% is given on wet basis (actual concentrations), then no such conversion of multiplying by $(1\text{-}w_{H_2O})$ is needed.

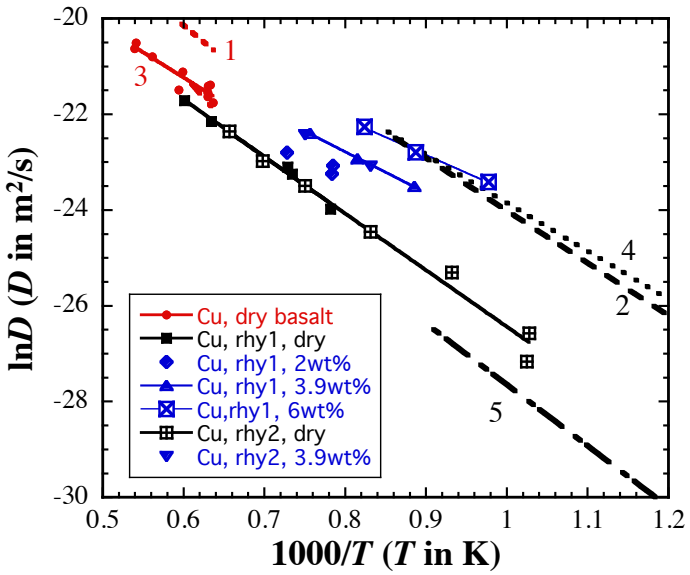

Figure 10. Cu diffusivity in rhyolite to basalt compared with diffusivity of Li, Na, and K. Red color for dry basalt. Black color for dry rhyolite. Blue color for wet rhyolite. Points with solid lines are for Cu diffusion data (Ni and Zhang 2016; Ni et al. 2017, 2018). The two lines for Cu diffusivity in dry rhyolite overlap and cannot be seen individually. Numbered lines are for diffusion data of Li, Na and K. 1 (red short-dash line): Li diffusivity in dry basalt (Lowry et al. 1981); 2 (black long-dash line): Li in dry rhyolite (Jambon and Semet 1978); 3 (red long-dash line): Na in dry basalt (Lowry et al. 1982). (Line 3 cannot be seen because it overlaps with Cu diffusion line in basalt); 4 (black short-dash line): Na in dry rhyolite (Jambon 1982); 5 (black dot-dash line): K in dry rhyolite (Jambon 1982).

In addition to the above studies, Von der Gonna and Russel (2000), and Kaufmann and Russel (2008, 2010, 2011) obtained Cu diffusivity in SiO_2-Na_2O, SiO_2-CaO-Na_2O, SiO_2-Al_2O_3-Na_2O, SiO_2-Al_2O_3-CaO-Na_2O melts using square wave voltametry. The Cu diffusivity data determined using the voltametry method are for a mixture of Cu^+ and Cu^{2+} at subequal proportions, and Kaufmann and Russel (2011) derived them to roughly equal to $2D_{Cu^{2+}}$, meaning that these diffusivities are expected to be much smaller than diffusivity of Cu^+ determined by Ni

and Zhang (2016) and Ni et al. (2017, 2018). Furthermore, the compositions are very different from natural silicate melts. Equation (44) cannot be applied to predict these diffusivities.

Diffusion of Sc, Y, and REE

Holycross and Watson (2016, 2018) produced high quality trace element diffusion data in both dry basalt8a and wet rhyolite14b containing ~4.1 wt% H_2O and ~6.2 wt% H_2O using diffusion couple experiments. The compositions of basalt8a and rhyolite14b are listed in Table 8. The chemical concentration gradients are only on some 20 trace elements, not on major elements. In principle, the presence of concentration gradients of other trace elements could affect the diffusivity of a given trace element. However, such effect is unlikely to be significant. Hence, the diffusivities are close to TED1. Holycross and Watson (2016, 2018) reported a large number of diffusion data and they are highly self consistent. Diffusion coefficients decrease slightly from La to Lu, by about 20% in dry basalt8a melt (Fig. 11), and slightly more in wet rhyolite14b melt.

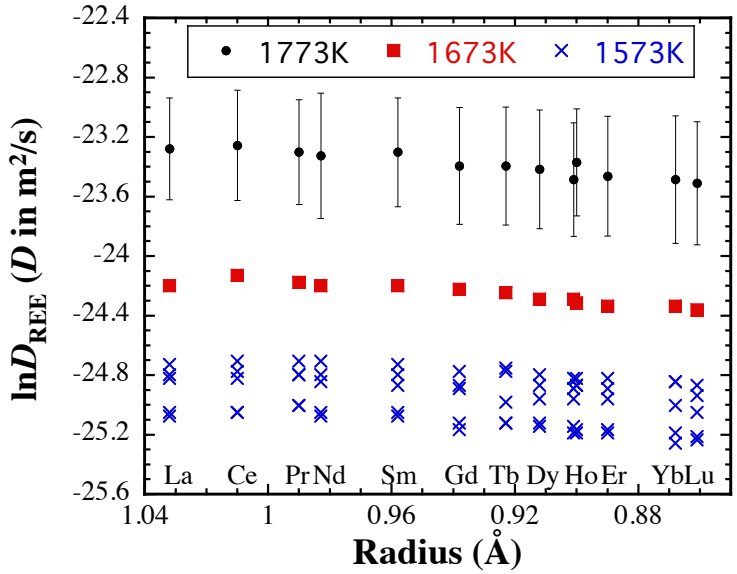

Figure 11. Diffusion coefficients of rare earth elements in basalt8a at three temperatures (Holycross and Watson, 2016) as a function of trivalent ionic radius in octahedral sites. Y diffusivity is also shown (almost overlapping with Ho). Error bars at 1σ level are shown at 1773K, and they are similar at other temperatures. Another measure of error is by comparison of the five experiments at 1573 K with different durations. It appears that Ce has the highest diffusivity among the REE, but the difference between Ce and La diffusivity is tiny (~0.04 ln$D$ units) compared to the error (~0.3 ln$D$ units). From La to Lu, ln$D$ decreases by about 0.2.

The activation energy E and pre-exponential factor D_0 based on diffusivities extracted from diffusion profiles for each element are listed in Table 9. From E and D_0 listed, D at a given temperature can be calculated using Equation (5). Holycross and Watson (2016) showed that both E and logD_0 depend roughly linearly on the REE-O bond length (Ciccico et al. 2013). For hydrous rhyolite, the relations with REE elemental sequence shown in Holycross and Watson (2018) are slightly curved. Because REE-O bond lengths are not available for all REE, we use ionic radius to fit all trivalent REE (excluding Eu) diffusion data in the three different melts:

$$\ln D_{REE^{3+}}^{\text{dry basalt8a}} = -10.03 - \frac{25131 - 1738r}{T}, \tag{45a}$$

$$\ln D_{REE^{3+}}^{\text{rhy14b+4.1wt\%H}_2\text{O}} = -9.12 - \frac{24194 + 16516(1.097 - r)^2}{T}, \tag{45b}$$

$$\ln D_{REE^{3+}}^{\text{rhy14b+6.2wt\%H}_2\text{O}} = -8.35 - \frac{23250 + 21657(1.069 - r)^2}{T}, \tag{45c}$$

where r is trivalent ionic radius of REE in Å in octahedral site from Shannon (1976) (listed in Table 9 for convenience), T is in K, and D is in m^2/s. Trial fittings show that adding a dependence of lnD_0 on the ionic radius does not improve the fitting. Equation (45a) reproduces all the diffusivities in Supplementary Table B of Holycross and Watson (2016) to within 0.22 ln$D$ units, and the REE diffusivities in Supplementary Table A to within 0.24 ln$D$ units. Equation (45b) reproduced experimental data of trivalent REE diffusivity in rhyolite14b containing ~4.1 wt% H_2O within 0.28 ln$D$ units. Equation (45c) reproduced experimental data of trivalent REE diffusivity in rhyolite14b containing ~6.2 wt% H_2O within 0.31 ln$D$ units. Such high accuracy reflects the high self-consistency of the REE diffusion data in Holycross and Watson (2016, 2018). Equations (45a)-(45c) should be able to predict Eu^{3+} (and hence assess the contribution of Eu^{3+} and Eu^{2+} to Eu diffusion) and Tm diffusivity even though no Tm diffusion data were

available in the literature. All three equations predict Y diffusion data in Holycross and Watson (2016, 2018) well, within 0.24 ln$D$ units, and Equation (45a) also predicts Sc diffusivity within 0.28 ln$D$ units. Using Equations (45b) and (45c) to predict Sc diffusivity would lead to large errors (1.0 ln$D$ units). Equations (45a)-(45c) mean that there is larger difference in La to Lu diffusivities in wet rhyolite14b melts than in dry basalt8a.

Table 9. Diffusion parameters for some trace elements

		basalt8a		rhy14b+4.1wt%H_2O		rhy14b+6.2wt%H_2O	
	r (Å)	E	logD_0	E	logD_0	E	logD_0
Li						39.31	-7.35
Rb		178.33	-4.69				
Sr		161.7	-5.10				
Ba		181.1	-4.67				
V	0.640	203.3	-4.06	185.0	-4.90	222.4	-2.67
Sc	0.745	202.6	-4.14	228.8	-3.42	211.4	-3.24
Y	0.900	195.1	-4.39	188.3	-4.66	165.7	-5.09
La	1.032	191.41	-4.43	188.31	-4.51	203.34	-3.21
Ce	1.01	192.75	-4.41	201.66	-3.97	198.90	-3.33
Pr	0.99	193.18	-4.40	194.63	-4.27	202.07	-3.28
Nd	0.983	193.36	-4.40	203.61	-3.93	200.60	-3.35
Sm	0.958	194.30	-4.37	206.69	-3.84	205.46	-3.18
Eu		188.98	-4.41	166.10	-4.98		
Gd	0.938	194.87	-4.37	209.08	-3.79	193.84	-3.74
Tb	0.923	195.55	-4.35	201.13	-4.14	203.97	-3.32
Dy	0.912	196.42	-4.33	214.66	-3.60	185.72	-4.17
Ho	0.901	196.77	-4.33	210.90	-3.80	190.93	-3.91
Er	0.890	197.42	-4.31	201.01	-4.22	210.29	-3.98
Yb	0.868	198.07	-4.30	218.59	-3.54	171.42	-4.90
Lu	0.861	198.86	-4.29	209.63	-3.93	196.97	-3.82
Zr		219.7	-3.85	182.4	-5.45	155.2	-6.36
Hf		223.8	-3.81	231.1	-3.52		
Th		213.4	-4.02			176.7	-5.10
U		212.0	-3.98	228.8	-3.42	267.8	-1.06
Nb		206.1	-4.18	214.5	-4.03	179.5	-4.91
Ta		218.2	-3.92				
P		147.0	-6.30				

The unit of E is kJ/mol. The unit of D_0 is m^2/s. Note logD_0 values rather than lnD_0 are listed following the original authors. Compositions of basalt8a and rhyolite14b (rhy14b) are listed in Table 8. Data are from Holycross and Watson (2016, 2018), except for Li (Holycross et al. 2018) and P (Watson et al. 2015). For REE, E and logD_0 are based on ratio-fitting method in Holycross and Watson (2016, 2018), which have better consistency. Ionic radii are

for trivalent cations in octahedral sites from Shannon (1976). A single coordination (octahedral) is used for consistency with no implication on the real coordination number.

Diffusivities of Li, Rb, Sr, Ba, Sn, V, Zr, Hf, Th, U, Nb and Ta

Holycross and Watson (2016, 2018) also reported high quality trace element diffusion (close to TED1) data for Rb, Sr, Ba, V, Zr, Hf, Th, U, Nb and Ta in dry basalt8a (Table 8), V, Zr, Hf, U, and Nb in rhyolite14b (Table 8) containing 4.1 wt% H_2O, and V, Zr, Th, U and Nb in rhyolite14b containing ~6.2 wt% H_2O. Watson et al. (2015) determined P diffusivity (POCGD) in dry basalt8a using diffusion couple experiments. The activation energies and pre-exponential factors for these elements in dry basalt8a and wet rhyolite14b are listed in Table 9. The diffusivities of tetravalent and pentavalent ions (HFSE) in basalts are shown in Fig. 12. They are similar to each other (within ~0.5 ln$D$ units in basalt8a), with

$$D_U \approx D_{Nb} > D_{Th} \geq D_{Zr} \geq D_{Ta} > D_{Hf} > D_P. \quad (46)$$

Si diffusivities in basalts with slightly different compositions (self diffusivity in basalt6 in Table 8, and POCGD in basalt11 (Juan de Fuca MORB), and interdiffusivity in synthetic basalts) are also shown in Fig. 12 for comparison. Due to slightly different compositions, direct comparison of HFSE diffusivities with Si diffusivity is not possible. By correcting to the same composition using Yu et al. (2019), Si diffusivity is equal to or slightly smaller than P diffusivity. The information is used in updating the diffusivity sequence in basalt (Eqn. 28). Fig. 12 also shows the high self-consistency in Si self diffusion and Si POCGD, but high variability in Si interdiffusivity in a given melt.

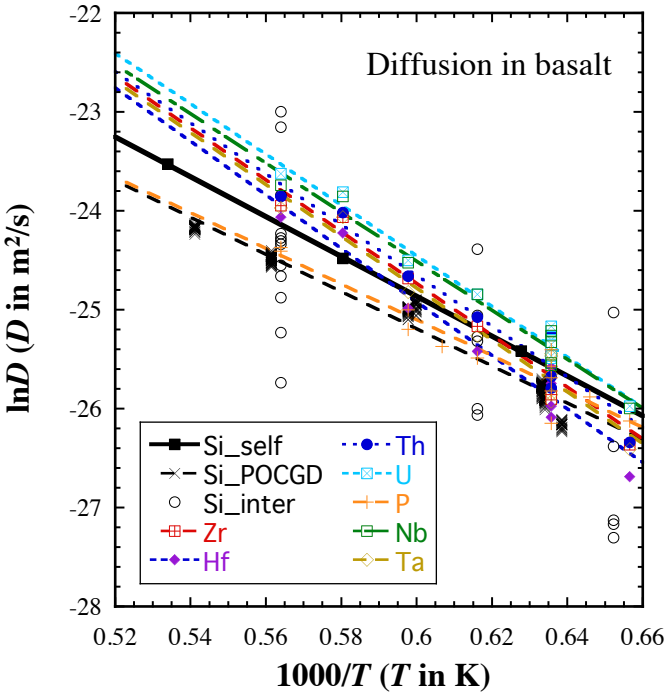

Figure 12. Comparison of HFSE diffusivities. Diffusivities of Zr, Hf, Th, U, P, Nb and Ta are for basalt8a (Table 8) at 1 GPa and are from Holycross et al. (2016) and Watson et al. (2015). Si self diffusivities are for composition basalt6 (Table 8) at 1 GPa from Lesher et al. (1996). Si POCGD values are for basalt11 (Table 8) from quartz dissolution experiments at 0.5 GPa by Yu et al. (2019). Si interdiffusivity values are for basalt11a and haplobasalt2 (Table 2) at 0.5 to 1 GPa from multicomponent diffusion experiments of Guo and Zhang (2016, 2018, 2020). The large variability of Si interdiffusivity is due to different counter-diffusion component.

Holycross et al. (2018) conducted Li diffusion couple experiments in wet rhyolite14b containing 6.0 wt% H_2O at 1063-1148 K and 1.0 GPa, and acquired Li trace element diffusivities (TED1) in addition to Li isotope fractionation profiles. Li diffusivities (TED1) in wet rhyolite at 1 GPa are higher by 1.8 ln$D$ units than Li tracer diffusion data in a dry rhyolite at 1 atm (Jambon and Semet 1978). The activation energy and pre-exponential factor are listed in Table 9.

Yang et al. (2016) carried out diffusive cassiterite dissolution experiments in various dry and wet rhyolites to determine Sn diffusivity. Sn diffusivity depends on its oxidation state (Sn^{2+} and Sn^{4+}). It was inferred that when graphite capsule is used, Sn in rhyolite melt is mostly divalent. The main concentration gradient is in SnO, and other components are diluted by additional SnO. Hence, the diffusion data are POCGD. Divalent Sn diffusivity in various reduced rhyolites at 1023-1373 K, 0.5 GPa, and 0-5.9 wt% H_2O can be described as follows:

$$\ln D_{\mathrm{SnO}}^{\text{silicic melts}} = -18.194 + 17(0.76 - w_{\mathrm{SiO_2}}) - \frac{19418 - 138900 w_{\mathrm{H_2O}}}{T}, \qquad (47)$$

where w_{SiO_2} and w_{H_2O} are mass fraction (not wt%) of SiO_2 and H_2O, T is in K, and D is in m^2/s.

Zhang and Xu (2016) carried out diffusive zircon dissolution experiments in various dry and wet rhyolites to determine Zr diffusivity. Even though zircon also contains SiO_2, the dissolution leads to mainly ZrO_2 concentration gradient and the rest are mostly dilution by ZrO_2. Hence, these diffusivities are close to POCGD's. They considered all Zr diffusion data available at the time and came up with the following equation to relate Zr POCGD with T (1270-1890 K), P (0.5-1.5 GPa), and melt composition in various dry and wet rhyolites:

$$\ln D_{Zr}^{rhyolites} = -14.42 - \frac{38784(Si+Al) - 1836P - 3172}{T}, \quad (48)$$

where Si+Al is the sum of Si and Al cation mole fractions calculated on wet basis (i.e., H^+ mole fraction is counted), P is in GPa, and T is in K. The effect of H_2O on Zr diffusivity seems to be simply its dilution of the network formers. The above equation reproduces the experimental Zr diffusion data of Zhang and Xu (2016) to within 0.59 ln$D$ units (1σ error 0.29 ln$D$ units). On the Zr diffusion data in rhyolites by Holycross and Watson (2018), the equation predicts six out of seven diffusivity values in the ~6.2 wt% H_2O rhyolite to within 0.27 ln$D$ units, but for the three diffusivities in the ~4.1 wt% rhyolite and the other diffusivity in the ~6.2 wt% H_2O rhyolite, the error ranges from 0.88 to 1.88 ln$D$ units. More effort is needed in the future to derive more accurate general expressions on the compositional dependence of Zr diffusivity.

SiO_2 diffusion

Yu et al. (2019) carried out quartz dissolution experiments in nominally dry rhyolite (NCO listed in Table 8) containing 0.10 wt% H_2O and nominally dry basalt11 (Table 8) containing 0.32 wt% H_2O, and determined effective binary diffusivity of SiO_2. SiO_2 is the major concentration gradient, and gradients of other oxides are largely due to the dilution of SiO_2 (also due to

multicomponent diffusion effects, Fig. 6). Hence, technically SiO_2 diffusivity is still POCGD even though the strong SiO_2 concentration gradient causes diffusion of many oxides. Previously, it was thought that SiO_2 diffusivity largely depends on SiO_2 concentration (e.g., Watson 1982; Koyaguchi 1989; Lesher and Walker 1986; Richter et al. 2003; Macris et al. 2018). An SiO_2 concentration profile during any single experiment can indeed be modeled well assuming $\ln D_{Si}$ is linear to SiO_2 concentration (Fig. 5), and Boltzmann analysis of SiO_2 concentration profile in every experiment using Equation (18) also shows such a dependence (Yu et al. 2019). However, when D_{Si} values extracted from quartz dissolution in rhyolite are compared to those from quartz dissolution in basalt, it becomes clear that D_{Si} depends on Si+Al rather than SiO_2 alone. As shown in Fig. 13, when $\ln D_{Si}$ is plotted against SiO_2 concentration, the trends for D_{Si} from quartz dissolution in rhyolite are offset from those for quartz dissolution in basalt. On the other hand, when $\ln D_{Si}$ is plotted against Si+Al cation mole fractions, the trends in rhyolite roughly line up with those in basalt.

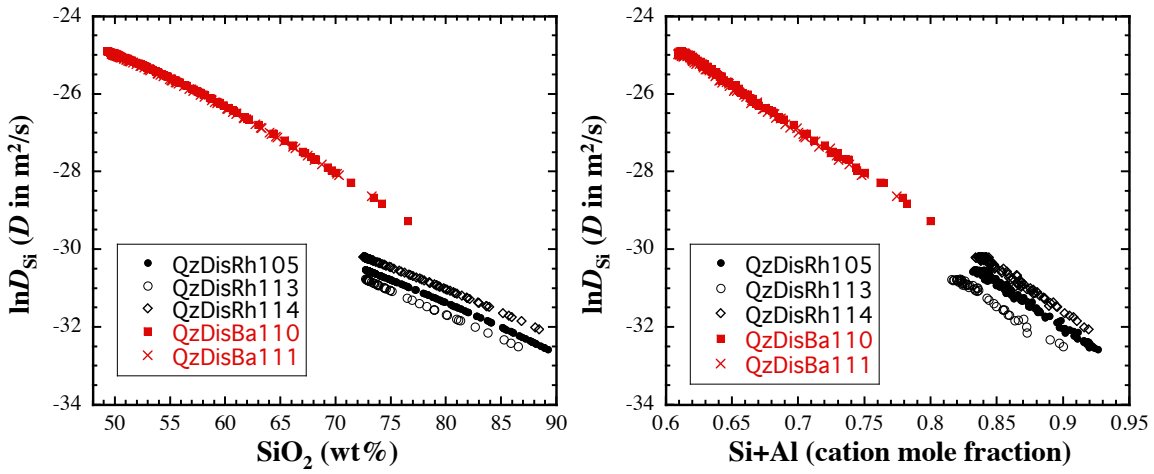

Figure 13. Si diffusivity from functional fitting results (points) as a function of SiO_2 concentration (left) and Si+Al mole fraction (right). Black points are from three quartz dissolution experiments in rhyolite (NCO, composition listed in Table 8) and red points are from two experiments in basalt (basalt11, composition listed in Table 8) melts at 1404±10°C.

Using Si+Al cation mole fraction on wet basis, Yu et al. (2019) obtained the following equation for SiO_2 diffusivity (POCGD) in basalt to rhyolite at 1123-1873 K and 0.5 GPa:

$$\ln D_{Si}^{\text{quartz dissolution}} = -11.41 - 2.758(\text{Si+Al}) - \frac{38829(\text{Si+Al}) - 3826}{T}, \quad (49)$$

where T is in K and D is in m^2/s. The above equation reproduces experimental data points in Yu et al. (2019) within 0.95 ln$D$ units (1σ error is 0.32 ln$D$ units). Hence, the accuracy in predicting D_{Si} using the above equation is much worse than that in predicting D_{Cu} using Equation (44), or in predicting REE diffusivities using Equations (45a)-(45c). Some of the inaccuracy is almost certainly due to the dependence of D_{Si} on concentrations of other major oxides, but such dependence cannot be quantified yet. Limited data examined by Yu et al. (2019) seem to indicate that the above equation would work for wet rhyolite too, meaning that the effect of H_2O on reducing D_{Si} is largely due to its dilution of Si+Al cation mole fraction. Equation (49) reproduces Si self diffusivities at 1 GPa (Lesher et al. 1996) within 0.23 ln$D$ units (excellent accuracy). The SiO_2 EBD values during shoshonite-rhyolite diffusion couple experiments (Gonzalez-Garcia et al. 2017) cannot be reproduced well, with maximum deviation of 2.3 ln$D$ units (one order of magnitude) and 1σ error of 0.66 ln$D$ units, reflecting the dependence of OEBD on concentration gradients. Due to much higher pressure (4-24 GPa) and higher MgO contents (37 wt%), the SiO_2 self diffusivity in peridotite at ultrahigh pressures (Posner et al. 2018) also cannot be reproduced well by Equation (49) (which is for 0.5 GPa), with maximum deviation of 3.1 ln$D$ units.

Self diffusion of O, Si, Mg and Ca, and interdiffusivity of Ni and Co in a peridotite melt

Posner et al. (2018) investigated the self diffusion of O, Si, Mg, and Ca, and interdiffusion of Ni and Co in a peridotite melt at 2150-2623 K and 4-24 GPa using diffusion couple experiments. The melt composition is listed in Table 8, with one side of the diffusion couple containing 1 wt%

NiO and the other side containing 1 wt% CoO. These are difficult experiments at extreme conditions. The pressure and temperature of the experiments co-varied and hence it is difficult to separate the effects of pressure and temperature on the diffusivities. By fixing the activation energy to some values, the self diffusivities presented by Posner et al. (2018) show a complicated pressure dependence. The diffusivities decrease with increasing pressure from 4 to 8 GPa, then increase with increasing pressure from 8 to 12 GPa, and then decrease again. For Ni and Co interdiffusivity, the pressure dependence is weaker.

Diffusion of Mo and W

Zhang et al. (2018) investigated Mo and W diffusion in a rhyolite melt (rhyolite3a in Table 8) using both diffusion couple and Mo saturation experiments on both dry and wet melts at 1273-1873 K and 1 GPa. Their work provided the first data (13 points) on Mo diffusion, and was the second investigation (4 points) on W diffusion in aluminosilicate melts. They found that in dry rhyolite3a melt, Mo and W have similar (within 0.16 ln$D$ units) diffusivities. Adding H_2O increases Mo diffusivity significantly. The Arrhenius relations for Mo and W diffusion are as follows:

$$\ln D_{\mathrm{Mo}}^{\text{Dry \& wet Rhyolite2}} = -4.47 - 200 w_{\mathrm{H_2O}} - \frac{44534 - 532358 w_{\mathrm{H_2O}}}{T}, \tag{50}$$

$$\ln D_{\mathrm{W}}^{\text{Dry Rhyolite2}} = -2.95 - \frac{47628}{T}, \tag{51}$$

where $w_{\mathrm{H_2O}}$ is the mass fraction of H_2O, T is in K and D is in m^2/s. Equation (50) reproduces Mo diffusion data in Zhang et al. (2018) to within 0.63 ln$D$ units (1σ uncertainty is 0.31 ln$D$ units). Equation (51) reproduces W diffusion data in dry rhyolite3a in Zhang et al. (2018) to within 0.14 ln$D$ units. Mo and W diffusivities in rhyolite3a are compared with those of Nb and Zr in

rhyolite14b in Fig. 14. Note that rhyolite14b is much more silicic than rhyolite3a (Table 8). The activation energy for Mo diffusion in rhyolite3a containing ~5 wt% H_2O is smaller than those for Nb and Zr diffusion in rhyolite14b containing ~4.1 and ~6.2 wt% H_2O, leading to $D_{Mo} > D_{Nb}$ at $T < 1200$ K, and $D_{Mo} < D_{Nb}$ at $T > 1400$ K. Nonetheless, Mo and W diffusivities are small and are not very different from other HFSE.

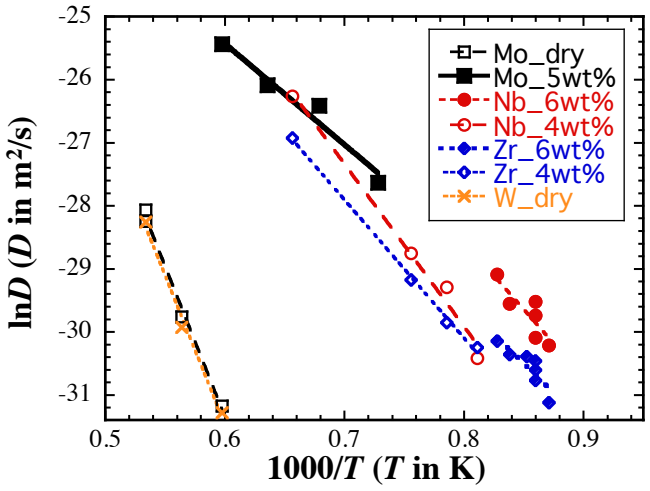

Figure 14. Mo and W trace element diffusivities (TED1) in rhyolite3a (Zhang et al. 2018) compared to Nb and Zr trace element diffusivities (TED1) in rhyolite14b (Holycross et al. 2018). The composition of rhyolite3a and rhyolite14b are listed in Table 8, and rhyolite14b is more silicic than rhyolite3a. The limited data shows smaller activation energy for Mo diffusion in wet rhyolite3a containing ~5.0 wt% H_2O than Nb and Zr diffusion in wet rhyolite14b containing ~4.1 wt% and ~6.2 wt% H_2O.

Diffusion of F, Cl, and S

Bohm and Schmidt (2013) studied F and Cl diffusion in a phonolite2 melt (Table 8) containing ≤ 2.4 wt% H_2O using diffusion couple experiments at 1073-1473 K and 0.1 GPa. In dry phonolite2, F diffusivity is higher than Cl diffusivity by about an order of magnitude. The composition and H_2O concentration range investigated are similar to those by Balcone-Boissard et al. (2009) but the diffusion data do not line up in one trend, either indicating subtle dependence on composition or inter-laboratory inconsistency. Bohm and Schmidt (2013) provided the following Arrhenius equations for F and Cl diffusivities:

$$\ln D_F^{\text{dry phonolite2}} = -18.24 - \frac{12003}{T}, \qquad (52a)$$

$$\ln D_{\mathrm{F}}^{\text{phonolite2+2.1wt\%H}_2\text{O}} = -17.36 - \frac{11678}{T}, \quad (52b)$$

$$\ln D_{\mathrm{Cl}}^{\text{dry phonolite2}} = -15.78 - \frac{18413}{T}, \quad (53a)$$

$$\ln D_{\mathrm{Cl}}^{\text{phonolite2+2.4wt\%H}_2\text{O}} = -13.72 - \frac{18570}{T}, \quad (53b)$$

where T is in K and D is in m^2/s.

Yoshimura (2018) examined Cl diffusion in a high-silica rhyolite containing ≤ 1.2 wt% H_2O and also reported Ca diffusion data as a byproduct. The composition of the rhyolite is similar to rhyolite14b in Table 8. The Cl diffusion data in dry rhyolite in Yoshimura (2018) are 2-3 orders of magnitude lower than those in Bai and Koster van Groos (1994). Yoshimura (2018) explained this by compromising of the latter data by Na infiltration. After removing the data by Bai and Koster van Groos (1994), Cl diffusivity decreases from basalt to phonolite to rhyolite.

Lierenfeld et al. (2018) examined sulfur diffusion in wet dacite melt (4.5-6.0 wt% H_2O) using diffusion couple experiments at 1223-1373 K, 0.20-0.25 GPa, and at $\log f_{O2}$ of FMQ-0.8 (S is dominantly S^{2-}) and FMQ+2.5 (S is dominantly S^{6+}). The composition of the dacite is listed as dacite3a in Table 7. The effect of oxidation state on sulfur diffusivity was anticipated but previously unresolved due to data scatter (Behrens and Stelling 2011). With well-designed experiments, Lierenfeld et al. (2018) clearly resolved the effect of $\log f_{O2}$ on S diffusivity, and found that S diffusivities at FMQ-0.8 is about 15 times those at FMQ+2.5. The equations to describe sulfur diffusivity in dacite containing 4.5 wt% H_2O at 0.2 GPa are as follows (Lierenfeld et al. 2018):

$$\ln D_{\text{S at QFM+2.5}}^{\text{Dacite+4.5wt\%H}_2\text{O}} = -13.63 - \frac{16513}{T}, \quad (54a)$$

$$\ln D_{\text{S at QFM}-0.8}^{\text{Dacite}+4.5\text{wt\%H}_2\text{O}} = -11.93 - \frac{15118}{T}, \quad (54b)$$

where T is in K. Their sulfur diffusion data at 6.0 wt% H_2O are scattered.

Major and trace element diffusion (OEBD) in shoshonite-rhyolite diffusion couple

Gonzalez-Garcia et al. (2017, 2018) carried out shoshonite-rhyolite diffusion couple experiments in both dry and wet (≤ 2.0 wt% H_2O) conditions at 1473 K and 0.05-0.5 GPa. The compositions of the shoshonite and rhyolite (rhylite8a) are listed in Table 8. Due to the presence of significant concentration gradients in all major oxides, the diffusivities belong to the other types of effective binary diffusivities (OEBD). Numerous elements (e.g., Al, Na, La, Ce, Pr, Nd, Sm, Gd, Tb) show uphill diffusion, and OEBD cannot be extracted for them. For 19 elements with monotonic concentration profiles (Si, Ti, Fe, Mg, Ca, K, Rb, Cs, Sr, Ba, Co, Sn, Eu, V, Cr, Hf, Th, U, Ta), they found that the shapes of the profiles indicate that the diffusivity of each element depends on the bulk composition, as expected since SiO_2 concentration varies from 53 to 73 wt%. They extracted a large number of diffusion coefficients using Boltzmann-Matano analysis. These diffusivities depend on the direction and magnitude of the concentration gradient of all major oxides in addition to the dependence on the bulk composition. Their best applicability is to investigate the kinetics and dynamics of shoshonite-rhyolite mixing. Importantly, Gonzalez-Garcia et al. (2017, 2018) provided data to examine how OEBD values of many elements depend on H_2O concentration, which were previously unavailable. Such dependence might be applicable to the diffusion of these elements under other conditions (such as tracer diffusivity or POCGD).

Data by Gonzalez-Garcia et al. (2017, 2018) show that many components move in coordinated fashion with similar diffusivities, which are in agreement with observations by

Watson (1982), Koyaguchi (1989), Richter et al. (2003), Macris et al. (2018), Yu et al. (2019), among others. Gonzalez-Garcia et al. (2017) found that OEDB values increases with increasing H_2O by 0.8-2.3 ln$D$ units per wt% of H_2O, and decreases with increasing SiO_2 by 0.02-0.12 ln$D$ units per wt% SiO_2. The latter is roughly consistent with Yu et al. (2019), but predicted D_{SiO_2} using Equation (49) is on average lower than OEBD of SiO_2 (Gonzalez-Garcia et al. 2017) by 0.7 ln$D$ units with large scatters, revealing the role of different concentration gradients in OEBD, or more generally, multicomponent effects. No general equations were provided by Gonzalez-Garcia et al. (2017, 2018) to relate D with melt composition and pressure.

DIFFUSIVE ELEMENTAL AND ISOTOPE FRACTIONATION DURING MAGMATIC PROCESSES

Diffusion is ubiquitous in magmas. Therefore, it is of interest to understand the possibility and magnitude of diffusive fractionation of isotopes and elements in magmas. Equilibrium fractionation of isotopes and elements is fairly well understood (e.g., Gast 1968; Shaw 1970; Allegre and Minster 1978, and numerous partitioning studies). On the other hand, attention on diffusive fractionation of isotopes and elements is more recent. Jambon (1980) first proposed that isotopes could be diffusively fractionated, which can be recorded by growing crystals from magmas. Richter et al. (1999) were the first to measure diffusive isotope fractionation of $^{48}Ca/^{40}Ca$ in CAS system and $^{76}Ge/^{70}Ge$ in GeO_2 melt using spiked isotopes. Chopra et al. (2012) investigated possible diffusive isotope fractionation in igneous rocks and showed that current instrumental capability can measure such fractionations. If isotope ratios can be fractionated,

elemental ratios and patterns can of course also be fractionated by diffusion. Holycross and Watson (2016, 2018) and Watson (2017) discussed diffusive elemental fractionation.

Diffusive fractionation requires different diffusivities. Elemental diffusivities for most elements are available (see reviews by Zhang et al., 2010 and this work) and can be used to discuss elemental fractionation. For isotope diffusion, differences in diffusivities of isotopes cannot be resolved by measuring diffusivities of individual isotopes. Instead, the ratio of diffusivities of different isotopes is determined from experimental isotope ratio profiles and related to the mass ratio. If each isotope diffuses freely as individual atoms, diffusivities of heavy and light isotopes can be related by Graham's law (Richter et al. 2003):

$$\frac{D_{\mathrm{H}}}{D_{\mathrm{L}}}=\sqrt{\frac{m_{\mathrm{L}}}{m_{\mathrm{H}}}}, \tag{55}$$

where m_{H} and m_{L} are the atomic masses, and D_{H} and D_{L} are the diffusivities of heavy and light isotopes. If heavy and light isotopes diffuse freely as individual neutral molecules, then

$$\frac{D_{\mathrm{H}}}{D_{\mathrm{L}}}=\sqrt{\frac{M_{\mathrm{L}}}{M_{\mathrm{H}}}}, \tag{56}$$

where M_{H} and M_{L} are the molecular masses of those containing heavy and light isotopes. If isotopes diffuse as clusters exchanging with other species, then (Richter et al. 2003)

$$\frac{D_{\mathrm{H}}}{D_{\mathrm{L}}}=\sqrt{\frac{M_{\mathrm{L}}(M_{\mathrm{H}}+M)}{M_{\mathrm{H}}(M_{\mathrm{L}}+M)}}, \tag{57}$$

where M is the mass of the counter-diffusing species. However, silicate melts are complicated and the diffusion species and mechanisms are complicated (e.g., see multicomponent diffusion eigenvectors) and not accurately known. Hence, an empirical approach is used to characterize the relation between D_{H} and D_{L} as follows (Richter et al. 1999):

$$\frac{D_{\mathrm{H}}}{D_{\mathrm{L}}}=\left(\frac{m_{\mathrm{L}}}{m_{\mathrm{H}}}\right)^{\beta}, \tag{58}$$

where β is an empirical fit parameter.

Consider isotope fractionation of a given element in a diffusion couple. Suppose the left hand side has a lower concentration and the right hand side has a higher concentration. Treat the diffusion as effective binary diffusion. The element diffuses from the right hand side to the left hand side. The light isotope diffuses more rapidly, and hence is enriched in the LHS. In other words, the LHS is depleted in the heavy isotope, and the RHS is enriched in the heavy isotope. Quantitatively, the concentration profile of each isotopes is an error function (Eqn. 7). Hence, if the effective binary diffusivity is roughly constant, the isotope ratio, using ^{41}K/^{39}K as an example, is expressed as follows:

$$\frac{^{41}\mathrm{K}}{^{39}\mathrm{K}}=\frac{0.5(C_{41,\mathrm{LHS}}+C_{41,\mathrm{RHS}})+0.5(C_{41,\mathrm{RHS}}-C_{41,\mathrm{LHS}})\mathrm{erf}\dfrac{x-x_0}{\sqrt{4D_{41}t}}}{0.5(C_{39,\mathrm{LHS}}+C_{39,\mathrm{RHS}})+0.5(C_{39,\mathrm{RHS}}-C_{39,\mathrm{LHS}})\mathrm{erf}\dfrac{x-x_0}{\sqrt{4D_{39}t}}}, \tag{59}$$

where x_0 is the interface position, x increases from LHS to RHS, and subscript 41 and 39 means ^{41}K and ^{39}K. Converting to the δ-notation and using the initial ratio as standard lead to:

$$\delta\frac{^{41}\mathrm{K}}{^{39}\mathrm{K}}=\left(\frac{(1+\dfrac{C_{\mathrm{RHS}}}{C_{\mathrm{LHS}}})+(\dfrac{C_{\mathrm{RHS}}}{C_{\mathrm{LHS}}}-1)\mathrm{erf}\dfrac{x-x_0}{\sqrt{4D_{39}(m_{39}/m_{41})^{\beta}t}}}{(1+\dfrac{C_{\mathrm{RHS}}}{C_{\mathrm{LHS}}})+(\dfrac{C_{\mathrm{RHS}}}{C_{\mathrm{LHS}}}-1)\mathrm{erf}\dfrac{x-x_0}{\sqrt{4D_{39}t}}}-1\right)1000‰, \tag{60}$$

where $C_{\mathrm{RHS}}/C_{\mathrm{LHS}}$ is the initial concentration ratio of the RHS to the LHD (or concentration contrast). Model calculations (Fig. 15) using Equation (60) show that the magnitude of diffusive isotope fractionation depends on two parameters, one is the β value, and the other is the concentration ratio of the high concentration side to the low concentration side of the diffusion couple. By increasing the β value, or the concentration ratio, the magnitude of isotope

fractionation increases. For example, if β = 0.12 and the concentration ratio is 60, then the total variation of $\delta^{41}K/^{39}K$ would be about 10‰. If β = 0.12 and the concentration ratio is 2, then the variation of $\delta^{41}K/^{39}K$ would be about 1‰. Both of these fractionations are measurable (Zhang et al. 2019). One example of real data and fit is shown in Fig. 16.

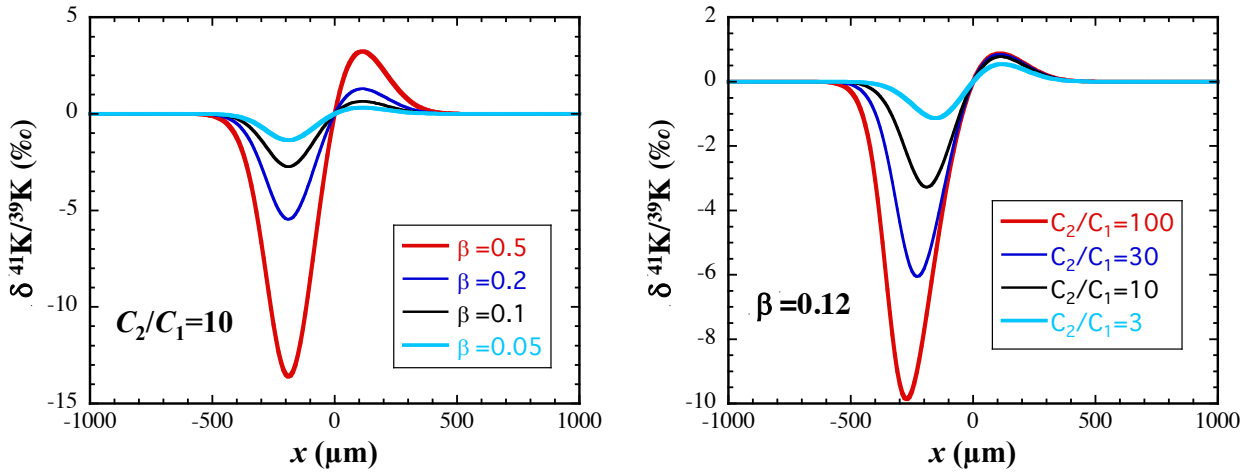

Figure 15. Calculated isotope fractionation in a diffusion couple as a function of β and concentration ratio $C_2/C_1 = C_{RHS}/C_{LHS}$. If β = 0 or $C_2/C_1 = 1$, there would be no isotope fractionation using effective binary treatment.

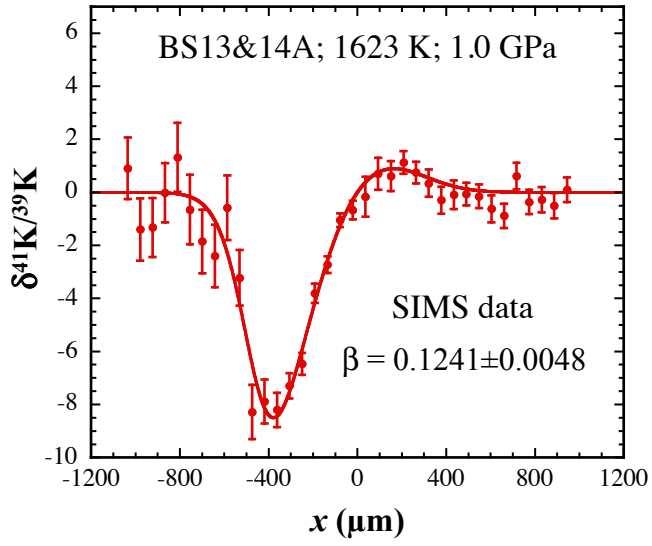

Figure 16. A $^{41}K/^{39}K$ isotope ratio profile (Zhang et al., 2019) in a multicomponent diffusion couple experiment by Guo and Zhang (2018). The measurement is made by Secondary Ion Mass Spectrometry at Caltech Microanalysis Center. The initial concentration of K_2O is ~0.05 wt% at $x < 0$, and 3.06 wt% at $x > 0$. From Zhang et al. (2019).

Richter et al. (1999) were the first to determine β values in CAS and GeO_2 melts. Richter et al. (2003, 2008, 2009) experimentally evaluated diffusive fractionation of $^{7}Li/^{6}Li$, $^{26}Mg/^{24}Mg$, $^{44}Ca/^{40}Ca$, and $^{56}Fe/^{54}Fe$ in dry basalt-rhyolite diffusion couple and obtained: $\beta_{Li} = 0.215$, $\beta_{Mg} = 0.05$, $\beta_{Ca} = 0.075$, and $\beta_{Fe} = 0.03$. Watkins et al. (2009, 2011, 2014) examined $^{26}Mg/^{24}Mg$ and $^{44}Ca/^{40}Ca$ fractionation in basalt-rhyolite, albite-anorthite, and albite-diopside diffusion couples and SiO_2-CaO-Na_2O system, and found that β_i (where i is an element) increases with D_i/D_{Si}. Watkins et al. (2014) developed the theory to treat isotope diffusion in the context of multicomponent diffusion. More experimentally determined β values and the associated experimental conditions can be found in Table 10.

Table 10. Experimentally determined β values for diffusive isotope fractionation

Isotopes	β	D_i/D_{Si}	Melt	T (K)	P (GPa)	Ref
$^{7}Li/^{6}Li$	0.215±0.005	290	basalt-rhyolite	1623-1723	1.2-1.3	1
$^{7}Li/^{6}Li$	0.228	2560	wet rhyolite	1103	1.2	2
$^{26}Mg/^{24}Mg$	0.05±0.01	~1	basalt-rhyolite	1673	1.0-1.2	3
$^{26}Mg/^{24}Mg$	0.10±0.01	1.5	albite-diopside	1723	0.8	4
$^{26}Mg/^{24}Mg$	0.045	~1	basalt-rhyolite	1773	1.45	5
$^{41}K/^{39}K$	0.12	1.64	basalt	1623	1.0	6
$^{48}Ca/^{40}Ca$	~0.08		CAS	1773	1.0	7
$^{44}Ca/^{40}Ca$	0.075±0.025	1.6	basalt-rhyolite	1623-1723	1.2-1.3	1
$^{44}Ca/^{40}Ca$	0.035±0.005	2.2	basalt-rhyolite	1723	1.0-1.3	8
$^{44}Ca/^{40}Ca$	0.21±0.015	23	albite-anorthite	1723	0.8	4
$^{44}Ca/^{40}Ca$	0.165±0.01	6.3	albite-diopside	1723	0.8	4
$^{44}Ca/^{40}Ca$	0.10		NCS(Ca-Na)	1523	0.8	9
$^{44}Ca/^{40}Ca$	0.035	~1	NCS(Ca-Si)	1523	0.8	9
$^{56}Fe/^{54}Fe$	0.03±0.01	1.3	basalt-rhyolite	1673	1.0-1.2	10
$^{76}Ge/^{70}Ge$	< 0.025		GeO_2	1673	0.5	7

Melt: CAS means CaO-Al_2O_3-SiO_2 system; NCS(Ca-Na) means CaO-Na_2O interdiffusion in Na_2O-CaO-SiO_2 system; NCS(Ca-Si) means CaO-SiO_2 interdiffusion in Na_2O-CaO-SiO_2 system;
References: 1. Richter et al. (2003); 2. Holycross et al. (2018); 3. Richter et al. (2008); 4. Watkins et al. (2011); 5. Chopra et al. (2012); 6. Zhang et al. (2019); 7. Richter et al. (1999); 8. Watkins et al. (2009); 9. Watkins et al. (2014); 10. Richter et al. (2009)

Diffusion also leads to elemental fractionation in magmas (Holycross and Watson 2016, 2018; Watson 2017). Holycross and Watson (2016) examined the fractionation of La/Lu ratio in a diffusion couple and found that diffusive fractionation can be significant and measurable. Here, we use REE diffusion coefficients in Equations (45a)-(45c) to model diffusive fractionation of REE patterns in dry basalt to wet rhyolite along a diffusion couple profile. Eu diffusivity is assumed to be 2 times Eu^{3+} diffusivity. To illustrate an extreme (unrealistic) case, we set the initial concentration contrast to be 200: the left hand side initially has the same REE concentration as in chondrites and the right hand side initially contains 200 times chondrite REE concentration. Some calculated REE patterns in basalt and wet rhyolites are shown in Fig. 17. In this extreme case, the REE pattern is fractionated significantly, and more so in rhyolite than in basalt due to larger differences between La and Lu diffusivities in rhyolite. There is also a large Eu anomaly ($Eu/Eu^* \approx 3$). As the initial concentration contrast decreases, the maximum fractionation decreases and the location of the maximum fractionation moves closer to the interface. If the concentration contrast is reduced to a factor of 2, then the REE pattern is much less fractionated, with normalized $(La/Lu)_{CI}$ ratio fractionated by $\leq 2.1\%$ in basalt and $\leq 8.4\%$ in rhyolite+6.2 wt% H_2O, and $Eu/Eu^* \leq 1.074$.

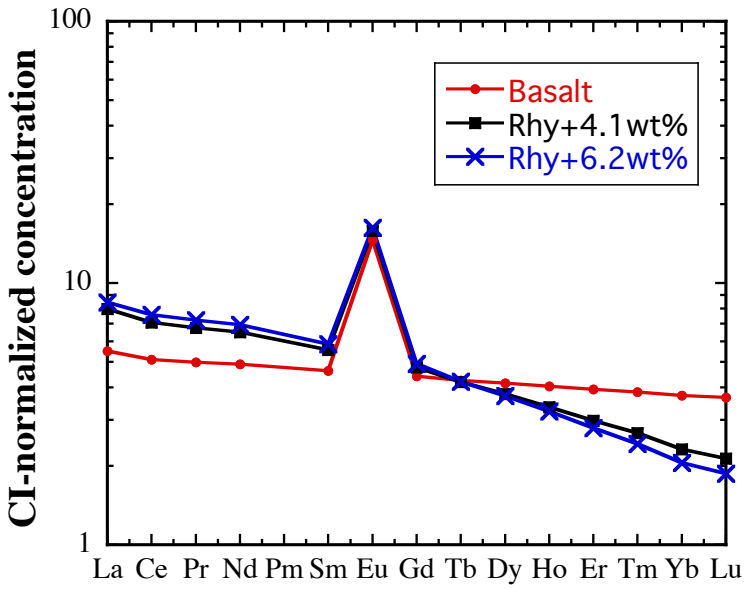

Figure 17. Calculated REE patterns due to diffusive fractionation in a diffusion couple. The initial concentrations in the diffusion couple are: same as chondrite at $x < 0$, and 200 times chondrite at $x > 0$. The diffusivities are calculated from Equations (45a)-(45c), at 1473 K for basalt, 1273 K for rhyolite+4.1 wt% H_2O, and 1173 K for rhyolite+6.2 wt% H_2O. D_{Eu} is set to be two times the diffusivity of Eu^{3+}. The patterns shown here are at $x = -1.5(Dt)^{1/2}$, where D is the average for all trivalent REE. This is roughly the position where the largest diffusive fractionation occurs.

DIFFUSIVITY IN CRYSTAL-BEARING AND BUBBLE-BEARING MAGMAS

Many diffusion media in geology are heterogeneous media, either due to the presence of multiple phases (such as mantle rocks, or magmas containing phenocrysts and/or bubbles), or the presence of boundaries that show different diffusion properties (e.g., Dohmen and Milke 2010). In such a system, diffusion at a length scale much larger than the heterogeneity (i.e., grain size) may be characterized by a bulk diffusivity or effective diffusivity, which for a given component i may be defined by:

$$\mathbf{J}_{i,\text{bulk}} = -D_{i,\text{bulk}} \nabla C_{i,\text{ave}}, \tag{61}$$

where $\mathbf{J}_{i,\text{bulk}}$ is the bulk flux, $D_{i,\text{bulk}}$ is the bulk diffusivity and $C_{i,\text{ave}}$ is the average concentration (in kg/m^3 or mol/m^3) of component i. $C_{i,\text{ave}}$ is defined as:

$$C_{i,\text{ave}} = \phi_1 C_{i,1} + \phi_2 C_{i,2} + ..., \tag{62}$$

where ϕ_1 and ϕ_2 are volume fractions of phases 1 and 2, and $C_{i,1}$ and $C_{i,2}$ are concentrations (in kg/m^3 or mol/m^3). To treat bulk diffusion in a heterogeneous medium, it is necessary to know

how the bulk diffusivity is related to individual-phase diffusivity. To simplify the task, all ϕ_i's are assumed to be constant so that growth and dissolution of crystals and bubbles are not considered in this section. Including growth and dissolution would require another set of kinetic equations to be solved together with diffusion and is beyond the scope of this review.

To the authors' knowledge, Brady (1983) first introduced the treatment of diffusion in heterogeneous media to geology literature and derived relations between bulk diffusivity and individual-phase diffusivities using the similarity between diffusivity and thermal conductivity. Unfortunately, the similarity does not hold perfectly, leading to errors in the derived relations. These errors were also found in other studies and famous books (e.g., Bell and Crank 1974; Crank 1975, Chapter 12; Davis et al. 1975; Cussler 1997, section 6.5.2). Zhang and Liu (2012) identified the error by realizing a key difference between diffusivity and conductivity. During thermal conduction, the heat flux is written to be proportional to temperature gradient. During diffusion, mass flux is normally written to be proportional to the concentration gradient. The difference is that temperature is a continuous function when a phase boundary is crossed, but concentration of a component is not continuous at local equilibrium. The discontinuity means that earlier derived relations for bulk or effective diffusivity in heterogeneous media only apply when the partition coefficient is 1 between the phases. Once this is realized, because chemical potential is continuous across phase boundaries, new analogy equations can be written between diffusion mobility and thermal conductivity where diffusion mobility M is defined as:

$$\mathbf{J}_i = -M_i \nabla \frac{\mu_i}{RT}, \tag{63}$$

$\mathbf{J}_i$ is mass flux, μ_i is chemical potential, and M_i is the mobility of component i. Zhang and Liu (2012) showed that in ideal and roughly ideal mixtures (note that Fick's law only applies to ideal and roughly ideal systems),

$$M_i \approx D_i C_i. \tag{64}$$

Hence, in deriving the relation between bulk diffusivity and individual-phase diffusivity, D_iC_i together (rather than D_i alone) should replace thermal conductivity in relating bulk conductivity and individual-phase conductivity. Zhang and Liu (2012) discussed some applications of the new analogy relations. Here we discuss bulk (or effective) diffusivity in crystal-bearing and bubble bearing magmas. We limit our discussion to low percentages of crystals and bubbles so that they do not interact with each other. What exactly is meant by low percentage is not precisely defined, but we expect that the derived relations are applicable at a volume fraction $\phi \leq 0.1$ and possibly at ϕ up to 0.2.

Thermal conductivity and electrical conductivity for heterogeneous media follow similar relations (Kerner 1956; Hashin and Shtrikman 1963). Maxwell (1873, p. 365) derived an expression for electrical resistivity when there are numerous spheres of phase 1 in phase 2, which can be written in terms of electrical conductivity:

$$\sigma_{\text{bulk}} = \frac{2\sigma_2 + \sigma_1 - 2\phi(\sigma_2 - \sigma_1)}{2\sigma_2 + \sigma_1 + \phi(\sigma_2 - \sigma_1)}\sigma_2 , \tag{65}$$

where σ means electrical conductivity, and ϕ means the volume fraction of phase 1 in the continuous phase 2. Using Zhang and Liu (2012) analogy between diffusivity and thermal conductivity, we obtain:

$$\frac{D_{\text{bulk}}}{D_2} = \frac{2 + KD_1/D_2 - 2\phi(1 - KD_1/D_2)}{2 + KD_1/D_2 + \phi(1 - KD_1/D_2)} \frac{C_2}{C_{\text{ave}}} , \tag{66}$$

where D_1 and C_1 are diffusivity and concentration (kg/m^3 or mol/m^3) in the dispersed phase 1 (such as crystals and/or bubbles), D_2 and C_2 are diffusivity and concentration (kg/m^3 or mol/m^3) in the continuous phase 2 (the melt in this work), $K = C_1/C_2 = \rho_1 w_1/(\rho_2 w_2)$ is the partition coefficient (taking into consideration the density difference between crystals and melt), and C_{ave}

$= \phi C_1 + (1-\phi) C_2$. The above derivation assumes that local equilibrium is reached between the dispersed spherical particles (all of which are the same phase, defined as phase 1) and the continuous melt (phase 2). That is, the diffusion distance in the continuous phase must be ≥ 10 times the particle diameter, and that in the dispersed spheres must be about the same as the radius for the equation to apply.

The bulk diffusivity is further elucidated below. If one plots bulk concentration (Eqn. 62) versus distance, the diffusivity obtained from fitting the profile is the bulk diffusivity. In addition, if one plots the concentration in any individual phase versus distance, the diffusivity obtained from fitting the profile is also the bulk diffusivity. This is illustrated in Fig. 18 for the case of melt and one phenocryst phase, with four panels: (a) a hypothetical measured concentration profile as one moves along a line that encounters both phases (this profile has spikes and cannot be fit by a constant D), (b) the average concentration profile, (c) the concentrations measured in the melt, and (d) the concentrations measured in phenocryst grains. Note that the average concentration, the concentration in the melt, and the concentration in phenocryst grains, are all proportional to one another. Hence, the three profiles in Fig. 18b,c,d are identical when normalized to the concentration at $x = 0$, and this normalized profile is characterized by a diffusivity equaling D_{bulk}. Therefore, in the case of diffusion in crystal or bubble-bearing magma, assuming local equilibrium between crystals and melt and between bubbles and melt, the diffusivity obtained by measuring concentrations profiles in any single phase (continuous phase, or many discrete grains along a direction) is also the bulk diffusivity or the effective diffusivity.

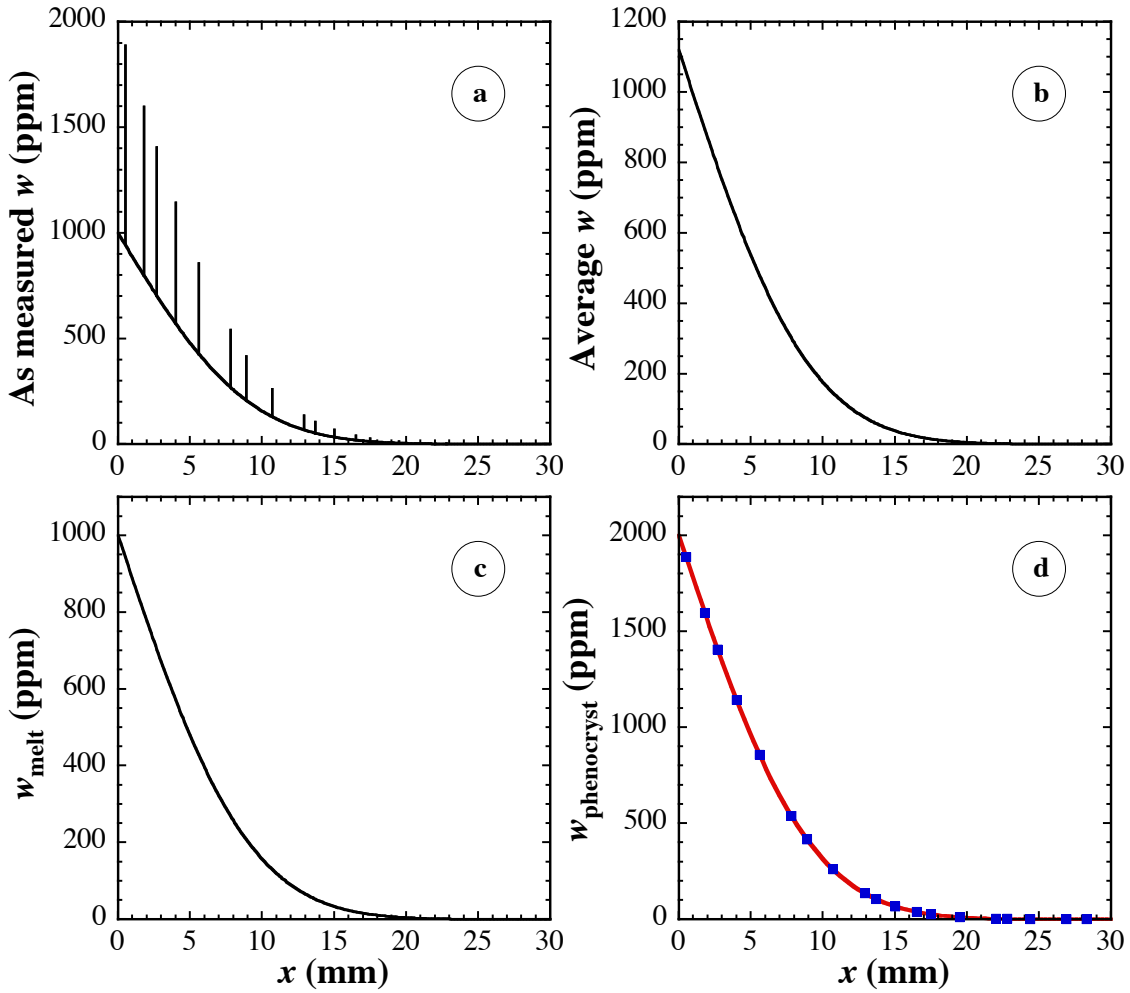

Figure 18. Calculated concentration profiles in a microphenocryst-bearing magma for the case of semi-infinite diffusion from one surface. Equilibrium elemental partition is assumed and the concentration in the microphenocryst is 2 times that in the melt. (a) A hypothetical measured profile when the measured points often encounter melt (glass) but occasionally encounter microphenocryst grains (spikes in the curve); (b) Calculated average concentration profile based on constant microphenocryst fraction; (c) Concentration profile by measuring points in the melt; (d) concentration profile by measuring points (blue squares) in different grains of the microphenocryst and fit to the points.

Crystal-bearing magmas

Here we apply Equation (66) to estimate bulk diffusivity in crystal-bearing magmas assuming equilibrium is reached between crystals and the melt. Let phase 1 be crystals, and phase 2 (continuous phase) be melt in Equation (66). Some limiting cases of interest are discussed below.

At the limit of very small $KD_{crystal}/D_{melt} << 1$ (this applies to essentially all components), Equation (66) becomes

$$\frac{D_{bulk}}{D_{melt}} = \frac{2(1-\phi)}{2+\phi}\frac{1}{\phi K + (1-\phi)}. \quad (67)$$

The above equation applies when the following conditions are satisfied:

(1) Diffusion distance in the melt is much greater than the diameter of the phenocrysts;

(2) Diffusion in the phenocrysts roughly reached the center of average phenocrysts, so that the phenocrysts are roughly in local equilibrium with the melt.

We temporarily define diffusion reaching the center to mean the center concentration reaching at least 72% equilibrium (which means that the whole phenocrysts reached >91.5% equilibrium), leading to $D_{crystal}t/a^2 \geq 0.2$ where a is radius (Crank 1975, p. 92). For typical diffusivities in minerals and melts, when condition 2 is satisfied, then condition 1 is also satisfied. For example, if the average phenocryst diameter is 0.1 mm (a = 0.05 mm), $D_{crystal}$ = 10^{-15} m^2/s (Spandler and O'Neill 2010), and $D_{melt} = 5x10^{-12}$ m^2/s, then $D_{crystal}t/a^2 \geq 0.2$ means $t \geq$ 5.79 days. After this time the diffusion distance in the melt is ≥1.58 mm, much greater than the phenocryst diameter. Therefore, condition 1 is also satisfied.

For a highly incompatible element (K<<1), Equation (66) becomes:

$$\frac{D_{bulk}}{D_{melt}} = \frac{1}{1+0.5\phi}. \quad (68)$$

To apply Equation (68), the two conditions listed below Equation (67) as well as K <<1 must be satisfied.

The variation of D_{bulk}/D_{melt} as a function of ϕ and K is plotted in Fig. 19. It can be seen that D_{bulk} is always smaller than D_{melt}. For K < 1, the effect of a small fraction of phenocrysts is

within uncertainty of diffusion data (~30%, Zhang et al. 2010). However, for highly compatible elements, D_{bulk} can be a factor of 3 lower than D_{melt} at 20% vol% of phenocrysts.

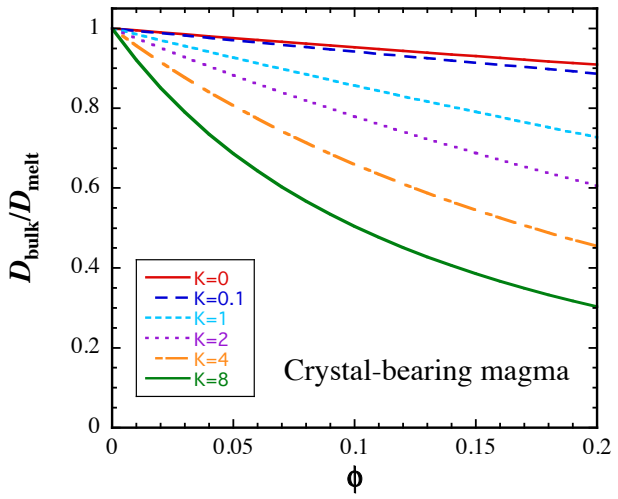

Figure 19. The dependence of D_{bulk}/D_{melt} on the volume fraction of crystals and partition coefficient $K = C_1/C_2 = \rho_1 w_1/(\rho_2 w_2)$ (where subscript "1" means crystal and "2" means melt) at the limit of $KD_1/D_2 << 1$.

If there is no rough equilibrium between the phenocrysts and melt, condition 2 below Equation (67) is not satisfied. Then Equation (67) cannot be applied. We consider another limiting case of constant crystal composition during a short-duration experiment. Because the phenocryst particles do not participate in the diffusion, one may just consider diffusion in the melt by ignoring partitioning. In this case, the phenocrysts play the role of small inert (non-active) blocks increasing tortuosity because atoms must diffuse around these particles, but do not participate in the compositional exchange. Mathematically, this may be treated using Equation (66) by adopting $K = 0$. Therefore, the effective diffusivity in the melt is given by Equation (68). That is, Equation (68) also describes how the tortuosity effect reduces the effective melt diffusivity in the limiting case that the crystals do not participate in the diffusion. Note that C_{ave} is irrelevant in the case of nonreactive phenocrysts because concentrations in the phenocrysts may be high or low but they do not participate in diffusion. Hence, effective diffusivity in the

melt is a better term than bulk diffusivity to describe diffusion in this case. We temporarily define nonreactive crystals by $D_{crystal}t/a^2 \le 10^{-4}$. For example, if the average phenocryst diameter is 100 μm (a = 50 μm), $D_{crystal} = 10^{-15}$ m^2/s = 10^{-3} μm^2/s (Spandler and O'Neill 2010), then t must be ≤ 250 s, meaning diffusion distance in the crystal is $(D_{crystal}t)^{1/2}$ =0.5 μm, for Equation (68) to be applicable. In such a case, if ϕ = 0.2, then D_{eff}/D_{melt} = 0.91. Because experimental diffusivities in silicate melts often have a relative error of 30% (e.g., Chen and Zhang 2008, 2009; Zhang et al. 2010), the effect of ≤20% nonreactive crystals is within diffusion data/model uncertainty.

For the time regime of $10^{-4} < D_{crystal}t/a^2 < 0.2$, one may use Equations (68) and (67) to find the lower and upper limits of D_{eff} in the melt. For a more precise estimation, a weighted average of the upper and lower limits is taken using the degree of equilibrium of the phenocrysts as weight:

$$\frac{D_{eff}}{D_{melt}} = \frac{2(1-\phi)}{2+\phi}\frac{1}{\phi K+(1-\phi)}\left(\frac{\Delta M_t}{\Delta M_\infty}\right)+\left(\frac{1-\phi}{1+0.5\phi}\right)\left(1-\frac{\Delta M_t}{\Delta M_\infty}\right), \quad (69)$$

where $\Delta M_t/\Delta M_\infty$ (which may be estimated using Eqn. 13c or 14c) means the degree of equilibrium for diffusion in phenocryst grains.

Bubble-bearing magmas

We now estimate bulk diffusivity in bubble-bearing magmas using Equation (66), with phase 1 being bubbles, and phase 2 being melt. Equation (66) for this specific case can be written as

$$\frac{D_{bulk}}{D_{melt}} = \frac{2+KD_{bubble}/D_{melt}-2\phi(1-KD_{bubble}/D_{melt})}{2+KD_{bubble}/D_{melt}+\phi(1-KD_{bubble}/D_{melt})}\frac{1}{\phi K+(1-\phi)}, \quad (70)$$

where $K_i = C_{i,bubble}/C_{i,melt}$, where $C_{i,bubble}$ and $C_{i,melt}$ must be in kg/m^3 or mol/m^3. There is only one condition for Equation (70) to be applicable: the diffusion distance in the melt must be much greater than the diameter of the bubbles. Adopting the unit of kg/m^3 for concentrations in both

phase, then $C_{i,\text{bubble}} = W_i X_{i,\text{bubble}} P/(RT)$ where $X_{i,\text{bubble}}$ is mole fraction of component i in the bubble and W_i is the molar mass of i in kg/mol, and $C_{i,\text{melt}} = w_{i,\text{melt}}\rho_{\text{melt}}$, where $w_{i,\text{melt}}$ is the mass fraction of i in the melt. Hence,

$$K_i = \frac{C_{i,\text{bubble}}}{C_{i,\text{melt}}} = \left(\frac{W_i X_{i,\text{bubble}} P}{w_{i,\text{melt}}\rho_{\text{melt}} RT}\right) = \frac{W_i}{S_i \rho_{\text{melt}} RT}, \tag{71}$$

where $S_i = w_{i,\text{melt}}/(X_{i,\text{bubble}}P)$ is solubility of i in the melt in mass fraction per Pa. The estimated values of K_i for H_2O and CO_2 at some conditions are listed in Table 11. For CO_2 and other gas species with solubility proportional to pressure, K_i is a constant in a given melt. For H_2O, K_i increases as pressure increases. The values of $K_i D_{i,\text{bubble}}/D_{i,\text{melt}}$ are listed in the last column of Table 10 as Ratio. It can be seen that $K_i D_{i,\text{bubble}}/D_{i,\text{melt}}$ for gas species is much greater than 1.

Table 11. Estimated values of K_i for H_2O and CO_2

Melt	Species	P MPa	T K	$C_{i,\text{bubble}}$ kg/m^3	$D_{i,\text{bubble}}$ μm^2/s	$w_{i,\text{melt}}$	$C_{i,\text{melt}}$ kg/m^3	K_i	$D_{i,\text{melt}}$ μm^2/s	Ratio
Rhyolite	H_2O	200	1100	394	72,000	0.0603	139	2.84	63.4	3,220
Rhyolite	H_2O	50	1200	90.3	328,000	0.0256	58.8	1.53	16.7	30,100
Rhyolite	H_2O	1	1400	1.55	2.07×10^7	0.00245	5.64	0.27	3.71	1.5×10^6
Basalt	CO_2	200	1500	706	26,400	0.001	2.7	261	6.07	1.1×10^6
Basalt	CO_2	1	1500	3.53	5.28×10^6	0.000005	0.0135	261	7.86	1.8×10^8

H_2O and CO_2 solubilities are calculated based on Zhang et al. (2007). Bubble is assumed to be pure H_2O for the first three cases and pure CO_2 for the last two cases. Melt density is taken as 2300 kg/m^3 for rhyolite and 2700 kg/m^3 for basalt. $D_{i,\text{bubble}}$ is estimated using elementary theory of diffusion in gases ($D=lv/3$ where l is the mean free path and v is the mean thermal speed). $D_{i,\text{melt}}$ is calculated from Ni and Zhang (2018) for H_2O, and Zhang and Ni (2010) for CO_2. Ratio = $K_i D_{i,\text{bubble}}/D_{i,\text{melt}}$.

For the limiting rare case of $K_i D_{i,\text{bubble}}/D_{i,\text{melt}} << 1$ (i.e., for a component that does not go into the bubbles at all), Equation (70) simplifies to:

$$\frac{D_{\text{bulk}}}{D_{\text{melt}}} = \frac{1}{1+0.5\phi}. \tag{72}$$

Note that Equation (72) is the same as Equation (68), meaning that the presence of bubbles increases the tortuosity of the diffusion path. Because $D_{i,\text{bubble}}/D_{i,\text{melt}}$ is typically >> 1 (decreasing with increasing pressure in the bubbles) and most components have some solubility in the vapor

phase, the applicability of Equation (72) is very limited because K_i would need to be really small (e.g., $<10^{-6}$). For example, a rough estimation for TiO_2 component in pure H_2O fluid phase in equilibrium with a basalt results in a $K_i \approx 0.003$ at 1273 K and 600 MPa (~100 ppm Ti in fluid, Antignano and Manning, 2008; ~2 wt% TiO_2 in hydrous basalt, Ryerson and Watson, 1987) and $K_i D_{i,\text{bubble}}/D_{i,\text{melt}} > 3$ depending on the pressure and how dissolved H_2O in basalt melt increases $D_{\text{Ti,melt}}$. Hence, even for the TiO_2 component that has low solubility in a fluid phase, Equation (72) still does not apply at 1273 K and 600 MPa.

A more widely applicable limiting case is $K_i D_{i,\text{bubble}}/D_{i,\text{melt}} >> 1$. Then Equation (70) simplifies to:

$$\frac{D_{\text{bulk}}}{D_{\text{melt}}} = \frac{(1+2\phi)}{(1-\phi)} \frac{1}{\phi K + (1-\phi)} . \tag{73}$$

Equation (73) is expected to apply well to H_2O and CO_2 and most other gas components (some $K_i D_{i,\text{bubble}}/D_{i,\text{melt}}$ values are listed in the last column of Table 11). Note that accurate values of $D_{i,\text{bubble}}$ and $D_{i,\text{melt}}$ are not needed as long as $K_i D_{i,\text{bubble}}/D_{i,\text{melt}} >> 1$. Fig. 20 displays how $D_{\text{bulk}}/D_{\text{melt}}$ depends on ϕ and K. Note that D_{bulk} may be greater or smaller than D_{melt} depending the value of K. When K is large (e.g., > 100, for CO_2), $D_{\text{bulk}}/D_{\text{melt}}$ can be much smaller than 1 even at a few percent of bubbles.

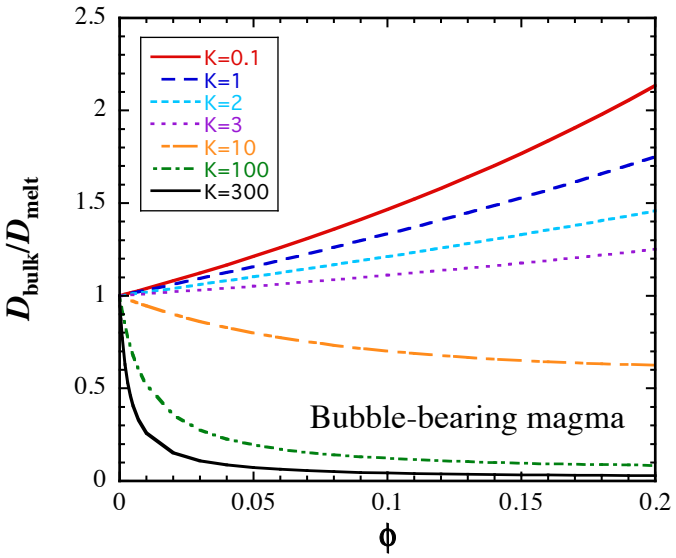

Figure 20. The dependence of D_{bulk}/D_{melt} on the volume fraction of bubbles and partition coefficient K at the limit of $KD_{bubble}/D_{melt} >> 1$. The relation applies to essentially all gas components. Table 11 gives some estimated K and KD_{bubble}/D_{melt} values. No $K = 0$ limiting curve is shown because it violates the condition that $KD_{bubble}/D_{melt} >> 1$.

In literature studies of H_2O diffusion, often there were a few volume percent of bubbles present in the experimental charges. The authors stated that a few volume percent of bubbles would not affect the extracted diffusion coefficient of H_2O significantly (e.g., Zhang et al. 1991a). Our results in Fig. 20 show the presence of 2 vol% of bubbles would increase the bulk diffusivity by less than 10%, and hence validate their statement. On the other hand, the effect of 2 vol% of bubbles could decrease the bulk diffusivity of CO_2 in melt by a factor of 6. The reduction of bulk diffusivity in the melt may sound counterintuitive. The reason is that even at 2 vol% of bubbles, most CO_2 is in bubbles, rather than in the melt. Although diffusion in bubbles is rapid, bubbles are isolated from one another. Hence, CO_2 transport is by diffusion in the melt, whereas bubbles buffer the CO_2 concentration in the melt to some degree. Hence, as CO_2 diffuses in the melt, CO_2 concentration in the melt does not change so much as in the case of no bubbles, leading to a decrease in the effective CO_2 diffusivity. Because the presence of bubbles may significantly impact on CO_2 diffusivity as well as diffusivity of other gases (such as noble

gases) with low solubility in silicate melts, it is critical to prevent bubbles in the experimental charges for diffusion of these gases (e.g., Spickenbom et al. 2010).

CONCLUSIONS

This review on diffusion in silicate melts and magmas mostly covers the progresses since the publication of *Diffusion in Minerals and Melts* as volume 72 of *Reviews in Mineralogy and Geochemistry* in 2010. Major advancement has been made in a number of fields. Multicomponent diffusion studies have made it possible to roughly predict diffusion of all major components in basalt melt during mixing of different basalts or mineral dissolution and growth. Diffusive isotope fractionation in melts has been examined for various elements in different melts, and simultaneous treatment of isotope diffusion and multicomponent diffusion has been developed. Theory has become available to treat diffusion in crystal-bearing or bubble-bearing magmas. In terms of diffusion data, great efforts have been made by some authors to generate a large number of data, which have been applied to model and understand diffusive elemental fractionation and have applications in many other diffusion problems.

ACKNOWLEDGEMENT

We thank an anonymous reviewer for constructive and insightful comments. This work is partially supported by NSF grants EAR-1829822 and EAR-2020603, and NASA grant 80NSSC19K0782.

REFERENCES

Acosta-Vigil A, London D, Morgan VI GB (2012) Chemical diffusion of major components in granitic liquids: implications for the rates of homogenization of crustal melts. Lithos

153:308-323
Allegre CJ, Minster JF (1978) Quantitative models of trace element behavior in magmatic processes. Earth Planet Sci Lett 38:1-25
Amalberti J, Burnard P, Tissandier L, Laporte D (2018) The diffusion coefficients of noble gases (He-Ar) in a synthetic basaltic liquid: one-dimensional diffusion experiments. Chem Geol 480:35-43
Antignano A, Manning CE (2008) Rutile solubility in H_2O, H_2O-SiO_2, and H_2O-$NaAlSi_3O_8$ fluids at 0.7-2.0 GPa and 700-1000°C: implications for mobility of nominally insoluble elements. Chem Geol 255:283-293
Bai TB, Koster van Groos AF (1994) Diffusion of chlorine in granitic melts. Geochim Cosmochim Acta 58:113-123
Balcone-Boissard H, Baker DR, Villemant B, Boudon G (2009) F and Cl diffusion in phonolitic melts: influence of the Na/K ratio. Chem Geol 263:89-98
Behrens H (2010) Noble gas diffusion in silicate glasses and melts. Rev Mineral Geochem 72:227-267
Behrens H (2010) Ar, CO_2 and H_2O diffusion in silica glasses at 2 kbar pressure. Chem Geol 272:40-48
Behrens H, Hahn M (2009) Trace element diffusion and viscous flow in potassium-rich trachytic and phonolitic melts. Chem Geol 259:63-77
Behrens H, Stelling J (2011) Diffusion and redox reactions of sulfur in silicate melts. Rev Mineral Geochem 73:79-111
Behrens H, Zhang Y (2001) Ar diffusion in hydrous silicic melts: implications for volatile diffusion mechanisms and fractionation. Earth Planet Sci Lett 192:363-376
Behrens H, Zhang Y (2009) H_2O diffusion in peralkaline to peraluminous rhyolitic melts. Contrib Mineral Petrol 157:765-780
Behrens H, Zhang Y, Leschik M, Miedenbeck M, Heide G, Frischat GH (2007) Molecular H_2O as carrier for oxygen diffusion in hydrous silicate melts. Earth Planet Sci Lett 254:69-76
Behrens H, Zhang Y, Xu Z (2004) H_2O diffusion in dacitic and andesitic melts. Geochim Cosmochim Acta 68:5139-5150
Bell GE, Crank J (1974) Influence of imbedded particles on steady-state diffusion. J Chem Soc Faraday Trans II 70:1259-1273
Bohm A, Schmidt BC (2013) Fluorine and chlorine diffusion in phonolitic melt. Chem Geol 346:162-171
Brady JB (1975) Reference frames and diffusion coefficients. Am J Sci 275:954-983
Brady JB (1983) Intergranular diffusion in metamorphic rocks. Am J Sci 283-A:181-200
Carroll MR (1991) Diffusion of Ar in rhyolite, orthoclase and albite composition glasses. Earth Planet Sci Lett 103:156-168
Carroll MR, Stolper EM (1991) Argon solubility and diffusion in silica glass: implications for the solution behavior of molecular gases. Geochim Cosmochim Acta 55:211-225
Carslaw HS, Jaeger JC (1959) Conduction of Heat in Solids. Clarendon Press, Oxford
Chakraborty S, Dingwell DB, Rubie DC (1995a) Multicomponent diffusion in ternary silicate melts in the system K_2O-Al_2O_3-SiO_2: I. Experimental measurements. Geochim Cosmochim Acta 59:255-264
Chakraborty S, Dingwell DB, Rubie DC (1995b) Multicomponent diffusion in ternary silicate melts in the system K_2O-Al_2O_3-SiO_2: II. mechanisms, systematics, and geological applications. Geochim Cosmochim Acta 59:265-277

Chen Y, Zhang Y (2008) Olivine dissolution in basaltic melt. Geochim Cosmochim Acta 72:4756-4777
Chen Y, Zhang Y (2009) Clinopyroxene dissolution in basaltic melt. Geochim Cosmochim Acta 73:5730-5747
Cherniak DJ, Hervig RL, Koepke J, Zhang Y, Zhao D (2010) Analytical methods in diffusion studies. Rev Mineral Geochem 72:107-170
Chopra R, Richter FM, Watson EB, Scullard CR (2012) Magnesium isotope fractionation by chemical diffusion in natural settings and in laboratory analogues. Geochim Cosmochim Acta 88:1-18
Cicconi MR, Giuli G, Paris E, Courtial P, Dingwell DB (2013) XAS investigation of rare earth elements in sodium disilicate glasses. J Non-Cryst Sol 362:162-168
Claireaux C, Chopinet MH, Burov E, Gouillart E, Roskosz M, Toplis MJ (2016) Atomic mobility in calcium and sodium aluminosilicate melts at 1200°C. Geochim Cosmochim Acta 192:235-247
Claireaux C, Chopinet MH, Burov E, Montigaud H, Roskosz M, Toplis MJ, Gouillart E (2019) Influence of temperature on multicomponent diffusion in calcium and sodium aluminosilicate melts. J Non-Cryst Sol 505:170-180
Cooper AR (1968) The use and limitations of the concept of an effective binary diffusion coefficient for multi-component diffusion. *In*: Mass Transport in Oxides. Vol 296. Wachman JB, Franklin AD, (eds). Nat. Bur. Stand. Spec. Publ., p 79-84
Crank J (1975) The Mathematics of Diffusion. Clarendon Press, Oxford
Cunningham GJ, Henderson P, Lowry RK, Nolan J, Reed SJB, Long JVP (1983) Lithium diffusion in silicate melts. Earth Planet Sci Lett 65:203-205
Cussler EL (1997) Diffusion: Mass Transfer in Fluid Systems. Cambridge Univ Press, Cambridge, England
Davis HT, Valencourt LR, Johnson CE (1975) Transport processes in composite media. J Am Ceram Soc 58:446-452
De Groot SR, Mazur P (1962) Non-Equilibrium Thermodynamics. Interscience, New York
De Koker N, Stixrude L (2010) Theoretical computation of diffusion in minerals and melts. Rev Mineral Geochem 72:971-996
Delaney JR, Karsten JL (1981) Ion microprobe studies of water in silicate melts: concentration-dependent water diffusion in obsidian. Earth Planet Sci Lett 52:191-202
Dingwell DB (1990) Effects of structural relaxation on cationic tracer diffusion in silicate melts. Chem Geol 82:209-216
Dohmen R, Milke R (2010) Diffusion in polycrystalline materials: grain boundaries, mathematical models, and experimental data. Rev Mineral Geochem 72:921-970
Doremus RH (1969) The diffusion of water in fused silica. *In*: Reactivity of Solids. Mitchell JW, Devries RC, Roberts RW, Cannon P, (eds). Wiley, New York, p 667-673
Einstein A (1905) The motion of small particles suspended in static liquids required by the molecular kinetic theory of heat. Ann Phys 17:549-560
Eyring H (1936) Viscosity, plasticity, and diffusion as examples of absolute reaction rates. J Chem Phys 4:283-291
Fanara S, Behrens H, Zhang Y (2013) Water diffusion in potassium-rich phonolitic and trachytic melts. Chem Geol 346:149-161
Fanara S, Sengupta P, Becker H-W, Rogalla D, Chakraborty S (2017) Diffusion across the glass transition in silicate melts: systematic correlations, new experimental data for Sr and Ba in

calcium-aluminosilicate glass and general mechanisms of ionic transport. J Non-Cryst Sol 455:6-16
Fortin M-A, Watson EB, Stern R (2017) The isotope mass effect on chlorine diffusion in dacite melt, with implications for fractionation during bubble growth. Earth Planet Sci Lett 480:15-24
Freda C, Baker DR, Romano C, Scarlato P (2003) Water diffusion in natural potassic melts. Geol Soc Spec Publ 213:53-62
Frischat GH, Szurman M (2011) Role of sulfur and its diffusion in silicate glass melts. Appl Glass Sci 2:47-51
Gast PW (1968) Trace element fractionation and the origin of tholeiitic and alkaline magma types. Geochim Cosmochim Acta 32:1057-1086
Giordano D, Russel JK, Dingwell D (2008) Viscosity of magmatic liquids: a model. Earth Planet Sci Lett 271:123-134
Gonzalez-Garcia D, Behrens H, Petrelli M, Vetere F, Morgavi D, Zhang C, Perugini D (2017) Water-enhanced interdiffusion of major elements between natural shoshonite and high-K rhyolite melts. Chem Geol 466:86-101
Gonzalez-Garcia D, Petrelli M, Behrens H, Vetere F, Fischer LA, Morgavi D, Perugini D (2018) Diffusive exchange of trace elements between alkaline melts: implications for element fractionation and time scale estimations during magma mixing. Geochim Cosmochim Acta 233:95-114
Guo C, Zhang Y (2016) Multicomponent diffusion in silicate melts: SiO_2-TiO_2-Al_2O_3-MgO-CaO-Na_2O-K_2O system. Geochim Cosmochim Acta 195:126-141
Guo C, Zhang Y (2018) Multicomponent diffusion in basaltic melts at 1350°C. Geochim Cosmochim Acta 228:190-204
Guo C, Zhang Y (2019a) Corrigendum to ‘‘Multicomponent diffusion in silicate melts: SiO_2-TiO2-Al_2O_3-MgO-CaO-Na_2O-K_2O system” [Geochim. Cosmochim. Acta 195 (2016) 126–141]. Geochim Cosmochim Acta 259:412
Guo C, Zhang Y (2019b) Corrigendum to ‘‘Multicomponent diffusion in basaltic melts at 1350 °C’’ [Geochim. Cosmochim. Acta 228 (2018) 190–204]. Geochim Cosmochim Acta 259:413
Guo C, Zhang Y (2020) Multicomponent diffusion in a basaltic melt: temperature dependence. Chem Geol 549: 119700
Harrison TM, Watson EB (1983) Kinetics of zircon dissolution and zirconium diffusion in granitic melts of variable water content. Contrib Mineral Petrol 84:66-72
Hashin Z, Shtrikman S (1963) Conductivity of polycrystals. Phys Rev 130:129-133
Henderson P, Nolan J, Cunningham GC, Lowry RK (1985) Structural controls and mechanisms of diffusion in natural silicate melts. Contrib Mineral Petrol 89:263-272
Hess K, Dingwell DB (1996) Viscosities of hydrous leucogranitic melts: a non-Arrhenian model. Am Mineral 81:1297-1300
Hofmann AW, Giletti BJ, Yoder HS, Yund RA (eds) (1974) Geochemical Transport and Kinetics. Carnegie Institution of Washington Publ., Washington, DC
Holycross ME, Watson EB (2016) Diffusive fractionation of trace elements in basaltic melt. Contrib Mineral Petrol 171:80(15 pages)
Holycross ME, Watson EB (2018) Trace element diffusion and kinetic fractionation in wet rhyolitic melt. Geochim Cosmochim Acta 232:14-29
Holycross ME, Watson EB, Richter FM, Villeneuve J (2018) Diffusive fractionation of Li isotopes in wet, highly silicic melts. Geochem Persp Lett 6:39-42

Huber C, Bachmann O, Manga M (2009) Homogenization processes in silicic magma chambers by stirring and mushification (latent heat buffering). Earth Planet Sci Lett 283:38-47
Hui H, Zhang Y (2007) Toward a general viscosity equation for natural anhydrous and hydrous silicate melts. Geochim Cosmochim Acta 71:403-416
Jambon A (1980) Isotopic fractionation: a kinetic model for crystals growing from magmatic melts. Geochim Cosmochim Acta 44:1373-1380
Jambon A (1982) Tracer diffusion in granitic melts: experimental results for Na, K, Rb, Cs, Ca, Sr, Ba, Ce, Eu to 1300°C and a model of calculation. J Geophys Res 87:10797-10810
Jambon A, Carron JP (1976) Diffusion of Na, K, Rb and Cs in glasses of albite and orthoclase composition. Geochim Cosmochim Acta 49:897-903
Jambon A, Semet MP (1978) Lithium diffusion in silicate glasses of albite, orthoclase, and obsidian compositions: an ion-microprobe determination. Earth Planet Sci Lett 37:445-450
Jambon A, Zhang Y, Stolper EM (1992) Experimental dehydration of natural obsidian and estimation of D_{H2O} at low water contents. Geochim Cosmochim Acta 56:2931-2935
Karsten JL, Holloway JR, Delaney JR (1982) Ion microprobe studies of water in silicate melts: temperature-dependent water diffusion in obsidian. Earth Planet Sci Lett 59:420-428
Kaufmann J, Russel C (2008) Redox behavior and diffusion of copper in soda-lime-silica melts. J Non-Cryst Sol 354:4614-4619
Kaufmann J, Russel C (2010) Diffusion of copper in soda-silicate and soda-lime-silicate melts. J Non-Cryst Sol 356:1158-1162
Kaufmann J, Russel C (2011) Diffusivity of copper in aluminosilicate melts, studied by square wave voltametry. Phys Chem Glas 52:101-106
Kerner EH (1956) The electrical conductivity of composite media. Proc Phys Soc B 69:802-807
Kirkaldy JS, Young DJ (1987) Diffusion in the Condensed State. The Institute of Metals, London
Koepke J, Behrens H (2001) Trace element diffusion in andesitic melts: an application of synchrontron X-ray fluorescence analysis. Geochim Cosmochim Acta 65:1481-1498
Koyaguchi T (1985) Magma mixing in a conduit. J Volcanol Geotherm Res 25:365-369
Koyaguchi T (1989) Chemical gradient at diffusive interfaces in magma chambers. Contrib Mineral Petrol 103:143-152
Lasaga AC (1983) Geospeedometry: an extension of geothermometry. *In*: Kinetics and Equilibrium in Mineral Reactions. Saxena SK, (ed) Springer-Verlag, New York
Lasaga AC (1998) Kinetic Theory in the Earth Sciences. Princeton University Press, Princeton, NJ
Lasaga AC, Kirkpatrick RJ (eds) (1981) Kinetics of Geochemical Processes. Mineralogical Society of America
Lesher CE (2010) Self-diffusion in silicate melts: theory, observations and applications to magmatic systems. Rev Mineral Geochem 72:269-309
Lesher CE, Walker D (1986) Solution properties of silicate liquids from thermal diffusion experiments. Geochim Cosmochim Acta 50:1397-1411
Lesher CE, Hervig RL, Tinker D (1996) Self diffusion of network formers (silicon and oxygen) in naturally occurring basaltic liquid. Geochim Cosmochim Acta 60:405-413
Liang Y (2000) Dissolution in molten silicates: effects of solid solution. Geochim Cosmochim Acta 64:1617-1627
Liang Y (2010) Multicomponent diffusion in molten silicates: theory, experiments, and geological applications. Rev Mineral Geochem 72:409-446

Liang Y, Davis AM (2002) Energetics of multicomponent diffusion in molten CaO-Al_2O_3-SiO_2. Geochim Cosmochim Acta 66:635-646
Liang Y, Richter FM, Chamberlin L (1997) Diffusion in silicate melts, III: empirical models for multicomponent diffusion. Geochim Cosmochim Acta 61:5295-5312
Liang Y, Richter FM, Davis AM, Watson EB (1996a) Diffusion in silicate melts, I: self diffusion in CaO-Al_2O_3-SiO_2 at 1500°C and 1 GPa. Geochim Cosmochim Acta 60:4353-4367
Liang Y, Richter FM, Watson EB (1996b) Diffusion in silicate melts, II: multicomponent diffusion in CaO-Al_2O_3-SiO_2 at 1500°C and 1 GPa. Geochim Cosmochim Acta 60:5021-5035
Lierenfeld MB, Zajacz Z, Bachmann O, Ulmer P (2018) Sulfur diffusion in dacitic melt at various oxidation states: implications for volcanic degassing. Geochim Cosmochim Acta 226:50-68
Lierenfeld MB, Zhong X, Reusser E, Kunze K, Putlitz B, Ulmer P (2019) Species diffusion in clinopyroxene solid solution in the diopside-anorthite system. Contrib Mineral Petrol 174:46
Liu Y, Zhang Y (2000) Bubble growth in rhyolitic melt. Earth Planet Sci Lett 181:251-264
Liu Y, Zhang Y, Behrens H (2004) H_2O diffusion in dacitic melt. Chem Geol 209:327-340
Lowry RK, Henderson P, Nolan J (1982) Tracer diffusions of some alkali, alkaline-earth and transition element ions in a basaltic and andesitic melt, and the implications concerning melt structure. Contrib Mineral Petrol 80:254-261
Lowry RK, Reed SJB, Nolan J, Henderson P, Long JVP (1981) Lithium tracer-diffusion in an alkali-basaltic melt - an ion-microprobe determination. Earth Planet Sci Lett 53:36-40
Macris CA, Asimow PD, Badro J, Eiler JM, Zhang Y, Stolper EM (2018) Seconds after impact: insights into the thermal history of impact ejecta from diffusion between lechateliertite and host glass in tektites and experiments. Geochim Cosmochim Acta 241:69-94
Matano C (1933) On the relation between the diffusion coefficient and concentrations of solid metals. Japan J Phys 8:109-113
Maxwell JC (1873) Treatise on Electricity and Magnetism. Oxford Univ Press, London
Mungall JE (2002) Empirical models relating viscosity and tracer diffusion in magmatic silicate melts. Geochim Cosmochim Acta 66:125-143
Mungall JE, Dingwell DB, Chaussidon M (1999) Chemical diffusivities of 18 trace elements in granitoid melts. Geochim Cosmochim Acta 63:2599-2610
Mungall JE, Romano C, Dingwell DB (1998) Multicomponent diffusion in the molten system K_2O-Na_2O-Al_2O_3-SiO_2-H_2O. Am Mineral 83:685-699
Newcombe ME, Beckett JR, Baker MB, Newman S, Guan Y, Eiler JM, Stolper EM (2019) Effects of pH_2O, pH_2, and fO_2 on the diffusion of H-bearing species in lunar basaltic liquid and an iron-free basaltic analog at 1 atm. Geochim Cosmochim Acta 250:316-343
Newcombe ME, Fabbrizio A, Zhang Y, Ma C, Le Voyer M, Guan Y, Eiler JM, Saal AE, Stolper EM (2014) Chemical zonation in olivine-hosted melt inclusions. Contrib Mineral Petrol 168:1030
Newcombe ME, Plank T, Zhang Y, Holycross M, Barth A, Lloyd AS, Ferguson D, Hauri E (2020) Magma pressure-temperature-time paths during mafic explosive eruptions. Frontiers, accepted.
Ni H (2012) Compositional dependence of alkali diffusivity in silicate melts: mixed alkali effect and pseudo-alkali effect. Am Mineral 97:70-79
Ni H, Zhang Y (2008) H_2O diffusion models in rhyolitic melt with new high pressure data. Chem Geol 250:68-78

Ni P, Zhang Y (2016) Cu diffusion in a basaltic melt. Am Mineral 101:1474-1482
Ni H, Behrens H, Zhang Y (2009b) Water diffusion in dacitic melt. Geochim Cosmochim Acta 73:3642-3655
Ni H, Hui H, Steinle-Neumann G (2015) Transport properties of silicate melts. Rev Geophys 53:715-744
Ni H, Liu Y, Wang L, Zhang Y (2009a) Water speciation and diffusion in haploandesitic melts at 743-873 K and 100 MPa. Geochim Cosmochim Acta 73:3630-3641
Ni H, Shi H, Zhang L, Li W-C, Guo X, Liang T (2018) Cu diffusivity in granitic melts with application to the formation of porphyry Cu deposits. Contrib Mineral Petrol 173:50
Ni H, Xu Z, Zhang Y (2013) Hydroxyl and molecular H_2O diffusivity in a haploandesitic melt. Geochim Cosmochim Acta 103:36-48
Ni P, Zhang Y, Guan Y (2017) Volatile loss during homogenization of lunar melt inclusions. Earth Planet Sci Lett 478:214-224
Ni P, Zhang Y, Simon A, Gagnon J (2017) Cu and Fe diffusion in rhyolitic melts during chalcocite "dissolution": implications for porphyry ore deposits and tektites. Am Mineral 102:1287-1301
Nowak M, Behrens H (1997) An experimental investigation on diffusion of water in haplogranitic melts. Contrib Mineral Petrol 126:365-376
Obukhovsky VV, Kutsyk AM, Nikonova VV, Ilchenko OO (2017) Nonlinear diffusion in multicomponent liquid solutions. Phys Rev E 95:022133
Oishi Y, Nanba M, Pask JA (1982) Analysis of liquid-state interdiffusion in the system CaO-Al_2O_3-SiO_2 using multiatomic ion models. J Am Cer Soc 65:247-253
Okumura S, Nakashima S (2004) Water diffusivity in rhyolitic glasses as determined by in situ IR spectroscopy. Phys Chem Minerals 31:183-189
Okumura S, Nakashima S (2006) Water diffusion in basaltic to dacitic glasses. Chem Geol 227:70-82
Pablo H, Schuller S, Toplis MJ, Gouillart E, Mostefaoui S, Charpentier T, Roskosz M (2017) Multicomponent diffusion in sodium borosilicate glasses. J Non-Cryst Sol 478:29-40
Persikov ES, Bukhtiyarov PG, Nekrasov AN, Bondarenko GV (2014) Concentration dependence of water diffusion in obsidian and dacitic melts at high pressures. Geochem Int 52:365-371
Persikov ES, Newman S, Bukhtiyarov PG, Nekrasov AN, Stolper EM (2010) Experimental study of water diffusion in haplobasaltic and haploandesitic melts. Chem Geol 276:241-256
Posner ES, Schmickler B, Rubie DC (2018) Self-diffusion and chemical diffusion in peridotite melt at high pressure and implications for magma ocean viscosities. Chem Geol 502:66-75
Proussevitch AA, Sahagian DL (1998) Dynamics and energetics of bubble growth in magmas: analytical formulation and numerical modeling. J Geophys Res 103:18223-18251
Reid JE, Poe BT, Rubie DC, Zotov N, Wiedenbeck M (2001) The self-diffusion of silicon and oxygen in diopside ($CaMgSi_2O_6$) liquid up to 15 GPa. Chem Geol 174:77-86
Richter FM, Davis AM, DePaolo DJ, Watson EB (2003) Isotope fractionation by chemical diffusion between molten basalt and rhyolite. Geochim Cosmochim Acta 67:3905-3923
Richter FM, Liang Y, Davis AM (1999) Isotope fractionation by diffusion in molten oxides. Geochim Cosmochim Acta 63:2853-2861
Richter FM, Watson EB, Chaussidon M, Mendybaev R, Christensen JN, Qiu L (2014) Isotope fractionation of Li and K in silicate liquids by Soret diffusion. Geochim Cosmochim Acta 138:136-145
Richter FM, Watson EB, Mendybaev RA, Dauphas N, Georg B, Watkins JM, Valley JW (2009)

Isotopic fractionation of the major elements of molten basalt by chemical and thermal diffusion. Geochim Cosmochim Acta 73:4250-4263
Richter RM, Watson EB, Mendybaev RA, Teng FZ, Janney PE (2008) Magnesium isotope fractionation in silicate melts by chemical and thermal diffusion. Geochim Cosmochim Acta 72:206-220
Ryerson FJ, Watson EB (1987) Rutile saturation in magmas: implication for Ti-Nb-Ta depletion in island-arc basalts. Earth Planet Sci Lett 86:225-239
Ryerson FJ, Durham WB, Cherniak DJ, Lanford WA (1989) Oxygen diffusion in olivine: effect of oxygen fugacity and implications for creep. J Geophys Res 94:4105-4118
Sauer VF, Freise V (1962) Diffusion in binaren Gemischen mit Volumenanderung. Z Elektrochem Angew Phys Chem 66:353-363
Shang LB, Chou IM, Lu WJ, Burruss RC, Zhang Y (2009) Determination of diffusion coefficients of hydrogen in fused silica between 296 and 523 K by Raman spectroscopy and application of fused silica capillaries in studying redox reactions. Geochim Cosmochim Acta 73:5435-5443
Shannon RD (1976) Revised effective ionic radii and systematic studies of interatomic distances in halides and chalcogenides. Acta Cryst A32:751-767
Shaw DM (1970) Trace element fractionation during anatexis. Geochim Cosmochim Acta 34:237-243
Shaw HR (1974) Diffusion of H_2O in granitic liquids, I: experimental data; II: mass transfer in magma chambers. *In*: Geochemical Transport and Kinetics. Vol 634. Hofmann AW, Giletti BJ, Yoder HS, Yund RA, (eds). Carnegie Institution of Washington Publ., Washington, DC, p 139-170
Shewmon PG (1989) Diffusion in Solids. Minerals, Metals & Materials Society, Warrendale, PA
Shimizu N, Kushiro I (1984) Diffusivity of oxygen in jadeite and diopside melts at high pressures. Geochim Cosmochim Acta 48:1295-1303
Spandler C, O'Neill HSC (2010) Diffusion and partition coefficients of minor and trace elements in San Carlos olivine at 1300°C with some geochemical implications. Contrib Mineral Petrol 159:791-818
Sparks RSJ (1978) The dynamics of bubble formation and growth in magmas: A review and analysis. J Volcanol Geotherm Res 3:1-37
Spickenbom K, Sierralta M, Nowak M (2010) Carbon dioxide and argon diffusion in silicate melts: insights into the CO2 speciation in magmas. Geochim Cosmochim Acta 74:6541-6564
Stanton TR, Holloway JR, Hervig RL, Stolper EM (1985) Isotopic effect on water diffusivity in silicic melts. Eos 66:1131
Stolper EM (1982a) Water in silicate glasses: an infrared spectroscopic study. Contrib Mineral Petrol 81:1-17
Stolper EM (1982b) The speciation of water in silicate melts. Geochim Cosmochim Acta 46:2609-2620
Sugawara H, Nagata K, Goto KS (1977) Interdiffusivities matrix of CaO-Al_2O_3-SiO_2 melt at 1723 K to 1823 K. Metall Trans 8B:605-612
Tinker D, Lesher CE (2001) Self diffusion of Si and O in dacitic liquid at high pressures. Am Mineral 86:1-13
Tinker D, Lesher CE, Baxter GM, Uchida T, Wang Y (2004) High-pressure viscometry of polymerized silicate melts and limitations of the Eyring equation. Am Mineral 89:1701-1708
Tinker D, Lesher CE, Hucheon ID (2003) Self-diffusion of Si and O in diopside-anorthite melt at

high pressures. Geochim Cosmochim Acta 67:133-142
Trail D, Cherniak DJ, Watson EB, Harrison TM, Weiss BP, Szumila I (2016) Li zoning in zircon as a potential geospeedometer and peak temperature indicator. Contrib Mineral Petrol 171:25, DOI 10.1007/s00410-00016-01238-00418
Trial AF, Spera FJ (1994) Measuring the multicomponent diffusion matrix: experimental design and data analysis for silicate melts. Geochim Cosmochim Acta 58:3769-3783
Varshneya AK, Cooper AR (1972) Diffusion in the system K_2O-SrO-SiO_2, III: interdiffusion coefficients. J Am Ceram Soc 55:312-317
Von der Gonna G, Russel C (2000) Diffusivity of various polyvalent elements in a $Na_2O{\cdot}2SiO_2$ glass melt. J Non-Cryst Solids 261:204-210
Vrentas JS, Vrentas CM (2016) Diffusion and Mass Transfer. CRC Press
Wang H, Xu Z, Behrens H, Zhang Y (2009) Water diffusion in Mount Changbai peralkaline rhyolitic melt. Contrib Mineral Petrol 158:471-484
Wasserburg GJ (1988) Diffusion of water in silicate melts. J Geol 96:363-367
Watkins JM, DePaolo DJ, Huber C, Ryerson FJ (2009) Liquid composition-dependence of calcium isotope fractionation during diffusion in molten silicates. Geochim Cosmochim Acta 73:7341-7359
Watkins JM, DePaolo DJ, Ryerson FJ, Peterson BT (2011) Influence of liquid structure on diffusive isotope separation in molten silicates and aqueous solutions. Geochim Cosmochim Acta 75:3103-3118
Watkins JM, DePaolo DJ, Watson EB (2017) Kinetic fractionation of non-traditional stable isotopes by diffusion and crystal growth reactions. Rev Mineral Geochem 82:85-125
Watkins JM, Liang Y, Richter F, Ryerson FJ, DePaolo DJ (2014) Diffusion of multi-isotopic chemical species in molten silicates. Geochim Cosmochim Acta 139:313-326
Watson EB (1976) Two-liquid partitioning coefficients: experimental data and geochemical implications. Contrib Mineral Petrol 56:119-134
Watson EB (1982) Basalt contamination by continental crust: some experiments and models. Contrib Mineral Petrol 80:73-87
Watson EB (2017) Diffusive fractionation of volatiles and their isotopes during bubble growth in magmas. Contrib Mineral Petrol 172:61 (21 pages)
Watson EB, Cherniak DJ, Holycross ME (2015) Diffusion of phosphorus in olivine and molten basalt. Am Mineral 100:2053-2065
Watson EB, Muller T (2009) Non-equilibrium isotopic and elemental fractionation during diffusion-controlled crystal growth under static and dynamic conditions. Chem Geol 267:111-124
Williams EL (1965) Diffusion of oxygen in fused silica. J Am Ceram Soc 48:190-194
Yang Y, Zhang Y, Simon A, Ni P (2016) Cassiterite dissolution and Sn diffusion in silicate melts of variable water content. Chem Geol 441:162-176
Yoshimura S (2018) Chlorine diffusion in rhyolite under low-H_2O conditions. Chem Geol 483:619-630
Yu Y, Zhang Y, Chen Y, Xu Z (2016) Kinetics of anorthite dissolution in basaltic melt. Geochim Cosmochim Acta 179:257-274
Yu Y, Zhang Y, Yang Y (2019) Kinetics of quartz dissolution in natural silicate melts and dependence of SiO2 diffusivity on melt composition. ACS Earth Space Chem 3:599-616
Zhang Y (1993) A modified effective binary diffusion model. J Geophys Res 98:11901-11920
Zhang Y (1994) Reaction kinetics, geospeedometry, and relaxation theory. Earth Planet Sci Lett

122:373-391
Zhang Y (1999) H_2O in rhyolitic glasses and melts: measurement, speciation, solubility, and diffusion. Rev Geophys 37:493-516
Zhang Y (2008) Geochemical Kinetics. Princeton University Press, Princeton, NJ
Zhang Y (2010) Diffusion in minerals and melts: theoretical background. Rev Mineral Geochem 72:5-59
Zhang Y (2013) Kinetics and dynamics of mass-transfer-controlled mineral and bubble dissolution or growth: a review. Eur J Mineral 25:255-266
Zhang Y, Behrens H (2000) H2O diffusion in rhyolitic melts and glasses. Chem Geol 169:243-262
Zhang Y, Cherniak DJ (eds) (2010) Diffusion in Minerals and Melts. Mineralogical Society of America
Zhang Y, Liu L (2012) On diffusion in heterogeneous media. Am J Sci 312:1028-1047
Zhang Y, Ni H (2010) Diffusion of H, C, and O components in silicate melts. Rev Mineral Geochem 72:171-225
Zhang Y, Stolper EM (1991) Water diffusion in basaltic melts. Nature 351:306-309
Zhang Y, Xu Z (2016) Zircon saturation and Zr diffusion in rhyolitic melts, and zircon growth geospeedometer. Am Mineral 101:1252-1267
Zhang Y, Gan T, Guan Y (2019) K isotope fractionation in diffusion couples of molten basalts. Abstract , Goldschmidt Conference
Zhang L, Guo X, Li W-C, Ding J, Zhou D, Zhang L, Ni H (2019) Reassessment of pre-eruptive water content of lunar volcanic glass based on new data of water diffusivity. Earth Planet Sci Lett 522:40-47
Zhang L, Guo X, Wang Q, Ding J, Ni H (2017) Diffusion of hydrous species in model basaltic melt. Geochim Cosmochim Acta 215:377-386
Zhang Y, Jenkins J, Xu Z (1997) Kinetics of the reaction $H_2O + O = 2OH$ in rhyolitic glasses upon cooling: geospeedometry and comparison with glass transition. Geochim Cosmochim Acta 61:2167-2173
Zhang Y, Ni H, Chen Y (2010) Diffusion data in silicate melts. Rev Mineral Geochem 72:311-408
Zhang Y, Stolper EM, Ihinger PD (1995) Kinetics of reaction $H_2O + O = 2OH$ in rhyolitic glasses: preliminary results. Am Mineral 80:593-612
Zhang Y, Stolper EM, Wasserburg GJ (1991a) Diffusion of water in rhyolitic glasses. Geochim Cosmochim Acta 55:441-456
Zhang Y, Stolper EM, Wasserburg GJ (1991b) Diffusion of a multi-species component and its role in the diffusion of water and oxygen in silicates. Earth Planet Sci Lett 103:228-240
Zhang Y, Walker D, Lesher CE (1989) Diffusive crystal dissolution. Contrib Mineral Petrol 102:492-513
Zhang Y, Xu Z, Liu Y (2003) Viscosity of hydrous rhyolitic melts inferred from kinetic experiments, and a new viscosity model. Am Mineral 88:1741-1752
Zhang Y, Xu Z, Zhu M, Wang H (2007) Silicate melt properties and volcanic eruptions. Rev Geophys 45:RG4004, doi:4010.1029/2006RG000216
Zhang P, Zhang L, Wang Z, Li WC, Guo X, Ni H (2018) Diffusion of molybdenum and tungsten in anhydrous and hydrous granitic melts. Am Mineral 103:1966-1974